Design of an Abiotic, Stimulus-Responsive, Foldamer for the Study of Latent Free Energy and Frustration

Adam Jesse Sowers

A dissertation submitted to the faculty of the University of North Carolina at Chapel Hill in partial fulfillment of the requirements for the degree of Doctor of Philosophy in the Department of Chemistry in the College of Arts and Sciences.

Chapel Hill
2022

Approved by:

Marcey L. Waters

Michel R. Gagné

Abigail S. Knight

Frank A. Leibfarth

David A. Nicewicz

ABSTRACT

Adam Jesse Sowers: Design of an abiotic, stimulus-responsive, foldamer for the study of latent free energy and frustration
(Under the direction of Marcey L. Waters)

Noncovalent networks (NCN) are complex webs of non-covalent interactions that give proteins their structure and play a role in functions, such as allostery and signal transduction. These functions rely on long-distance communication through the NCN within the protein. Despite their role, there is a lack of molecular understanding of their mode of action due to their size and complexity with proteins. Herein, I report the system design and evaluation of a water-soluble, stimulus-responsive foldamer, based on an established aromatic donor-acceptor foldamer and a novel, pH-sensitive aromatic monomer.

To my loving wife, Mercedes,
my eternal source of frustration.

Table of Contents

LIST OF TABLES

LIST OF FIGURES

LIST OF SCHEMES

List of Abbreviations and Symbols

1D	1-dimensional
°C	degrees Celsius
δ	chemical shift
λ_{max}	wavelength at maximum absorbance
µL	microliter
µm	micrometer
µM	micromolar
Å	angstrom or ångström
AAN	aminoalkoxynaphthalene
$AANH^+$	protonated AAN
Ac	acetyl
acceptor	A
aedamer	aromatic electron donor-acceptor foldamer
AHN	aminohydroxynaphthalene
Aib	2-aminoisobutyric residue
Alloc	N-allyloxycarbonyl
Alloc-Cl	allyloxycarbonyl chloride
aq	aqueous
Boc	N-*tert*-butoxycarbonyl
Boc_2O	di-*tert*-butyl dicarbonate
^{13}C	carbon-13
calcd	calculated
CD	circular dichroism

$CDCl_3$	chloroform-*d*1
cm	centimeter
conc	concentrated
CT	charge transfer
D_2O	deuterium oxide
D_2SO_4	deuterated sulfuric acid
donor	D
DAN	dialkoxynaphthalene
DCM	dichloromethane
DHN	dihydroxynaphthalene
DIC	N,N'-diisopropylcarbodiimide
DIPEA	diisoproylethylamine
DMF	dimethylformamide
DMSO-*d*6	dimethylsulfoxide-*d*6
DSS	sodium trimethylsilylpropanesulfonate
equiv	equivalence
ESI	electrospray ionization
ESP	electrostatic potential map
Et_2O	diethyl ether
EtOAc	ethyl acetate
EtOH	ethanol
Fmoc	N-fluorenylmethyloxycarbonyl
g	gram
GdmCl	guanidinium chloride

Gen 1	generation 1 switchable foldamer
Gly	glycine
GPCR	G-protein coupled receptor
h	hour
^{1}H	hydrogen-1
H^{+}	proton
H_2O	water
H_3PO_4	phosphoric acid
HCl	hydrochloric acid
HOMO	hightest occupied molecular orbital
HPLC	high-performance liquid chromatography
HRMS	high-resolution mass spectrometry
Hz	hertz
J	coupling constant
K	Kelvin
K_a	association constant
$K_2CO_{\#}$	potassium carbonate
kcal	kilocalorie
KD_2PO_4	potassium dideuterophosphate
$KHCO_3$	potassium bicarbonate
KI	potassium iodide
KOD	potassium deuteroxide
KOH	potassium hydroxide
LCMS	liquid chromotagraphy-mass spectrometry

LUMO	lowest unoccupied molecular orbital
Lys	lysine
M	left-handed screw sense or molar
MeCN	acetonitrile
mg	milligram
MHz	megahertz
min	minute
mL	milliliter
mm	millimeter
mM	millimolar
mmol	millimole
mol	mole
MRE	mean residue ellipticity
N_2	nitrogen gas
NCN	non-covalent network
NDCA	naphthalenedicarboxyanhydride
NDI	naphthalenediimide
NEt_3	triethylamine
nm	nanometer
NMR	nuclear magnetic resonance
NOE	nuclear Overhauser effect
NOESY	nuclear Overhauser effect spectroscopy
Oxyma	ethyl cyanohydroxyiminoacetate
P	right-handed screw sense

ppm	parts per million
quant	quantitative
R	substituent
R_f	retention factor
rt	room temperature
SPPS	solid phase peptide synthesis
temp	temperature
TFA	trifluoroacetic acid
THF	tetrahydrofuran
TLC	thin layer chromatography
TMS	tetramethylsilane
UV-Vis	Ultraviolet-visible region

CHAPTER ONE:

INTRODUCTION AND BACKGROUND

1.1 Introduction

Non-covalent networks (NCN) are complex webs of non-covalent interactions that are present in proteins when they are folded into their three-dimensional structures.[1–3] These networks are comprised of electrostatics (charge repulsions and ion pairing), hydrogen-bonding, van der Waals interactions, aromatic interactions, and water-mediated hydrophobic interactions.[4] Within a protein, it is hypothesized that perturbations to the network gives rise to functional activities, such as enzymatic catalysis,[5] molecular recognition,[6,7] and cell signaling.[8,9] The perturbations and resulting changes in the network can result in structural reorganizations that can be viewed as a form of long-range communication that transmits information through the protein. This phenomenon of long-range communication is important for biological processes such as allostery[10,11] and transmembrane signal transduction.[12]

Despite the role NCNs play in protein function, there is a lack of molecular understanding of their mode of action. This can be explained in part by the overall size and complexity of protein systems that rely on them to function. The size of the NCN in a protein directly relates to the number of interactions which comprise it. As the magnitude of interactions increases, the number of conformational states with fully optimized interactions decreases.[13,14] This leads to a subset of non-optimal, or *frustrated,* interactions within the NCN that contribute to its functionality.[15] Well-defined

synthetic systems can be used as model systems, but there are few examples of small molecule systems in the literature.[16,17] Small molecule systems are generally lacking in size and complexity to build a functional NCN.[18–23]

Herein, I describe a water-soluble foldamer system that bridges the size and complexity between proteins and small molecules. The foldamer incorporates non-optimal (frustrated) interactions and a molecular pH switch to facilitate a conformational change to a new folded state from a single point of perturbation. This design provides insights into the action of NCNs in long-range communication and the role of frustration, as well as the new concept of latent free energy, the potential energy of the non-optimal noncovalent interactions. Furthermore, it establishes a working model for designing artificial responsive NCNs.

1.2 Background

1.2.1 Principle of minimal frustration

Proteins exist at equilibrium as ensembles of conformational states rather than as unique static structures.[24–27] Following its specific funneled energy landscape as it folds, a protein samples many partial folded states seeking to optimize the interactions within the resulting NCN.[28,29] As mentioned previously, NCNs are complex webs with many interactions at play, so it is improbable that one folded conformation can perfectly optimize each interaction to their own lowest energy orientation. This leads to an ensemble of frustrated lowest energy states that contains both optimal and non-optimal interactions.

The concept of frustration in proteins, first introduced by Wolynes,[14] interprets the optimization of interactions in a protein from a global perspective. The principle of minimal frustration states that a protein cannot optimize every interaction within its NCN,

so it must manage by reducing the non-optimal interactions without significantly compromising optimal interactions.[15,30] The final “structure” is an ensemble of many conformational states that each have similar energies with respect to both optimal and non-optimal interactions. This is represented in an energy landscape as a “rugged” funnel with a definite number of minima of similar energies at the bottom of the energy funnel.[31]

Frustrated sites in proteins have been suggested to facilitate their functions.[29,32,33] In a study of frustration in enzymes, Wolynes reported a common trend of highly frustrated residues in the active site and a secondary shell of weakly frustrated interactions around the site, and the frustration of the active site was relieved when the substrate was bound.[34,35] In another study, Wolynes compared frustration analyses of native proteins to designed proteins and found that the native proteins contained more frustrated interactions.[36] The designed protein was optimized specifically with stability in mind, not function. Wolynes argues that nature must consider multiple requirements when designing proteins: structure and stability, function and activity, and regulation.

Waters and Gagné have previously studied the effect of frustrated non-covalent interactions on long-range communication through a responsive NCN.[37] In this study, mutations in a peptide [2]-catenane resulted in long-range changes in packing forming new and strengthened interactions to compensate the loss of other favorable interactions at a distant site, including the formation of a new hydrogen bond (Figure 1-1). The stabilizing energy of the new interactions drives the system to respond to a stimulus, in this case a destabilizing mutation from Aib to Gly.

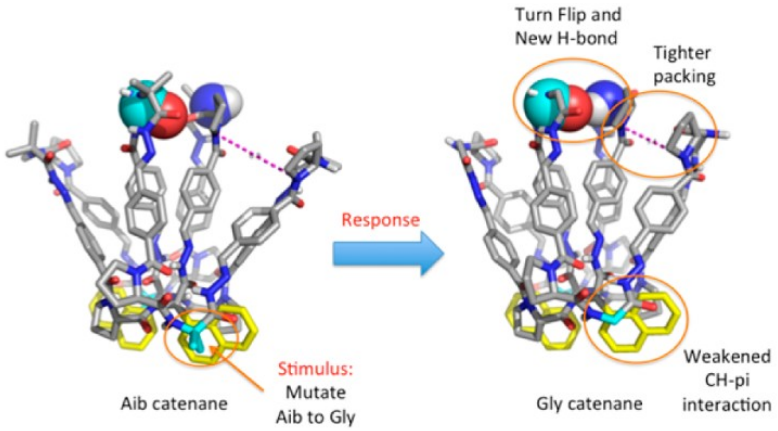

Figure 1-1. Representation of [2]-catenane system exhibiting long-range response in the NCN from an Aib to Gly mutation.[37] Reprinted with permission from ref 37. Copyright 2016 American Chemical Society.

They describe a responsive NCN as a system that stores potential energy in the form of non-optimal non-covalent interactions, such as the frustrated hydrogen bonding groups in the original structure, and is referred to as latent free energy. In effect, a NCN stores latent free energy by incorporating frustration into certain interactions that exhibit negative cooperativity. This negative cooperativity ultimately leads to a response from a stimulus.

1.2.2 Foldamers

Foldamers are a class of oligomers that exhibit a strong behavior to adopt a specific compact conformation.[38] They are designed by mimicking the principles that govern the folding of biomolecules, such as proteins. Three principles are of particular importance: (i) hierarchical organization of conformation; (ii) cooperativity in higher order structures; (iii) sequence heterogeneity.[39]

As foldamers fold into higher order structures, a NCN develops from the individual non-covalent interactions.[40–46] In this way, many foldamers have been reported that mimic the higher order folding of proteins, and some have been shown to mimic protein activities as well, such as enzyme catalysis[47,48] and signal

transduction.[49,50] Mimicking structure and function is not enough to gain insight into the behavior of proteins. To truly mimic the behavior of proteins, a foldamer must contain a responsive NCN that can respond to the environment around it.

One area of foldamer design is in developing systems for signaling transduction through a membrane. The most prevalent family of transmembrane signaling proteins are G-protein coupled receptors (GPCR).[51] GPCRs are known to respond to a variety of stimuli that initiate signal cascades leading to downstream responses in the cell, such as light, metals, and small molecules.[52–55] Without crossing the membrane, the stimulating signal delivers its information to the GPCR which transmits that information into the cell via long-distance conformational changes through the membrane.

One foldamer system designed to mimic signal transduction is the oligo-Aib 3_{10} helix.[56–59] Because Aib is achiral, these helices are known to rapidly interconvert between right- (P) and left-handed (M) screw sense conformers (Figure 1-2a). By incorporating a binding site capable of binding a chiral ligand, the chiral information can be transmitted through the helix to a chiral marker on the other end (Figure 1-2b). The helix interconverts between screw senses because the two conformation are of equal energies in the absence of a chiral stimulus. When the ligand interacts with the binding site, the energy of the corresponding conformation is lowered thereby increasing the helix's preference for that screw sense.

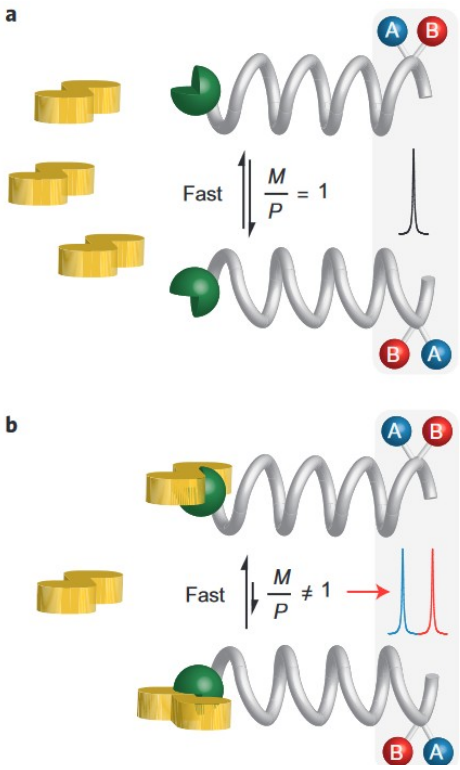

Figure 1-2. Schematic representation of Aib 3_{10} helix interconverting between screw sense conformers.[60] a) Fast exchange in the helical equilibrium results in equally populated M and P conformers appearing as a single signal for the chiral marker. b) The helical equilibrium is shifted by the binding of a chiral ligand inducing preference for one conformer over the other appearing as separate signals for the chiral marker. Reprinted by permission from ref 60. Copyright 2013 Springer Nature.

The Aib 3_{10} helix has been shown to transmit chirality even through a lipid bilayer membrane. This mechanism of information transmittance mimics signal transduction via transmembrane signaling proteins in a cell membrane. The Aib 3_{10} helical foldamer has been shown to mimic this process with a variety of ligand stimuli, including pH, metals, and light.[50,60–65]

This foldamer has a number of qualities that bring synthetic foldamers closer to the behavior of proteins, but it has minor discrepancies with real proteins. In an Aib 3_{10} helix, the energies for the two screw sense conformers are identical leading to a rapid global conformation change. In proteins, the NCN has a clear preference for one conformation over another. The preference changes to a new conformation only after

the stimulus event occurs. Furthermore, the Aib 3_{10} helix does not clearly demonstrate the concept of frustration in the switchable behavior. The goal of my research was to develop a new biomimetic foldamer that demonstrates the use of frustration to drive stimulus-responsive behavior between two folded states.

1.2.3 Aromatic electron donor-acceptor foldamers

I chose to work with a well-studied foldamer system that is comprised of only one type of non-covalent interaction. Aromatic electron donor-acceptor foldamers (aedamers), developed by Iverson, are oligomers that exploit aromatic donor-acceptor interactions in their folded structure.[66–70] The system design incorporates a well-known naphthalene-based donor-acceptor pair into a water-soluble peptide (Figure 1-3). The donor-acceptor pair are based on dialkoxynaphthalene (**DAN**) and naphthalenediimide (**NDI**) aromatic units which have been shown to have a relatively strong stacking interaction in water. This interaction is driven by aromatic stacking, strengthened by donor-acceptor charge-transfer interactions resulting in a pleated stacked columnar structure.

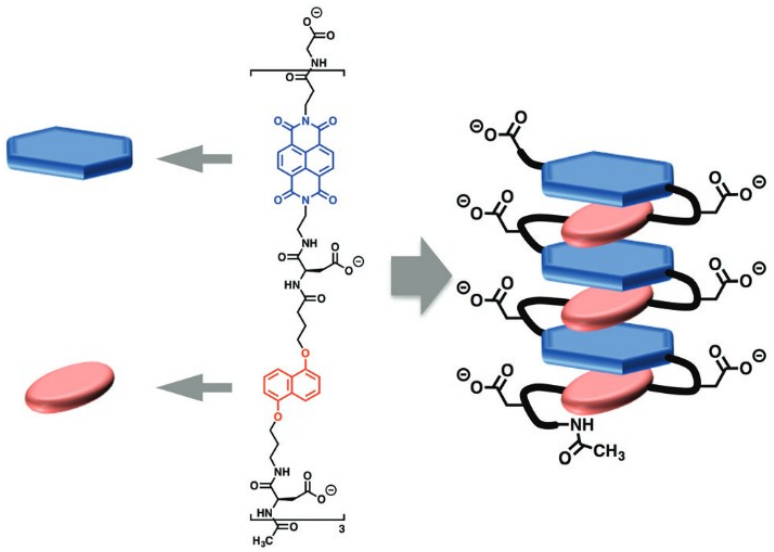

Figure 1-3. Schematic representation of the pleated stacked columnar structure between **NDI** (blue) and **DAN** (red) in the aedamer peptide system.[71] Reproduced with permission from Ref. 71. Copyright 2016 Royal Society of Chemistry.

Charge-transfer interactions are a type of molecular orbital coupling in which the highest occupied molecular orbital (HOMO) of the donor compound favorably interacts with the lowest unoccupied molecular orbital (LUMO) of the acceptor compound. The coupling of the donor (D) and acceptor (A) can lead to a photoinduced single-electron transfer from the HOMO to the LUMO resulting in a transient radical cation-anion charge attraction ($D^{\bullet+}$-$A^{\bullet-}$).

The difference in strength between only the standard aromatic stacking (quadrupole-quadrupole interaction) and the additional charge-transfer interaction is shown for the aromatic monomers below. The intermolecular binding strengths of the aromatic units in aqueous solution are as follows: **DAN**/**DAN** K_a = 20 M^{-1}; **NDI**/**NDI** K_a = 245 M^{-1}; **DAN**/**NDI** K_a = 2045 M^{-1}.[71] There is a tenfold difference between **NDI**/**NDI** which stacks solely by aromatic stacking and **DAN**/**NDI** which has an additional donor-acceptor, charge-transfer interaction. This interaction is characterized by an absorption

signal in the UV-Vis spectrum called a charge-transfer band. The charge-transfer band for this donor-acceptor pair is in the visible region at 522 nm resulting in a red color.

The foldamer itself is a peptide oligomer that incorporates the aromatic units as amino acid monomers into the peptide backbone. The aromatic monomers are tethered together by aspartate residues which grant water solubility to the foldamer as a whole. Including the alkyl linkers on each monomer, Iverson looked at a diverse set of linkers and found that any linker that gave a total of at least eight atoms was sufficient for folding.[72] In another study, he showed that 11 atoms resulted the expected columnar folding between adjacent monomers, but linkers of 13 atoms allowed for alternative folding such as intercalative folding between monomers that are not in proximity to one another.[73]

My research aimed to use Iverson's aedamer as a foundation for a switchable foldamer that can access two conformational states using a switching component and a controlled stimulus. In Chapter 2, I will discuss the design and characterization of both the switchable foldamer and its novel, pH-sensitive switching component, aminoalkoxynaphthalene (**AAN**), which is based on the original **DAN** monomer. I will also report the evaluation of the switchable foldamer as it relates to a stimulus-responsive NCN, frustration, and latent free energy.

REFERENCES

(1) Dill, K. A.; Ozkan, S. B.; Shell, M. S.; Weiki, T. R. The Protein Folding Problem. *Annu. Rev. Biophys.* **2008**, *37*, 289–316. https://doi.org/10.1146/annurev.biophys.37.092707.153558.

(2) Wolynes, P. G. Energy Landscapes and Solved Protein–Folding Problems. *Phil. Trans. R. Soc. A.* **2005**, *363* (1827), 453–467. https://doi.org/10.1098/rsta.2004.1502.

(3) Onuchic, J. N.; Wolynes, P. G. Theory of Protein Folding. *Current Opinion in Structural Biology* **2004**, *14* (1), 70–75. https://doi.org/10.1016/j.sbi.2004.01.009.

(4) Dill, K. A. Dominant Forces in Protein Folding. *Biochemistry* **1990**, *29* (31), 7133–7155. https://doi.org/10.1021/bi00483a001.

(5) Clark, A. C. Caspase Allostery and Conformational Selection. *Chem. Rev.* **2016**, *116* (11), 6666–6706. https://doi.org/10.1021/acs.chemrev.5b00540.

(6) Stank, A.; Kokh, D. B.; Fuller, J. C.; Wade, R. C. Protein Binding Pocket Dynamics. *Acc. Chem. Res.* **2016**, *49* (5), 809–815. https://doi.org/10.1021/acs.accounts.5b00516.

(7) Levy, Y.; Wolynes, P. G.; Onuchic, J. N. Protein Topology Determines Binding Mechanism. *Proceedings of the National Academy of Sciences* **2004**, *101* (2), 511–516. https://doi.org/10.1073/pnas.2534828100.

(8) Nussinov, R.; Tsai, C.-J.; Ma, B. The Underappreciated Role of Allostery in the Cellular Network. *Annu. Rev. Biophys.* **2013**, *42*, 169–189. https://doi.org/10.1146/annurev-biophys-083012-130257.

(9) Tompa, P. The Principle of Conformational Signaling. *Chem. Soc. Rev.* **2016**, *45* (15), 4252–4284. https://doi.org/10.1039/C6CS00011H.

(10) Williams, D. H.; Zhou, M.; Stephens, E. Ligand Binding Energy and Enzyme Efficiency from Reductions in Protein Dynamics. *J. Mol. Bio.* **2006**, *355* (4), 760–767. https://doi.org/10.1016/j.jmb.2005.11.015.

(11) del Sol, A.; Tsai, C.-J.; Ma, B.; Nussinov, R. The Origin of Allosteric Functional Modulation: Multiple Pre-Existing Pathways. *Structure* **2009**, *17* (8), 1042–1050. https://doi.org/10.1016/j.str.2009.06.008.

(12) Grigoryan, G.; Moore, D. T.; DeGrado, W. F. Transmembrane Communication: General Principles and Lessons from the Structure and Function of the M2 Proton Channel, K^+ Channels, and Integrin Receptors. *Annu. Rev. Biochem.* **2011**, *80* (1), 211–237. https://doi.org/10.1146/annurev-biochem-091008-152423.

(13) Wolynes, P. G. Symmetry and the Energy Landscapes of Biomolecules. *Proc. Natl. Acad. Sci. U.S.A.* **1996**, *93* (25), 14249–14255. https://doi.org/10.1073/pnas.93.25.14249.

(14) Bryngelson, J. D.; Wolynes, P. G. Spin Glasses and the Statistical Mechanics of Protein Folding. *Proc. Natl. Acad. Sci. U.S.A.* **1987**, *84* (21), 7524–7528. https://doi.org/10.1073/pnas.84.21.7524.

(15) Ferreiro, D. U.; Komives, E. A.; Wolynes, P. G. Frustration in Biomolecules. *Quart. Rev. Biophys.* **2014**, *47* (4), 285–363. https://doi.org/10.1017/S0033583514000092.

(16) Chockalingam, K.; Blenner, M.; Banta, S. Design and Application of Stimulus-Responsive Peptide Systems. *Protein Eng. Des. Sel.* **2007**, *20* (4), 155–161. https://doi.org/10.1093/protein/gzm008.

(17) Rangel, A. E.; Hariri, A. A.; Eisenstein, M.; Soh, H. T. Engineering Aptamer Switches for Multifunctional Stimulus-Responsive Nanosystems. *Adv. Mater.* **2020**, *32* (50), 2003704. https://doi.org/10.1002/adma.202003704.

(18) Zhao, C.; Li, P.; Smith, M. D.; Pellechia, P. J.; Shimizu, K. D. Experimental Study of the Cooperativity of CH−π Interactions. *Org. Lett.* **2014**, *16* (13), 3520–3523. https://doi.org/10.1021/ol5014729.

(19) Rodriguez-Docampo, Z.; Pascu, S. I.; Kubik, S.; Otto, S. Noncovalent Interactions within a Synthetic Receptor Can Reinforce Guest Binding. *J. Am. Chem. Soc.* **2006**, *128* (34), 11206–11210. https://doi.org/10.1021/ja062389h.

(20) Rodriguez-Docampo, Z.; Eugenieva-Ilieva, E.; Reyheller, C.; Belenguer, A. M.; Kubik, S.; Otto, S. Dynamic Combinatorial Development of a Neutral Synthetic Receptor That Binds Sulfate with Nanomolar Affinity in Aqueous Solution. *Chem. Commun.* **2011**, *47* (35), 9798. https://doi.org/10.1039/c1cc13451e.

(21) Otto, S. Reinforced Molecular Recognition as an Alternative to Rigid Receptors. *Dalton Trans.* **2006**, No. 23, 2861. https://doi.org/10.1039/b515817f.

(22) Gunasekara, R. W.; Zhao, Y. Rationally Designed Cooperatively Enhanced Receptors To Magnify Host–Guest Binding in Water. *J. Am. Chem. Soc.* **2015**, *137* (2), 843–849. https://doi.org/10.1021/ja510823h.

(23) Carrillo, R.; Feher-Voelger, A.; Martín, T. Enantioselective Cooperativity Between Intra-Receptor Interactions and Guest Binding: Quantification of Reinforced Chiral Recognition. *Angew. Chem.* **2011**, *123* (45), 10804–10808. https://doi.org/10.1002/ange.201103970.

(24) Wrabl, J. O.; Gu, J.; Liu, T.; Schrank, T. P.; Whitten, S. T.; Hilser, V. J. The Role of Protein Conformational Fluctuations in Allostery, Function, and Evolution. *Biophys. Chem.* **2011**, *159* (1), 129–141. https://doi.org/10.1016/j.bpc.2011.05.020.

(25) Hilser, V. J. An Ensemble View of Allostery. *Science* **2010**, *327* (5966), 653–654. https://doi.org/10.1126/science.1186121.

(26) Guo, J.; Zhou, H.-X. Protein Allostery and Conformational Dynamics. *Chem. Rev.* **2016**, *116* (11), 6503–6515. https://doi.org/10.1021/acs.chemrev.5b00590.

(27) Nussinov, R. Introduction to Protein Ensembles and Allostery. *Chem. Rev.* **2016**, *116* (11), 6263–6266. https://doi.org/10.1021/acs.chemrev.6b00283.

(28) Okazaki, K.; Koga, N.; Takada, S.; Onuchic, J. N.; Wolynes, P. G. Multiple-Basin Energy Landscapes for Large-Amplitude Conformational Motions of Proteins: Structure-Based Molecular Dynamics Simulations. *Proc. Natl. Acad. Sci. U.S.A.* **2006**, *103* (32), 11844–11849. https://doi.org/10.1073/pnas.0604375103.

(29) Wolynes, P. G. Evolution, Energy Landscapes and the Paradoxes of Protein Folding. *Biochimie* **2015**, *119*, 218–230. https://doi.org/10.1016/j.biochi.2014.12.007.

(30) Röder, K.; Wales, D. J. Evolved Minimal Frustration in Multifunctional Biomolecules. *J. Phys. Chem. B* **2018**, *122* (49), 10989–10995. https://doi.org/10.1021/acs.jpcb.8b03632.

(31) Ferreiro, D. U.; Hegler, J. A.; Komives, E. A.; Wolynes, P. G. On the Role of Frustration in the Energy Landscapes of Allosteric Proteins. *Proc Natl Acad Sci USA* **2011**, *108* (9), 3499–3503. https://doi.org/10.1073/pnas.1018980108.

(32) Ferreiro, D. U.; Komives, E. A.; Wolynes, P. G. Frustration, Function and Folding. *Curr. Opin. Struct. Bio.* **2018**, *48*, 68–73. https://doi.org/10.1016/j.sbi.2017.09.006.

(33) Li, W.; Wolynes, P. G.; Takada, S. Frustration, Specific Sequence Dependence, and Nonlinearity in Large-Amplitude Fluctuations of Allosteric Proteins. *Proc Natl Acad Sci USA* **2011**, *108* (9), 3504–3509. https://doi.org/10.1073/pnas.1018983108.

(34) Freiberger, M. I.; Guzovsky, A. B.; Wolynes, P. G.; Parra, R. G.; Ferreiro, D. U. Local Frustration around Enzyme Active Sites. *Proc Natl Acad Sci USA* **2019**, *116* (10), 4037–4043. https://doi.org/10.1073/pnas.1819859116.

(35) Ferreiro, D. U.; Hegler, J. A.; Komives, E. A.; Wolynes, P. G. Localizing Frustration in Native Proteins and Protein Assemblies. *Proceedings of the National Academy of Sciences* **2007**, *104* (50), 19819–19824. https://doi.org/10.1073/pnas.0709915104.

(36) Truong, H. H.; Kim, B. L.; Schafer, N. P.; Wolynes, P. G. Funneling and Frustration in the Energy Landscapes of Some Designed and Simplified Proteins. *J. Chem. Phys.* **2013**, *139* (12), 121908. https://doi.org/10.1063/1.4813504.

(37) Chung, M.-K.; White, P. S.; Lee, S. J.; Gagné, M. R.; Waters, M. L. Investigation of a Catenane with a Responsive Noncovalent Network: Mimicking Long-Range Responses in Proteins. *J. Am. Chem. Soc.* **2016**, *138* (40), 13344–13352. https://doi.org/10.1021/jacs.6b07833.

(38) Hill, D. J.; Mio, M. J.; Prince, R. B.; Hughes, T. S.; Moore, J. S. A Field Guide to Foldamers. *Chem. Rev.* **2001**, *101* (12), 3893–4012. https://doi.org/10.1021/cr990120t.

(39) Gellman, S. H. Foldamers: A Manifesto. *Acc. Chem. Res.* **1998**, *31* (4), 173–180. https://doi.org/10.1021/ar960298r.

(40) Aromatic Oligoamide Foldamers. *Eur. J. Org. Chem.* **2003**, *2004* (1), 17–29. https://doi.org/0.1002/ejoc.200300495.

(41) Chandramouli, N.; Ferrand, Y.; Lautrette, G.; Kauffmann, B.; Mackereth, C. D.; Laguerre, M.; Dubreuil, D.; Huc, I. Iterative Design of a Helically Folded Aromatic Oligoamide Sequence for the Selective Encapsulation of Fructose. *Nature Chem* **2015**, *7* (4), 334–341. https://doi.org/10.1038/nchem.2195.

(42) Zhang, D.-W.; Zhao, X.; Li, Z.-T. Aromatic Amide and Hydrazide Foldamer-Based Responsive Host–Guest Systems. *Acc. Chem. Res.* **2014**, *47* (7), 1961–1970. https://doi.org/10.1021/ar5000242.

(43) Zhang, D.-W.; Zhao, X.; Hou, J.-L.; Li, Z.-T. Aromatic Amide Foldamers: Structures, Properties, and Functions. *Chem. Rev.* **2012**, *112* (10), 5271–5316. https://doi.org/10.1021/cr300116k.

(44) Saraogi, I.; Hamilton, A. D. Recent Advances in the Development of Aryl-Based Foldamers. *Chem. Soc. Rev.* **2009**, *38* (6), 1726. https://doi.org/10.1039/b819597h.

(45) Prince, R. B.; Barnes, S. A.; Moore, J. S. Foldamer-Based Molecular Recognition. *J. Am. Chem. Soc.* **2000**, *122* (12), 2758–2762. https://doi.org/10.1021/ja993830p.

(46) Licini, G.; Prins, L. J.; Scimin, P. Oligopeptide Foldamers: From Structure to Function. *Eur. J. Org. Chem.* **2005**, *2005* (6), 969–977. https://doi.org/10.1002/ejoc.200400521.

(47) Müller, M. M.; Windsor, M. A.; Pomerantz, W. C.; Gellman, S. H.; Hilvert, D. A Rationally Designed Aldolase Foldamer. *Angew. Chem. Int. Ed.* **2009**, *48* (5), 922–925. https://doi.org/10.1002/anie.200804996.

(48) Mayer, C.; Müller, M. M.; Gellman, S. H.; Hilvert, D. Building Proficient Enzymes with Foldamer Prostheses. *Angew. Chem. Int. Ed.* **2014**, *53* (27), 6978–6981. https://doi.org/10.1002/anie.201400945.

(49) Ousaka, N.; Inai, Y. Transfer of Noncovalent Chiral Information along an Optically Inactive Helical Peptide Chain: Allosteric Control of Asymmetry of the C-Terminal Site by External Molecule That Binds to the N-Terminal Site. *J. Org. Chem.* **2009**, *74* (4), 1429–1439. https://doi.org/10.1021/jo801686m.

(50) Gratzer, K.; Diemer, V.; Clayden, J. Signal Transduction in Oligoamide Foldamers by Selective Non-Covalent Binding of Chiral Phosphates at a Urea Binding Site. *Org. Biomol. Chem.* **2017**, *15* (17), 3585–3589. https://doi.org/10.1039/C7OB00660H.

(51) Katritch, V.; Cherezov, V.; Stevens, R. C. Structure-Function of the G Protein–Coupled Receptor Superfamily. *Annu. Rev. Pharmcol. Toxicol.* **2013**, *53*, 531–556. https://doi.org/10.1146/annurev-pharmtox-032112-135923.

(52) Rasmussen, S. G. F.; DeVree, B. T.; Zou, Y.; Kruse, A. C.; Chung, K. Y.; Kobilka, T. S.; Thian, F. S.; Chae, P. S.; Pardon, E.; Calinski, D.; Mathiesen, J. M.; Shah, S. T. A.; Lyons, J. A.; Caffrey, M.; Gellman, S. H.; Steyaert, J.; Skiniotis, G.; Weis, W. I.; Sunahara, R. K.; Kobilka, B. K. Crystal Structure of the B2 Adrenergic Receptor–Gs Protein Complex. *Nature* **2011**, *477* (7366), 549–555. https://doi.org/10.1038/nature10361.

(53) Tesmer, J. J. G.; Sunahara, R. K.; Gilman, A. G.; Sprang, S. R. Crystal Structure of the Catalytic Domains of Adenylyl Cyclase in a Complex with Gsα·GTPγS. *Science* **1997**, *278* (5345), 1907–1916. https://doi.org/10.1126/science.278.5345.1907.

(54) Kruse, A. C.; Ring, A. M.; Manglik, A.; Hu, J.; Hu, K.; Eitel, K.; Hübner, H.; Pardon, E.; Valant, C.; Sexton, P. M.; Christopoulos, A.; Felder, C. C.; Gmeiner, P.; Steyaert, J.; Weis, W. I.; Garcia, K. C.; Wess, J.; Kobilka, B. K. Activation and Allosteric Modulation of a Muscarinic Acetylcholine Receptor. *Nature* **2013**, *504* (7478), 101–106. https://doi.org/10.1038/nature12735.

(55) Kobilka, B. K. G Protein Coupled Receptor Structure and Activation. *Biochim. Biophys. Acta. Biomembr.* **2007**, *1768* (4), 794–807. https://doi.org/10.1016/j.bbamem.2006.10.021.

(56) Yashima, E.; Maeda, K.; Iida, H.; Furusho, Y.; Nagai, K. Helical Polymers: Synthesis, Structures, and Functions. *Chem. Rev.* **2009**, *109* (11), 6102–6211. https://doi.org/10.1021/cr900162q.

(57) Nakano, T.; Okamoto, Y. Synthetic Helical Polymers: Conformation and Function. *Chem. Rev.* **2001**, *101* (12), 4013–4038. https://doi.org/10.1021/cr0000978.

(58) Ousaka, N.; Takeyama, Y.; Iida, H.; Yashima, E. Chiral Information Harvesting in Dendritic Metallopeptides. *Nature Chem* **2011**, *3* (11), 856–861. https://doi.org/10.1038/nchem.1146.

(59) Clayden, J.; Castellanos, A.; Solà, J.; Morris, G. A. Quantifying End-to-End Conformational Communication of Chirality through an Achiral Peptide Chain. *Angewandte Chemie International Edition* **2009**, *48* (32), 5962–5965. https://doi.org/10.1002/anie.200901892.

(60) Brown, R. A.; Diemer, V.; Webb, S. J.; Clayden, J. End-to-End Conformational Communication through a Synthetic Purinergic Receptor by Ligand-Induced Helicity Switching. *Nature Chem* **2013**, *5* (10), 853–860. https://doi.org/10.1038/nchem.1747.

(61) Le Bailly, B. A. F.; Clayden, J. Dynamic Foldamer Chemistry. *Chem. Commun.* **2016**, *52* (27), 4852–4863. https://doi.org/10.1039/C6CC00788K.

(62) Mazzier, D.; Crisma, M.; De Poli, M.; Marafon, G.; Peggion, C.; Clayden, J.; Moretto, A. Helical Foldamers Incorporating Photoswitchable Residues for Light-Mediated Modulation of Conformational Preference. *J. Am. Chem. Soc.* **2016**, *138* (25), 8007–8018. https://doi.org/10.1021/jacs.6b04435.

(63) Lister, F. G. A.; Le Bailly, B. A. F.; Webb, S. J.; Clayden, J. Ligand-Modulated Conformational Switching in a Fully Synthetic Membrane-Bound Receptor. *Nat. Chem.* **2017**, *9* (5), 420–425. https://doi.org/10.1038/nchem.2736.

(64) Le Bailly, B. A. F.; Byrne, L.; Clayden, J. Refoldable Foldamers: Global Conformational Switching by Deletion or Insertion of a Single Hydrogen Bond. *Angew. Chem.* **2016**, *128* (6), 2172–2176. https://doi.org/10.1002/ange.201510605.

(65) Brioche, J.; Pike, S. J.; Tshepelevitsh, S.; Leito, I.; Morris, G. A.; Webb, S. J.; Clayden, J. Conformational Switching of a Foldamer in a Multicomponent System by PH-Filtered Selection between Competing Noncovalent Interactions. *J. Am. Chem. Soc.* **2015**, *137* (20), 6680–6691. https://doi.org/10.1021/jacs.5b03284.

(66) Scott Lokey, R.; Iverson, B. L. Synthetic Molecules That Fold into a Pleated Secondary Structure in Solution. *Nature* **1995**, *375* (6529), 303–305. https://doi.org/10.1038/375303a0.

(67) Nguyen, J. Q.; Iverson, B. L. An Amphiphilic Folding Molecule That Undergoes an Irreversible Conformational Change. *J. Am. Chem. Soc.* **1999**, *121* (11), 2639–2640. https://doi.org/10.1021/ja9838920.

(68) Martinez, C. R.; Iverson, B. L. Rethinking the Term “Pi-Stacking.” *Chem. Sci.* **2012**, *3* (7), 2191. https://doi.org/10.1039/c2sc20045g.

(69) Gabriel, G. J.; Iverson, B. L. Aromatic Oligomers That Form Hetero Duplexes in Aqueous Solution. *J. Am. Chem. Soc.* **2002**, *124* (51), 15174–15175. https://doi.org/10.1021/ja0275358.

(70) Cubberley, M. S.; Iverson, B. L. ^{1}H NMR Investigation of Solvent Effects in Aromatic Stacking Interactions. *J. Am. Chem. Soc.* **2001**, *123* (31), 7560–7563. https://doi.org/10.1021/ja015817m.

(71) Ikkanda, B. A.; Iverson, B. L. Exploiting the Interactions of Aromatic Units for Folding and Assembly in Aqueous Environments. *Chem. Commun.* **2016**, *52* (50), 7752–7759. https://doi.org/10.1039/C6CC01861K.

(72) Zych, A. J.; Iverson, B. L. Synthesis and Conformational Characterization of Tethered, Self-Complexing 1,5-Dialkoxynaphthalene/1,4,5,8-Naphthalenetetracarboxylic Diimide Systems. *J. Am. Chem. Soc.* **2000**, *122* (37), 8898–8909. https://doi.org/10.1021/ja0019225.

(73) Gabriel, G. J.; Sorey, S.; Iverson, B. L. Altering the Folding Patterns of Naphthyl Trimers. *J. Am. Chem. Soc.* **2005**, *127* (8), 2637–2640. https://doi.org/10.1021/ja046722y.

CHAPTER TWO:

DESIGN AND EVALUATION OF A STIMULUS-RESPONSIVE FOLDAMER

2.1 Introduction

Noncovalent networks (NCN) provide a protein with its structure, and a responsive NCN uses frustration to drive the dynamics that lead to its function.[1,2] For example, by incorporating frustration into the NCN, a protein can exhibit structural changes in response to a stimulus, as is well established in signal transduction with GPCRs.[3] While there are many artificial systems that mimic proteins in structure and function, there are few examples that mimic the overall complexity of a responsive NCN within proteins. To accurately model the complex behavior of a responsive NCN in a protein, the system must experience a structural change that begins at a single point of perturbation and propagates throughout. The goal of this work is to mimic this complexity by incorporating both frustrated interactions and a point of perturbation.

In this chapter, the design and rationale of a pH-sensitive, stimulus-responsive foldamer and novel switch component will be discussed. A brief synthetic overview of the aromatic monomer amino acids will also be provided. The system was evaluated using UV-Vis, ^{1}H NMR, and circular dichroism (CD) which support a pH-induced conformational change. This response was interpreted as a release of latent free energy that was driven by the relief of frustration within the NCN in the foldamer. I would also like to acknowledge that this project was completed in collaboration with Hanne Henriksen, a graduate student in the Waters lab.

2.2 System Design

The foldamer must fulfill three requirements. First, the foldamer must have two structural conformations that it switches between as a response to a stimulus, in this case pH. Second, the two conformational states must contain non-optimal interactions as the site of frustration. Third, the conformation change must propagate from a single point of perturbation.

We chose to use Iverson's aedamer as the basis for the design as it is well characterized, has conformational flexibility to allow for access to different folded states, and folds in aqueous solution.[4] When considering a new switching component, we wanted to minimize any undesired effects that may arise when altering the original system. To that end, we designed a new aromatic monomer, aminoalkoxynaphthalene (**AAN**), by replacing one of the ether substituents of the original monomer, **DAN**, with a secondary amine which behaves as a protonation site. In this way, the switch component is sensitive to a pH stimulus. **AAN** is more electron-rich than **DAN** at neutral pH, but the amine can be protonated at low pH, which makes the aromatic face electron-poor, as seen with the electrostatic potential (ESP) maps in Figure 2-1. Thus, we hypothesized that **AAN** will preferentially stack with the electron-poor **NDI** at neutral pH but will prefer to interact with **DAN** when protonated. This change in stacking partners is the basis for the foldamer conformational switch.

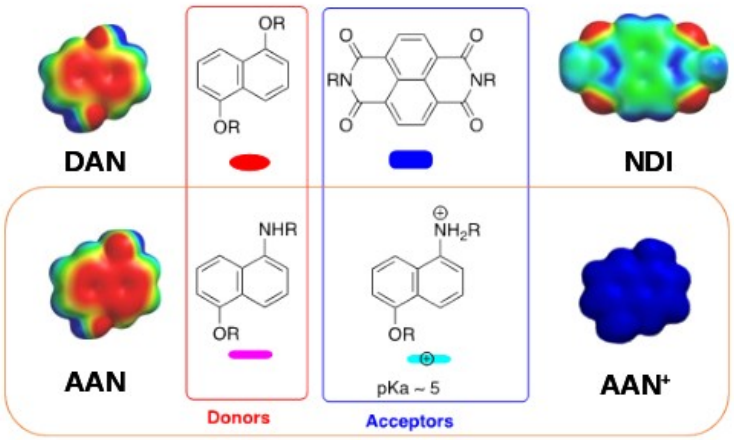

Figure 2-1. ESP maps (same scale) for **DAN**, **NDI**, **AAN**, and **AANH$^+$**.

The aryl amine on **AAN** resembles the amine on naphthylamine which has a pKa of 3.92.[5] **AAN** is more electron-rich than naphthylamine, so the pKa is expected to be similar or higher. A pH of two units above the pKa results in a speciation of 100:1 for unprotonated:protonated and the opposite for two units below. As such, the expected pH range for the switch is pH 3-7.

The design must include both optimal and non-optimal interactions within the NCN following the principle of minimal frustration. Iverson had shown that **DAN** and **NDI** stack most favorably (K_a = 2045 M^{-1}), but **NDI** can also form a homodimer that is about 10-fold weaker.[6] Thus, **NDI** optimally interacts with **DAN** but can also form a less favorable (frustrated) interaction with another **NDI**.

The Iverson aedamer uses aspartates as water-solubilizing linkers,[4] but the acidic conditions necessary for the pH switch conflicts with this strategy. Thus, the aspartates were changed to lysines in our design because they provide water solubility in the relevant pH range. The total linker length between aromatic groups is also important to consider because the different fold patterns between aromatic surfaces can occur. The desired folding pattern from the original Iverson aedamer is a pleated column

between adjacent aromatic surfaces (Figure 2-2a) as opposed to intercalative folding between every other surface (Figure 2-2b).[7] Iverson's studies demonstrated that a linker length of eight atoms and above allows the formation of the pleated column without alternative intercalative folding.[8] Linkers with eight atoms are too short and are incapable of folding into a pleated, columnar stack, whereas linkers with 13 atoms are too long and are capable of folding into an intercalative stack.[9]

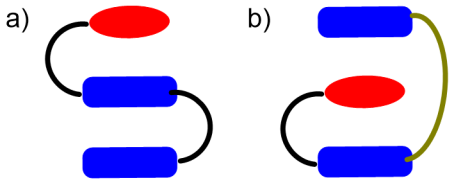

Figure 2-2. Representative three-monomer foldamer exhibiting two types of stacking. a) Pleated folding resulting from stacking of adjacent monomers tethered by linkers with 9-12 atoms (black). b) Intercalative folding resulting from stacking of one terminus with the other. The linker length necessary for this fold is 13 atoms or longer (tan).

Following the requirements outlined above, the first generation foldamer (**Gen 1**) shown in Figure 2-3a was designed as a structurally simple non-covalent network that contains four aromatic monomers: 2 **NDI**, **DAN**, and **AAN** (Figure 2-3b), with intervening lysines between each aromatic monomer and at each terminus for solubility. By exploiting the protonation states of **AAN** at both neutral and acidic pH, the design is predicted to achieve two folded structures. In this way, **AAN** behaves as a handle to introduce and relieve frustration to and from the system.

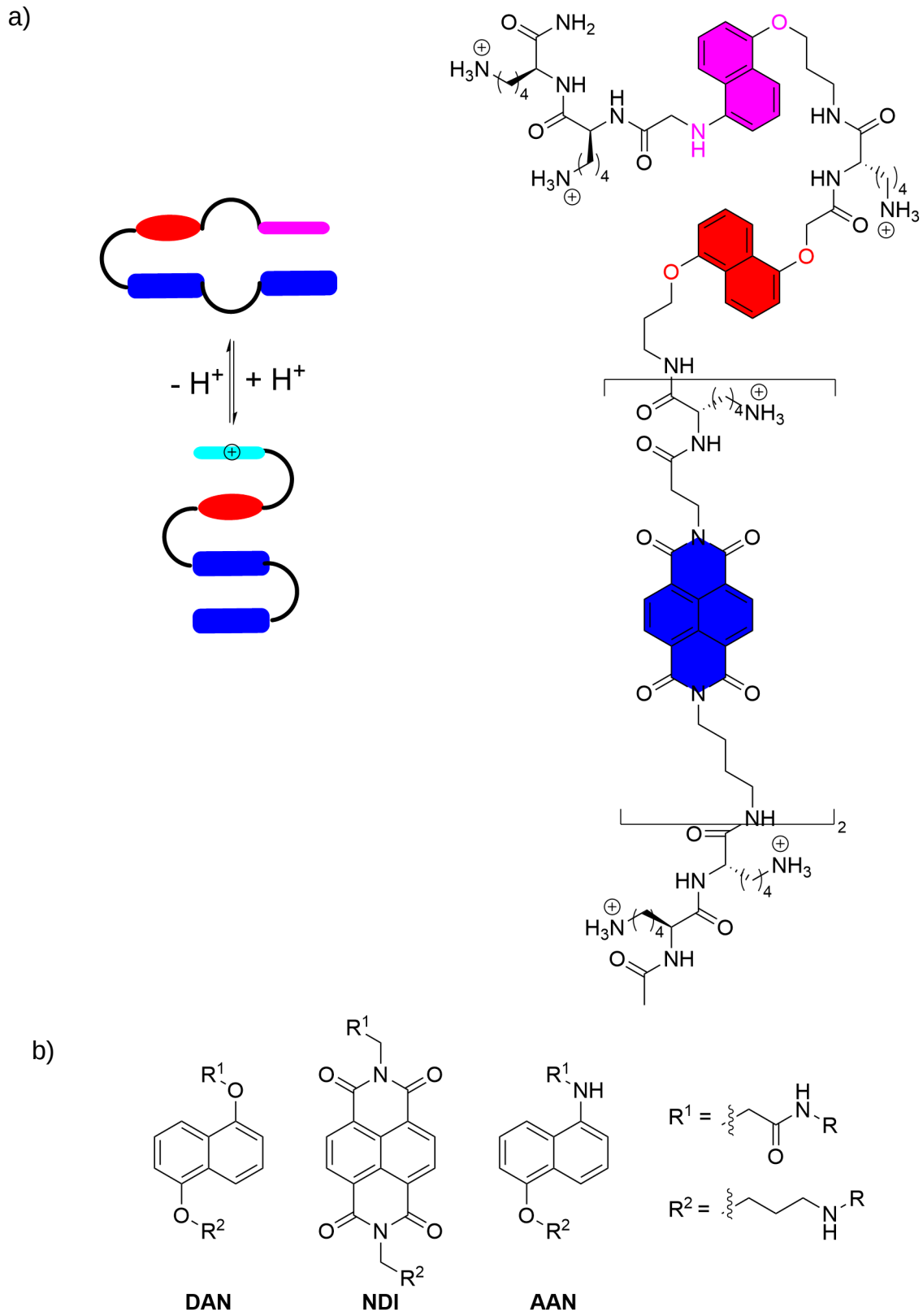

Figure 2-3. a) A schematic representation showing the **Gen 1** foldamer in its two predicted states, sheet-like (top) and columnar (bottom), in aqueous buffer. b) Chemical structures of **DAN**, **NDI**, and **AAN** amino residues within a peptide chain.

At neutral pH, the system is predicted to assume a sheet-like conformation that maximizes the number of favorable donor-acceptor interactions at the expense of water-exposed surface area with an internal **NDI**/**DAN** interaction and a terminal **NDI**/**AAN** interaction (Figure 2-3a, top). At acidic pH, **AAN** is protonated and becomes electron-poor. No longer a donor, **AANH**$^{+}$ cannot participate in a favorable donor-acceptor interaction with **NDI**, and we predict that stacking with **DAN** will be more favorable (Figure 2-3a, bottom). The terminal **NDI** is also predicted to stack with the adjacent **NDI** rather than being solvent exposed.[10] This interaction is electrostatically unfavorable since both rings are electron-poor, and is thus considered frustrated. The final structure is a pleated, columnar conformation that resembles the original aedamer folded conformation. Along with characterizing the behavior of the foldamer, each of the monomer peptides (in the form of Ac-Lys-monomer-Lys-NH_2) and relevant dimer peptides (Table 2-1) were characterized by UV-Vis, CD, and ^{1}H NMR to evaluate pairwise interactions at low and high pH.

Table 2-1. The relevant dimer peptide sequences and their abbreviations.

Peptide	Abbreviation
Ac-Lys-**NDI**-Lys-**AAN**-Lys-NH_2	**NDI-AAN**
Ac-Lys-**NDI**-Lys-**DAN**-Lys-NH_2	**NDI-DAN**
Ac-Lys-**NDI**-Lys-**NDI**-Lys-NH_2	**NDI-NDI**
Ac-Lys-**DAN**-Lys-**AAN**-Lys-NH_2	**DAN-AAN**

While the original aedamer developed by Iverson was well characterized in the literature,[4,6,8,9,11–13] there are significant changes that distinguish the aedamer in this work from the original. This includes the use of a novel aromatic monomer, the exposure of the aromatic monomers to both a neutral and acidic environment, and the replacement of aspartate residues with lysines. Thus, it became pertinent to verify the behavior of both the original monomers and the new in the dimer peptides.

To begin, the monomers were synthesized as Alloc-protected amino acids after solubility issues were observed with the standard Fmoc protecting group. The synthesis of the Alloc-protected amino acids of **DAN**, **NDI**, and **AAN** are shown in Schemes 2-1, 2-2, and 2-3, respectively. The synthesis of the peptides was completed using solid phase peptide synthesizer.

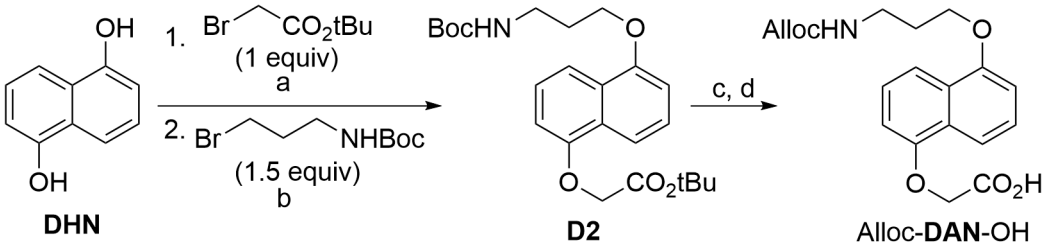

Scheme 2-1. The synthetic routes of Alloc-**DAN**-OH starting from **DHN**. (a) K_2CO_3 (2.5 equiv), acetone, reflux, 16 h, 42 %. (b) K_2CO_3 (2.5 equiv), MeCN, reflux, 16 h, 58 %. (c) TFA/DCM, 2 h. (d) Alloc-Cl (1.1 equiv), K_2CO_3 (5 equiv), THF/water, 16 h, 87 %.

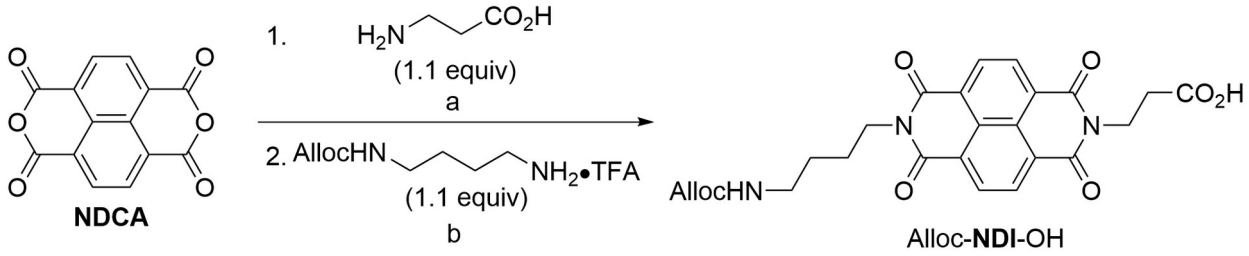

Scheme 2-2. The synthetic route of Alloc-**NDI**-OH starting from **NDCA**. (a) aq. KOH, then conc. H_3PO_4, pH 7, 110 °C, 16 h. (b) DIPEA (1.1 equiv), DMF, 110 °C, 16 h, 48 % overall.

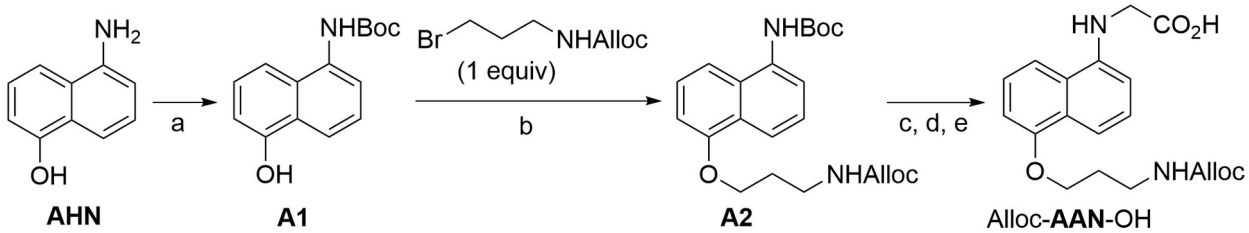

Scheme 2-3. The synthetic route of Alloc-**AAN**-OH starting from **AHN**. (a) GdmCl (0.2 equiv), Boc_2O (1 equiv), EtOH, 6 h, 86 %. (b) K_2CO_3 (4 equiv), KI (0.2 equiv), MeCN, reflux, 12 h, 73 %. (c) TFA/DCM, 2 h. (d) *tert*-butyl bromoacetate (3 equiv), $KHCO_3$ (4 equiv), KI (0.2 equiv), MeCN, reflux, 12 h, 65 %. (e) TFA/DCM, 2 h, 96 %.

2.3 Evaluating AAN as a pH-Sensitive Switch

To evaluate the viability of **AAN** behaving like a switch, we characterized the pH-dependent behavior of both the **AAN** monomer peptide, Ac-Lys-**AAN**-Lys-NH_2, and **NDI**-**AAN** (Table 2-1) using UV-Vis spectroscopy, circular dichroism (CD) and ^{1}H NMR spectroscopy.

UV-Vis characterization. The protonation of the Ac-Lys-**AAN**-Lys-NH_2 peptide was evaluated by UV-Vis spectroscopy (Figure 2-4). A comparison of the UV-Vis spectra at pH 7, 3, and 0 show that Ac-Lys-**AAN**-Lys-NH_2 (~ 30-60 μM) has an identical absorbance at pH 7 and 3 (λ_{max} 320 nm). This suggests that pH 3 is not acidic enough to protonate Ac-Lys-**AAN**-Lys-NH_2 because a blue shift should occur in its absorbance. A blue shift occurs in a UV-Vis spectrum when a conjugated system is reduced in length, and the maximum absorbance is shifted to a shorter wavelength. In the case of **AAN**, the protonation of the aryl amine prevents the lone pair from participating in the conjugation of the naphthalene ring. Ac-Lys-**AAN**-Lys-NH_2 was evaluated at a pH 0, and a noticeable blue shift (λ_{max} 301 nm) was observed. The blue shift confirms that pH 0 is necessary to protonate **AAN**. This is supported by the literature pKa of a similar amino acid, N-phenylglycine methyl ester, which has a neighboring electron-withdrawing group that lowers the pKa (pKa 2.0).[14] The N-phenyl α-amine is similar to the N-naphthyl α-amine on **AAN** which supports a pKa that is lower than predicted.

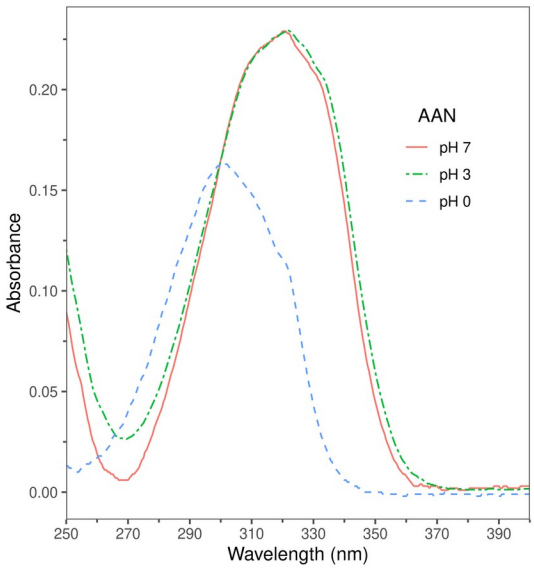

Figure 2-4. UV spectra of **AAN** (30 μM) in 50 mM potassium phosphate buffer, pH 7 (red), 50 mM citric acid-phosphate buffer, pH 3 (green), and 1 M sulfuric acid, pH 0 (blue), at 298 K.

At pH 7, **NDI**-**AAN** (Table 2-1) has a green color indicative of a favorable donor-acceptor interaction in a charge transfer (CT) complex. The spectrum shows an absorption at 613 nm at 2 mM (Figure 2-5). The CT absorbance for **NDI**-**AAN** suggests a nontrivial population of a folded state because donors and acceptors in a CT complex must be in proximity for a charge transfer event to occur. When the pH was lowered to pH 0, the solution turned colorless. In the visible spectrum, no CT absorption was present which I interpret is due to the loss of a donor-acceptor interaction when **AAN** transitions from electron-rich to electron-poor upon protonation. Thus, CT between **AAN** and **NDI** is pH-sensitive but at a pH much lower than expected.

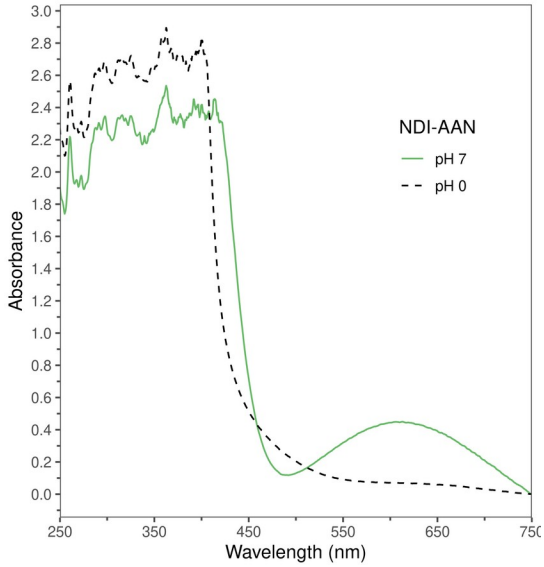

Figure 2-5. Visible spectra of **NDI**-**AAN** (2 mM) in 50 mM potassium phosphate buffer, pH 7 (green), and 1 M sulfuric acid, pH 0 (black), at 298 K.

The blue shift is also present in the UV region for **NDI**-**AAN** at pH 0 which supports that the loss of color arises from the protonation of **AAN** (Figure 2-6). All future low-pH experiments were performed at pH 0 in 1 M aq. sulfuric acid.

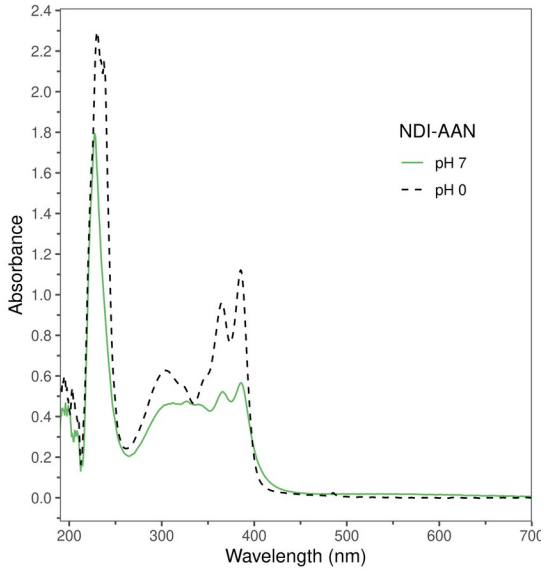

Figure 2-6. UV spectra of **NDI**-**AAN** (30 μM) in 50 mM potassium phosphate buffer, pH 7 (green), and 1 M sulfuric acid, pH 0 (black), at 298 K.

CD characterization. The loss of color in a charge transfer complex suggests a loss of a donor-acceptor interaction, but the folded/unfolded preference for **NDI**-**AAN**

still needed to be evaluated using CD and ^{1}H NMR. CD is a characterization technique that measures the absorbance of circularly polarized light for an optically active species. It is also used to indicate through-space interactions between chromophores which are not conjugated by identifying exciton coupling.[15] An exciton coupling occurs when two or more chromophores with similar excitation energies are in spatial proximity to each other. Because of their excitation energies, they cannot be excited independently, so each chromophores' excited state delocalizes over all chromophores within the system. This is known as an exciton. The excitons couple with one another resulting in a pair of intense absorbance bands with opposite signs in the CD spectrum, known as an exciton couplet, which corresponds to the transition wavelength of the chromophores.

When considering the folding of **NDI**-**AAN**, an exciton coupling will indicate a stacking interaction between the aromatic monomers. The charge transfer absorbance band in the visible spectrum for **NDI**-**AAN** at pH 7 suggests some degree of folding, so an exciton couplet was expected, too. At pH 0, the absence of a charge transfer absorbance band does not provide information about stacking, or lack of stacking, between aromatic monomers since **AANH^{+}** is no longer a donor and cannot participate in charge transfer. A protonated **AANH^{+}** is expected to stack with **NDI** much more weakly since both are electron-poor, so a weaker exciton couplet is expected.

The CD spectrum for **NDI**-**AAN** (200 μM) at pH 7 showed the expected exciton couplet at 225-245 nm (Figure 2-7). This supports the folded conformation necessary for the charge transfer event seen in the visible spectrum. The CD spectrum at pH 0 also shows an exciton couplet. This would suggest that **AANH^{+}** and **NDI** are also folding by a π-π stacking interaction. Even though the aromatic monomers are not expected to

interact in a donor-acceptor interaction, the exciton coupling indicates that they associate to some degree. ^{1}H NMR was used to evaluate this further.

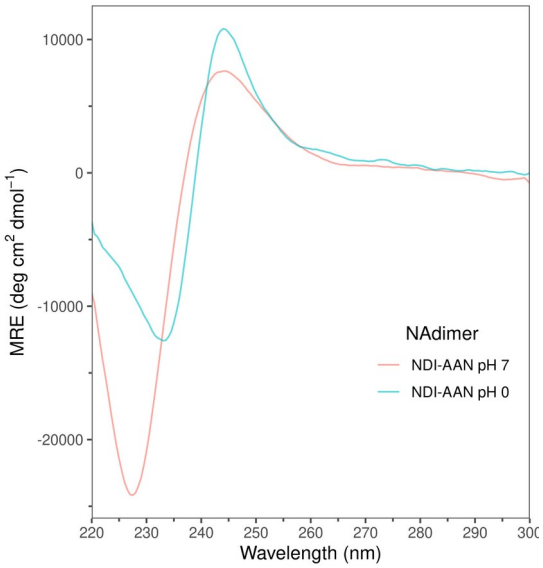

Figure 2-7. CD spectra of **NDI-AAN** (200 μM) in 50 mM potassium phosphate buffer, pH 7 (red), and 1 M sulfuric acid, pH 0 (blue), at 298 K.

^{1}H NMR characterization. ^{1}H-NMR spectroscopy is a powerful technique that can be used to characterize the stacking. By comparing the NMR spectra of **NDI-AAN** to the component monomer spectra, upfield shifting is observed for the aromatic signals of each monomer (Figure 2-8). The **AAN** monomer aromatic signals in the monomer peptide at pH 7 range from 6.60-7.77 ppm. The **AAN** signals at the same pH in the **NDI-AAN** dimer are upfield shifted to 5.91-7.05 ppm, a difference of ~ 0.7 ppm for the most upfield proton.

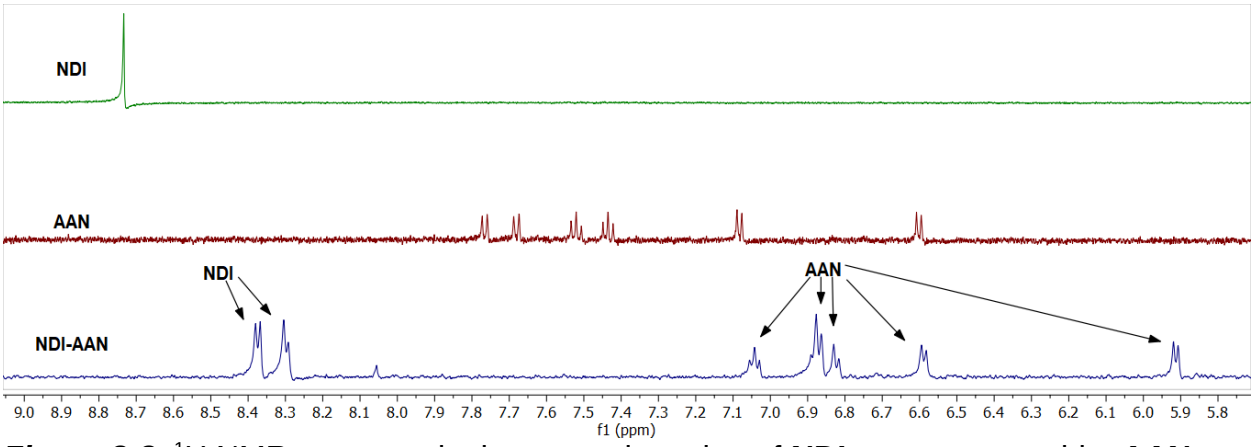

Figure 2-8. ^{1}H NMR spectrum in the aromatic region of **NDI** monomer peptide, **AAN** monomer peptide, and **NDI**-**AAN** in 50 mM potassium phosphate buffer, pH 7, at 298 K. All samples are at 100 μM. Note the upfield shifting of both the **NDI** and **AAN** signals.

The **NDI** aromatic signal in **NDI**-**AAN** at pH 7 is also upfield shifted in the dimer, indicating that it also experiences a significant difference in chemical environment due to stacking with **AAN**. In the aromatic monomer, the four aromatic protons are chemically identical appearing as a singlet at 8.74 ppm. In the dimer at pH 7, the four protons diverge into two sets of two equivalent protons appearing as two upfield shifted doublets at 8.30 and 8.38 ppm. The upfield shifting of all the aromatic protons across both **NDI** and **AAN** supports stacking rather than edge-to-face interactions. In edge-to-face interactions, an upfield shifting is still observed but only for the protons that are oriented into the quadrupole of an aromatic face. Upfield shifting of all aromatic protons is in agreement with the face-to-face orientations reported by Iverson in the characterization of the original DAN-NDI aedamer.[8]

The **NDI**-**AANH**$^{+}$ dimer spectrum at pH 0 also shows upfield shifting and two doublets for **NDI** (Figure 2-9). The aromatic signals of the **AANH**$^{+}$ monomer (7.19-8.51 ppm) are downfield shifted from the neutral **AAN** monomer signals (6.60-7.77 ppm) because the ammonium cation strongly deshields the ring by removing electron density. When stacked with **NDI** in the dimer, the aromatic signals for **AANH**$^{+}$ are shifted upfield

to 6.68-7.53 ppm, a difference of about 0.5 ppm for the most upfield proton. The **NDI** signals are shifted upfield from 8.74 ppm to 8.39 and 8.54 ppm, slightly less upfield shifted than at pH 7. This supports the stacking and folding of the aromatic surfaces even when no favorable donor-acceptor interactions are present.

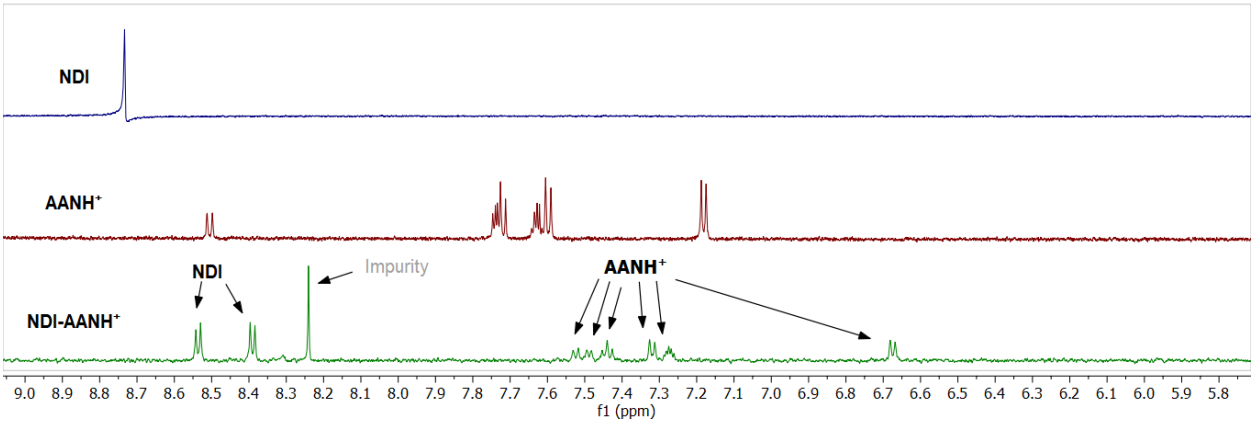

Figure 2-9. ^{1}H NMR spectrum in the aromatic region of **NDI**, **AANH^{+}**, and **NDI-AANH^{+}** in 1 M sulfuric acid solution, pH 0, at 298 K. All samples are at 100 μM. Note the upfield shifting of both the **NDI** and **AANH^{+}** signals.

Characterization Analysis. The UV-Vis and ^{1}H NMR for **NDI-AAN** data show that **AAN** is protonated at pH 0. This is shown by the blue shift in the UV spectrum, the loss of color in the visible spectrum, and the downfield shifting of the aromatic signals when **AAN** is protonated. However, the CD and ^{1}H NMR data also show that **AAN** cannot facilitate a conformational switch in a dimer alone as the **NDI-AANH^{+}** dimer still folds when protonated.

This stacking is not surprising in an aromatic dyad in water. Using NMR titration experiments to determine intermolecular binding energies, Iverson reported binding energies for both the optimal pair, **NDI/DAN**, and the non-optimal pairs, **DAN/DAN** and **NDI/NDI** (Table 2-2).

Table 2-2. Intermolecular binding energies in aqueous buffer for Iverson's aedamer.[7]

Dimer Pair	K_a (M^{-1})	ΔG (kcal/mol)
NDI/DAN	2045	-4.5
NDI/NDI	245	-3.3
DAN/DAN	20	-1.8

Each pair has a non-negligible *intermolecular* association in an aqueous environment, so the *intramolecular* stacking shown in the CD and ^{1}H NMR spectra for the **NDI**-**AANH$^+$** dimer peptide, which has a lower entropic cost due to increased effective molarity, is not surprising. Nonetheless, the magnitudes of the stacking interactions are all different. The non-optimal pairs, **DAN**/**DAN** and **NDI**/**NDI**, are 100- and 10-fold weaker, respectively, than the optimal pair **NDI**/**DAN**. Since we expect interactions with **AAN** to be of similar magnitude as those with **DAN**, this difference of strengths suggests that **AAN** can behave as a conformational switch but only when given the opportunity to form a new, more favorable interaction that is competitive with the **NDI**/**AANH$^+$** interaction. The **Gen 1** foldamer meets this requirement.

2.4 Evaluating Gen 1 as a pH-Sensitive Switchable Foldamer

To help characterize the **Gen 1** foldamer, each component dimer (Table 2-1) was synthesized and characterized along with **Gen 1** at both pH 7 and pH 0 using UV-Vis, CD, and ^{1}H-NMR.

UV-Vis characterization. The **NDI**-**DAN** dimer peptide has a visibly red color that matches the description from the original Iverson aedamer.[4] At millimolar concentrations, a charge transfer absorbance is present of 514 nm in both the pH 7 and pH 0 environments (Figure 2-10a). This is expected because neither **NDI** nor **DAN** is expected to be protonated in this pH range. The charge transfer absorbance for **NDI**-**DAN** supports the stacking conformation because donors and acceptors must be in

proximity for a charge transfer event to occur. Furthermore, no other change in the UV-vis spectrum was observed with a change in pH, supporting the fact that this interaction is unaffected by acid (Figure 2-10b).

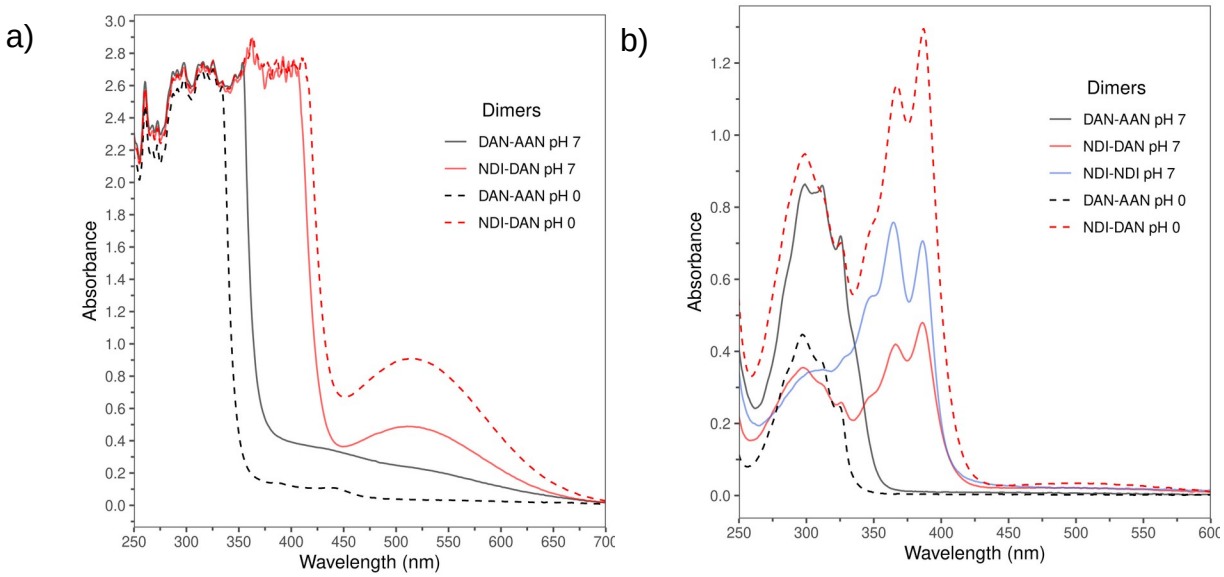

Figure 2-10. a) Visible (~ 2 mM) and b) UV (~ 30 μM) spectra for **NDI-DAN**, **NDI-NDI**, and **DAN-AAN** in 50 mM potassium phosphate buffer, pH 7, and 1 M sulfuric acid, pH 0, at 298 K.

The **DAN-AAN** dimer peptide is colorless in solution at both pH 7 and pH 0. At pH 7, the two electron-rich surfaces cannot participate in a donor-acceptor charge transfer that can be seen in the visible spectrum. The absorbance spectra overlap considerably, but the maxima for the individual monomers for **DAN** (λ_{max} 299 nm) and **AAN** (λ_{max} 312 nm) are different. At pH 0, **AANH$^+$** becomes electron-poor, but the dimer is still colorless. Donor-acceptor interactions rely on more than pairing of a donor and an acceptor; the energetics of the molecular orbital overlap must be in the visible range as described in Chapter One. The maximum at 312 nm shifts to shorter wavelengths at 297 nm at pH 0, however, as was observed for the **AAN** monomer, signifying protonation of **AAN**.

The **NDI**-**NDI** dimer peptide is also colorless at both pH 7 and pH 0. Two acceptors cannot participate in a charge transfer event, and no charge transfer absorbance was present at either pH. Furthermore, there was no change in the spectrum as **NDI** is not protonated at pH 0.

The **Gen 1** foldamer (Figure 2-11) has two distinct colors: black at pH 7 and red at pH 0. In the visible spectrum at pH 7, a charge transfer band (Figure 2-12a, black line) that matches the combined absorptions of **NDI**-**AAN** and **NDI**-**DAN** (Figure 2-12a, purple line) is seen spanning the length of the visible region, appearing as a black color. This is consistent with the sheet-like structure that was predicted at pH 7, with an internal **NDI**-**DAN** stack and a terminal **NDI**-**AAN** stack. At pH 0, the broad band is no longer present, but the **NDI**-**DAN** CT band is still present, resulting in a red color. In the UV region, the blue shift of **AAN** to **AANH**$^{+}$ is observed supporting the protonation of **AAN** as the stimulus for the color change (Figure 2-12b). This is consistent with the formation of the central **NDI**-**DAN** stack, but does not report on the folding of the **AAN** monomer and terminal **NDI** monomer. ^{1}H NMR was used to provide further information on the folding at pH 0 (*vide infra).*

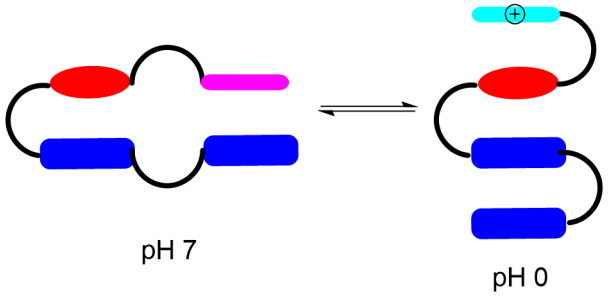

Figure 2-11. Schematic representation of **Gen 1** in its predicted folded structures for both pH 7 and 0.

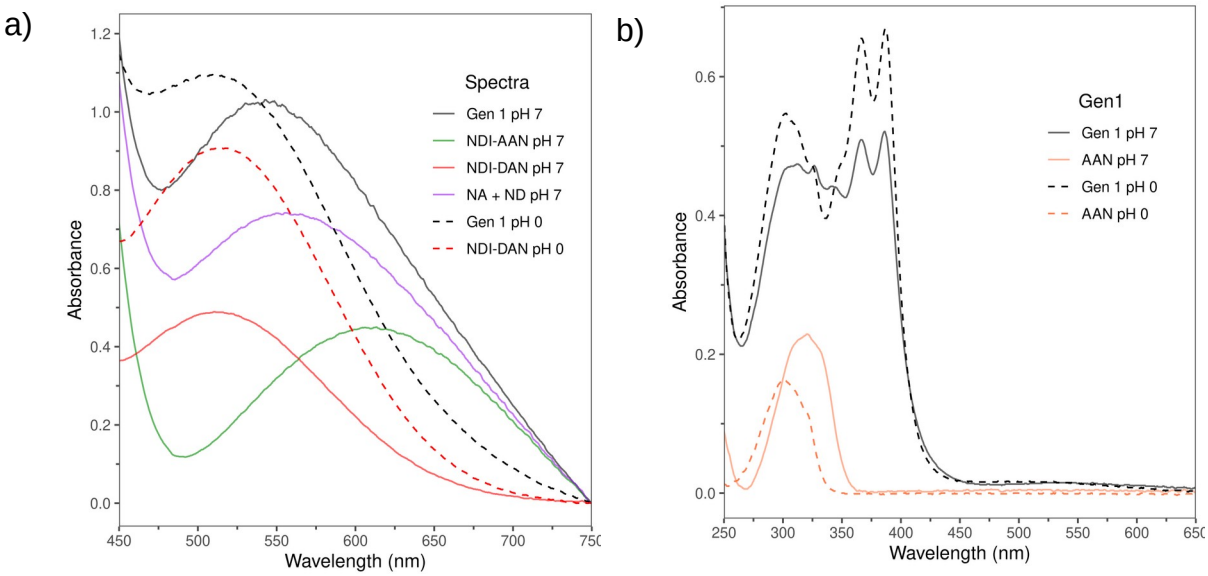

Figure 2-12. a) Visible spectra of **Gen 1**, **NDI-AAN**, and **NDI-DAN** (~ 2 mM) and b) UV spectra of **Gen 1** and **AAN** (~ 30 μM) in 50 mM potassium phosphate buffer, pH 7, and 1 M sulfuric acid, pH 0, at 298 K.

To verify that the observed charge transfer bands arise from intramolecular interactions, dilution experiments of **Gen 1** were conducted at pH 7 and 0 (Figure 2-13) in the relevant concentration range (1-2 mM). These studies show that the CT intensity is linear in this concentration range, confirming that the CT bands arise from intramolecular interactions, supporting a monomeric model of **Gen 1** at low millimolar concentrations.

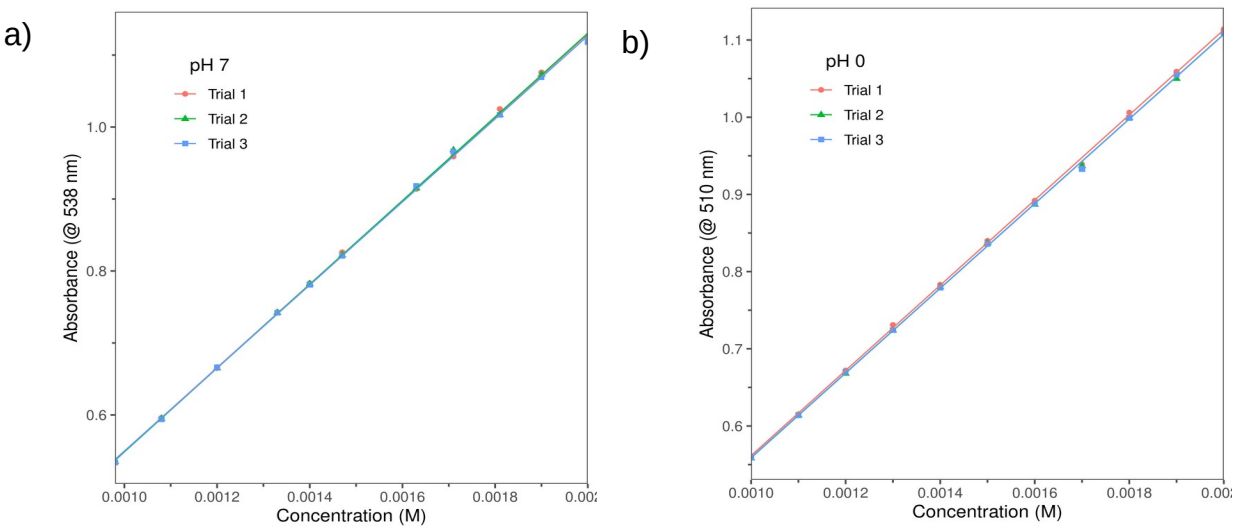

Figure 2-13. Plots from dilution experiments of **Gen 1** between 1-2 mM. a) pH 7, 50 mM potassium phosphate buffer, following 538 nm and b) pH 0, 1 M sulfuric acid solution, following 510 nm.

CD characterization. As with the **NDI-AAN** dimer, the other dimer peptides showed an exciton coupling between 220-250 nm at both pH 7 and 0 (Figure 2-14a). Because **NDI-AAN** and **NDI-DAN** are folded, it suggests the absorbance is characteristic of a folded dimer stack. Even dimers without a possible favorable donor-acceptor interaction have similar exciton couplets which supports a stacked association between tethered aromatic residues.

CD was employed to discern a change of the folded structure of the **Gen 1** foldamer at each pH (Figure 2-14b). The two spectra were different suggesting a change is conformation which supports the pH-sensitive responsive that was hypothesized for the system.

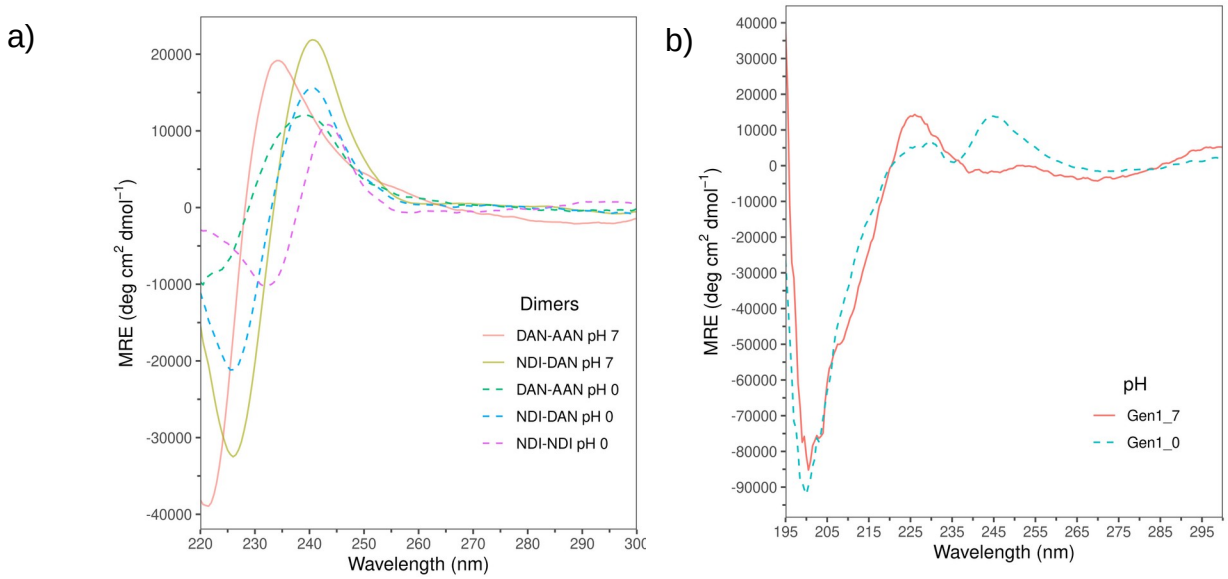

Figure 2-14. CD spectra in 50 mM potassium phosphate buffer, pH 7, and 1 M sulfuric acid solution, pH 0. a). Dimer peptides (200 μM): **DAN**-**AAN**, **NDI**-**DAN**, and **NDI**-**NDI** b). **Gen 1** (30 μM).

^{1}H NMR characterization. ^{1}H NMR was employed to characterize the folding of the relevant dimers and **Gen 1**. Upfield shifting was observed for the aromatic protons of each dimer peptide due to face-to-face stacking (Figure 2-15), similar to **NDI**-**AAN** which was previously discussed. The signals for the **NDI** monomer in **NDI**-**DAN** have a change in splitting pattern from singlet to a pair of doublets which is consistent with the stacking model in the literature.[8] This pattern matches the **NDI**-**AAN** spectrum suggesting the **NDI**-**AAN** dimer stacks similarly to the **NDI**-**DAN** dimer. The signals for the **NDI** monomers in the **NDI**-**NDI** dimer peptide have a change in splitting from singlet to three doublets. This supports that the two **NDI** monomers stack also stacking in a face-to-face orientation resulting in each proton experiencing the shielding from the adjacent **NDI**.

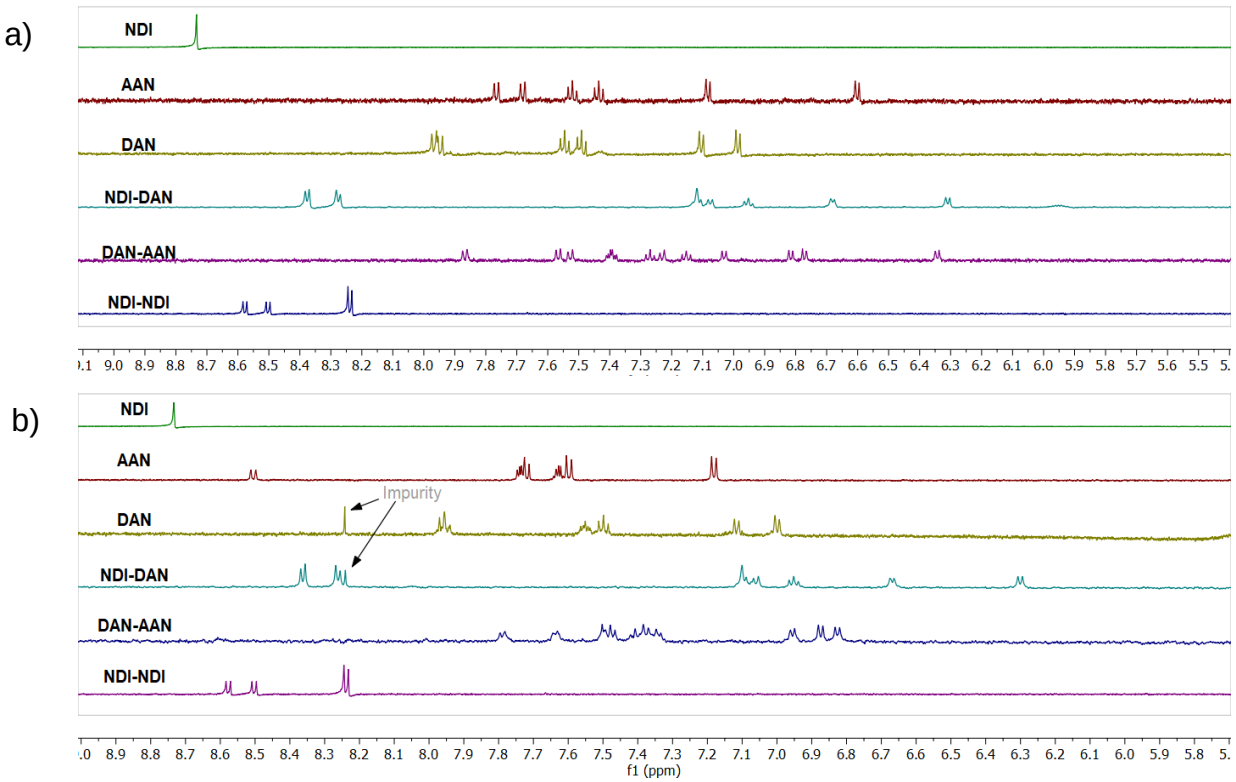

Figure 2-15. ^{1}H NMR spectra for the monomers (100 μM) **AAN**, **NDI**, **DAN**, and the dimers (100 μM) **NDI**-**DAN**, **DAN**-**AAN**, **NDI**-**NDI** in a) 50 mM potassium phosphate buffer, pH 7, at 298 K and b) 1 M sulfuric acid solution, pH 0, at 298 K.

For **Gen 1**, the signals were broad and unresolved at both pH 7 and 0, making it difficult to discern much other than the relative upfield shifting compared to the monomers and dimers. We expected that the peak broadening arose from intermediate exchange rates of the folded structure, since we had shown by UV-vis that the foldamer does not aggregate up to 2 mM.

Variable temperature NMR was used to explore this at pH 7 (Figure 2-16a) and pH 0 (Figure 2-16b). As the temperature was raised by 5 K for each step, the signals started to sharpen and resolve. At 318 K, the signals were well-resolved, but not significantly shifted, supporting intermediate rate exchange as the cause for the broad signals. The slower exchange rate in **Gen 1** relative to the dimers suggests that the

larger foldamer has an increased barrier to unfolding which may be a result of cooperativity from a larger NCN.

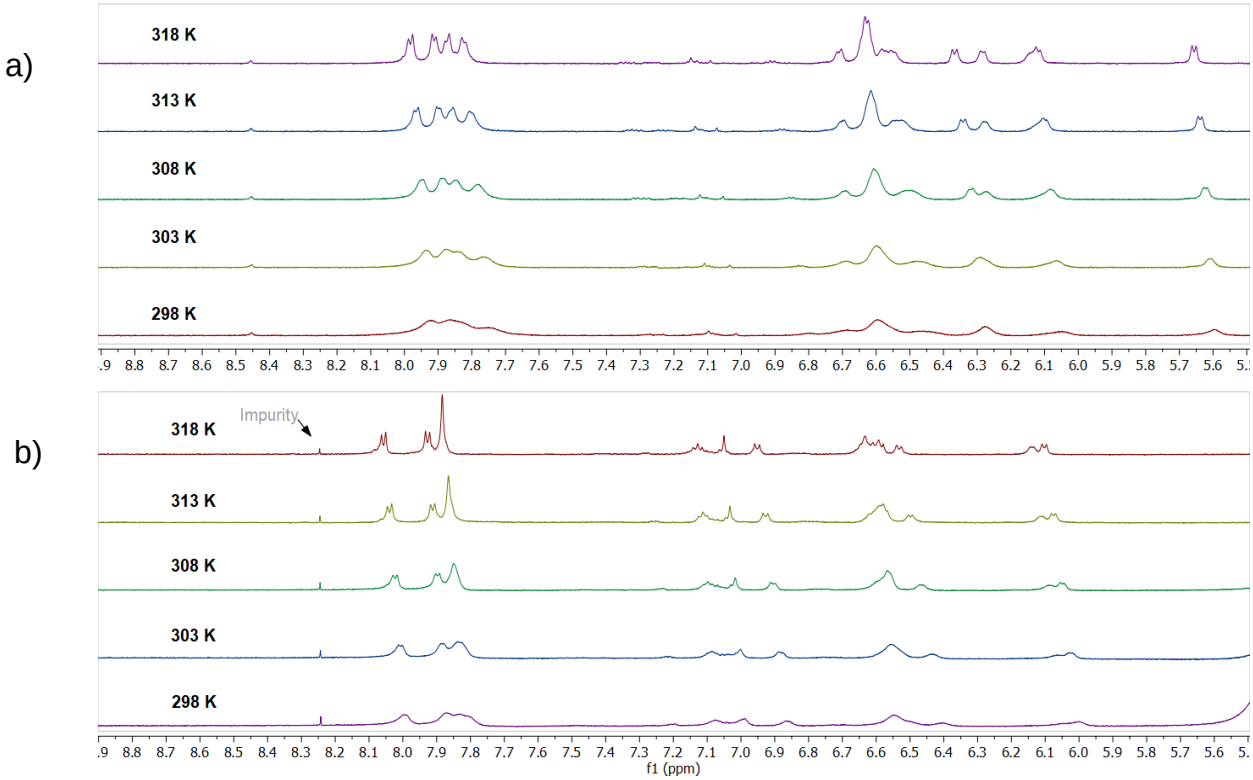

Figure 2-16. Variable Temp ^{1}H NMR for **Gen 1** (1 mM) in a) 50 mM potassium phosphate buffer, pH 7 and b) 1 M sulfuric acid solution, pH 0.

The **Gen 1** ^{1}H NMR spectrum exhibits greater upfield shifting than in the dimers in the spectra at both pH 7 and pH 0, as expected for a foldamer with two buried aromatic residues (Figure 2-17). The two **NDI** monomers in **Gen 1** also exhibit different splitting patterns between pH 7 and 0. At pH 7 and 318 K, the **NDI** region shows four doublets at 7.8-8.1 ppm. This is a cumulative pattern of the two doublets observed for both **NDI-AAN** and **NDI-DAN** which is consistent with a sheet-like conformation. At pH 0 and 318 K, the **NDI** region shows two doublets and a singlet. It appears that the singlet arises from coalescence of a pair of doublets that can be seen at lower temperatures, and may suggest a more dynamic terminal **NDI**.

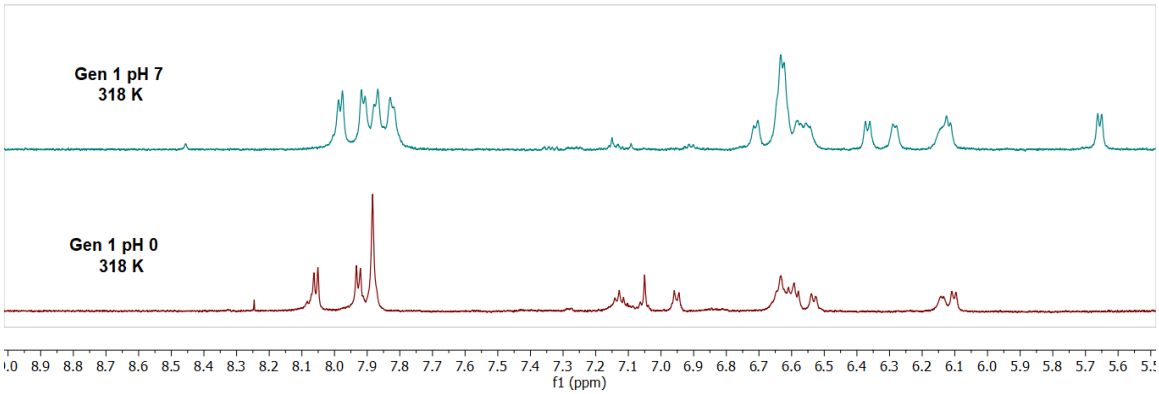

Figure 2-17. ^{1}H NMR spectra of the **Gen 1** foldamer (1 mM) at 318 K at a) pH 7 and b) pH 0.

Selective 1D NOESY (Nuclear Overhauser Effect Spectroscopy) experiments were used to help discern the conformation the foldamer is in at each pH. The nuclear Overhauser effect (NOE) arises when two nuclei have a through-space interaction. Selective NOESY experiments work by irradiating a target signal and observing the NOE signals that appear when the target proton interacts with another proton through-space. By choosing a specific signal, the NOE signals that appear can provide information on the conformation the foldamer is in. In the experiments with **Gen 1**, the entire **NDI** region was chosen to be irradiated for two reasons. First, it does not overlap with any signals from the other aromatic residues. Second, in the predicted folded conformations, the two **NDI** monomers stack with both **DAN** and **AAN** in the sheet-like structure at pH 7, but one stacks with **DAN** and the other with the internal **NDI** in the column at pH 0. Thus, for the predicted folded states, we would expect NOEs to both **DAN** and **AAN** at pH 7, but only to **DAN** at pH 0.

At pH 7, when the **NDI** protons were irradiated, NOE signals for the entire aromatic region appeared (Figure 2-18a) supporting interactions between one **NDI** and **DAN** and the other **NDI** and **AAN**. At pH 0, only part of the aromatic regions appeared as NOE signals, most notably the more upfield peaks, which correspond to **DAN** (Figure

2-18b). This suggests that the **AANH$^+$** and terminal **NDI** are not interacting in the folded conformation. These observations support a conformational change from sheet-like to columnar, but a discussion with respect to other possible structures is provided below. In summary, the 1D NOE experiments indicate that the **Gen 1** foldamer has an observable preference for one conformation over another at each pH.

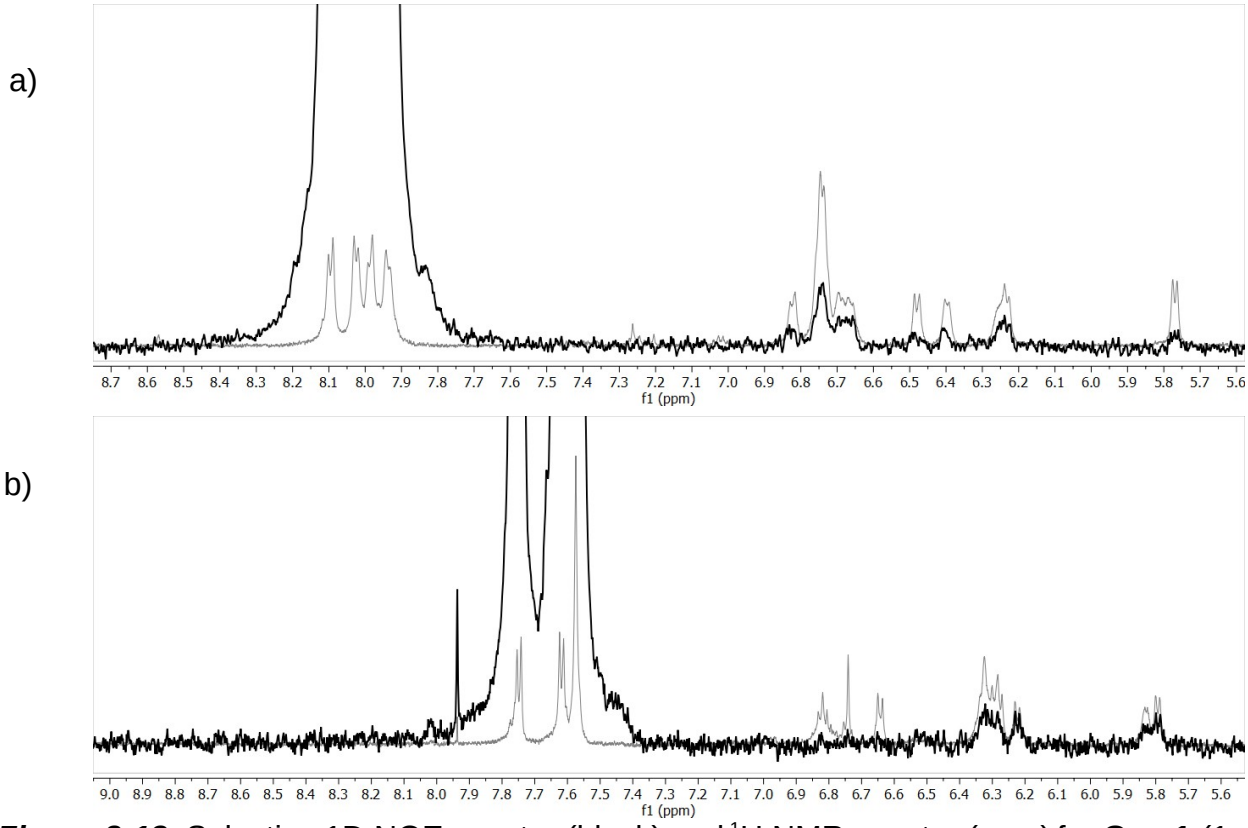

Figure 2-18. Selective 1D NOE spectra (black) and ^{1}H NMR spectra (gray) for **Gen 1** (1 mM) at 318 K in a) 50 mM potassium phosphate buffer, pH 7, irradiating 7.9-8.2 ppm and b) 1 mM sulfuric acid solution, pH 0, irradiating 7.5-7.8 ppm.

2.5 Discussion

The UV/Vis, CD, and ^{1}H NMR experiments described above demonstrate that the **Gen 1** foldamer results in a pH switch from a sheet-like conformation at pH 7 to a columnar structure at pH 0. The **Gen 1** foldamer has a visible response to a change in pH; a black color turns to red when the pH is lowered to 0. The dilution experiments show no aggregation in the system even at the highest concentration of 2 mM for the

visible absorbance experiments. Thus, the colors at each pH are from intramolecular charge transfer events. At pH 7, there is a charge band for **Gen 1** that matches the summation of the charge transfer bands of both **NDI**-**AAN** and **NDI**-**DAN** hence the black color. This is strong evidence that the foldamer is in the sheet-like conformation. At pH 0, there is a charge transfer that matches exactly with that of only **NDI**-**DAN** which is red in color. The color on its own is not enough to suggest a column because **NDI** and **AANH**$^{+}$ have been shown to associate by CD and ^{1}H NMR but do not result in a CT band.

The NMR experiments for **Gen 1** show intermediate exchange at 298 K evident by the broad signals in the spectra at both pH 7 and pH 0. The rate of exchange was increased by heating the samples to 318 K which sharpened and resolved the signals. This suggests the system is dynamic, which is expected for a non-covalent network because the aromatic stacking is not strong enough to lock one conformation over the another, or an unfolded state. However, the difference in exchange rates between the dimers, which give sharp peaks at 298 K, and the **Gen 1** system, indicate that there is a larger barrier in the **Gen 1** foldamer. Moreover, there is a perceivable preference for one folded state over the other at each pH. The selective NOE signals at pH 7 shows interactions between **NDI** and both **DAN** and **AAN** while the signals at pH 0 only show interactions between **NDI** and **DAN**. This supports preferences for a sheet-like conformation at pH 7 and a columnar conformation at pH 0.

The **Gen 1** foldamer is a multi-component, dynamic system that has other possible conformations. One possibility is the aggregation or higher order assembly of **Gen 1** resulting from intermolecular interactions between aromatic monomers. The dilution studies at both pH 7 and 0 confirm that the system is monomeric in structure,

and the observed response is from changes in intramolecular interactions. Other structures are possible by incomplete folding of the terminal monomers. The CT band (black color) and NOE signals observed at pH 7 supports a nontrivial population of the sheet-like conformational state. At pH 0, the CT band (red color) and NOE signals support the core **NDI**/**DAN** interaction is still present, but **AANH**$^+$ and terminal **NDI** could be unfolded. The dimer studies show that these monomers prefer to associate in a folded conformation rather than be exposed to the environment. Aggregation and partial folding are possible, but the evidence provides reasonable support for the predicted folded states at either pH.

At pH 0, the columnar structure is driven by two favorable donor-acceptor interactions, one between **AANH**$^+$ and **DAN** and one between **DAN** and **NDI**, as well as a less favorable stacking interaction between the two terminal **NDI** monomers which is considered the source of frustration (Figure 2-19). The combination of the **AANH**$^+$/**DAN** and **NDI**/**NDI** interactions in the columnar structure are more favorable than the **AANH**$^+$/**NDI** interaction that would be formed in the sheet-like structure. Nonetheless, the columnar structure contains a non-optimal/frustrated interaction due to a lack of a better stacking partner for the two **NDI** monomers.

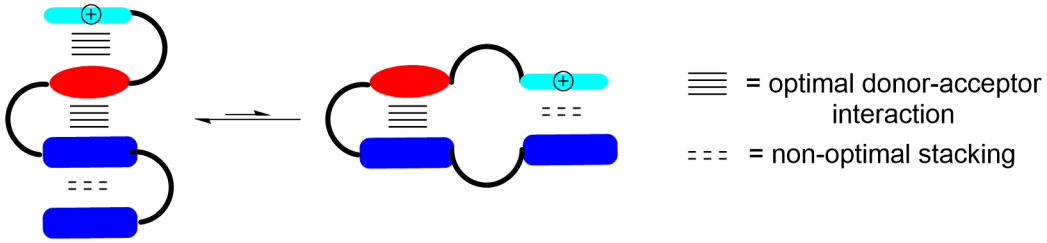

Figure 2-19. **Gen 1** conformers at pH 0: columnar structure (left) and sheet-like structure (right).

At pH 7, the sheet-like structure is driven by the relatively strong donor-acceptor interactions between each **NDI** with **DAN** and **AAN** (Figure 2-20). These two stacking

interactions are more favorable than the combination of donor-donor (**AAN**/**DAN**), donor-acceptor (**DAN**/**NDI**), and acceptor-acceptor (**NDI**/**NDI**) interactions that would exist in a columnar structure at pH 7. However, this conformation exposes more surface area to the aqueous environment than the columnar structure, so this is a source of frustration in the sheet-like structure.

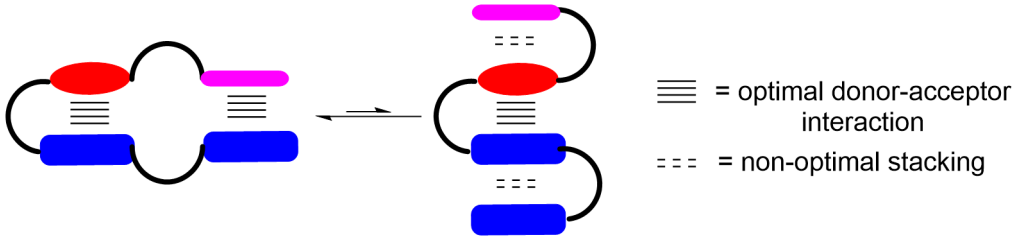

Figure 2-20. **Gen 1** conformers at pH 7: sheet-like structure (left) and columnar structure (right).

In summary, each folded state has a set of dominant noncovalent interactions and a site of frustration. These frustrated sites can be described as storing latent free energy – given the right stimulus, the frustration is relieved, and these sites can create new noncovalent interactions. The protonation state of **AAN** changes the energy landscape, changing the balance of powers between the two different sets of noncovalent interactions that contribute to each folded state, and the system responds by changing its preferred conformation.

In conclusion, we have designed and characterized a new stimulus-responsive foldamer using the concept of frustration as a design principle to achieve a switch between two folded states. Key lessons from this system are that frustration must be incorporated into both folded states, and that by doing so, the stimulus does not only turn “off” some noncovalent interactions, leading to unfolding, but turns on new ones, leading to reorganization to a new lowest energy state (Figure 2-21). This differs from early molecular machines, such as the rotaxane based systems, in which introduction of

a stimulus weakened one interaction, resulting in switching to the “second best” binding site, without changing its stability. This foldamer design is biomimetic, not so much in its structure but in its ability to adopt two different folded states in response to a stimulus and in the conceptual principles of frustration and latent free energy of which it is based. We expect that this conceptual framework will open up new approaches to the design of stimulus-responsive materials.

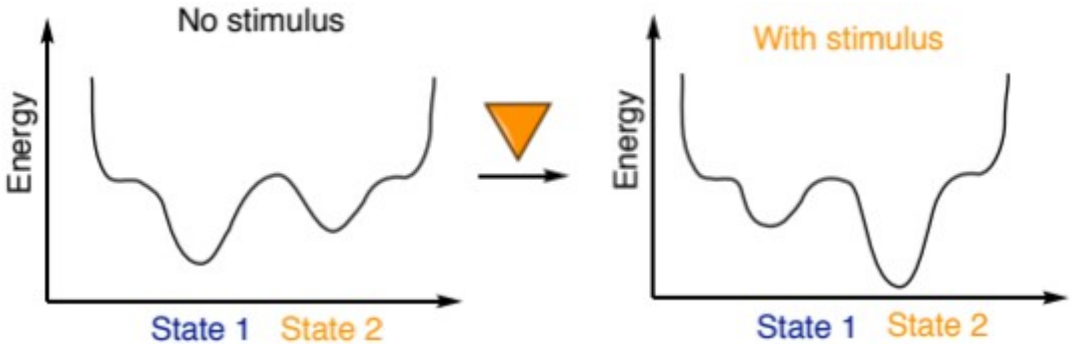

Figure 2-21. A representative change in the lowest energy state when a stimulus is introduced.

2.6 Experimental Section

Methods and Materials

General: Proton and carbon nuclear magnetic resonance spectra (^{1}H NMR and ^{13}C NMR) were recorded on a Bruker model Avance NEO 400 (^{1}H NMR at 400 MHz and ^{13}C NMR at 101 MHz) or a Bruker Avance III 600 (^{1}H NMR at 600 MHz and ^{13}C NMR at 151 MHz) spectrometer with solvent resonance (^{1}H NMR: $CDCl_3$ at 7.26 ppm and DMSO-d_6 at 2.50 ppm; ^{13}C NMR: $CDCl_3$ at 77.16 ppm and DMSO-d_6 at 39.52) or tetramethylsilane (TMS) as the internal standard. ^{1}H NMR data are reported as follows: chemical shift, multiplicity (s = singlet, br s = broad singlet, d = doublet, t = triplet, q = quartet, dd = doublet of doublets, td = triplet of doublets, ddd = doublet of doublet of doublets, ddt = doublet of doublet of triplets, m = multiplet), coupling constant (Hz), and integration. Mass spectra were obtained using a ThermoScientific Q Exactive HF-X mass spectrometer with electrospray introduction and external calibration. All samples were prepared in acetonitrile or methanol. Purification of the reaction products was carried out by manual flash column chromatography using Siliaflash-P60 silica gel (40-63 μm) purchased from Silicycle. A Biotage instrument with a refillable normal phase silica column was also used for purification of reaction products. A Biotage Initiator microwave reactor was used for reactions with microwave irradiation. Unless otherwise noted, all reactions were carried out under an atmosphere of dry nitrogen in flame-dried glassware with magnetic stirring. Reactions held at reflux were equipped with a water-cooled reflux condenser. Yield refers to isolated yield of pure material unless otherwise noted.

All chemicals were used as purchased unless otherwise noted. All chemicals purchased from Acros, Fisher Scientific, Oakwood Chemical Co., Sigma-Aldrich, Chem

Impex, NovaBioChem, and P3 Biosystems. Tetrahydrofuran (THF), diethyl ether (Et_2O), methylene chloride (DCM), toluene (PhMe), dimethylformamide (DMF), and triethylamine (NEt_3) were dried by passage through a column of neutral alumina under nitrogen prior to use. Deuterated solvents were purchased from Cambridge Isotope Laboratories and were stored over 3 Å molecular sieves.

Peptide samples for UV-Vis, CD, and ^{1}H NMR were made at two pHs: 50 mM potassium phosphate buffer, pH 7, and 1 M sulfuric acid solution, pH 0. Proton magnetic resonance spectra (^{1}H NMR) were recorded on a Bruker Avance III 600 (^{1}H NMR at 600 MHz) spectrometer with solvent resonance (^{1}H NMR: sodium trimethylsilylpropanesulfonate (DSS) at 0.00 ppm) as the internal standard. Samples were made using potassium dideuterophosphate (KD_2PO_4), deuterated sulfuric acid (D_2SO_4), deuterium oxide (H_2O), and potassium deuteroxide (KOD). NMR samples were made in 3 mm tubes. Before each sample was run, the pulse calibration (P1) was determined and the mixing time (d8) was set to 0.3 ms. Each sample was run using water suppression with a presaturation frequency of 4.9 Hz.

Circular dichroism (CD) spectroscopy was performed using an Applied Photophysics Chirascan. The mean residue ellipticity (MRE) was calculated using eq 1, where θ is MRE, *signal* is CD signal, *l* is path length, c is concentration, and *r* is the number of amino acid residues. A quartz cuvette with a path length of 0.1 cm was used to correct spectra.

$$\theta = \frac{signal}{10 * l * c * r} \qquad (1)$$

UV-Vis spectroscopy was performed on a ThermoFisher NanoDrop One with 80 µL samples in a quartz cuvette with a path length of 1 cm.

All chemicals were used as purchased unless otherwise noted. All chemicals purchased from Acros, Fisher Scientific, Oakwood Chemical Co., Sigma-Aldrich, Chem Impex, NovaBioChem, CEM, and P3 Biosystems. Deuterated chemicals were purchased from Cambridge Isotope Laboratories.

Peptide Synthesis. All peptides were synthesized on a CEM Liberty Blue peptide synthesizer using standard Fmoc-protected amino acids and Alloc-protected monomer amino acids on CEM Rink Amide ProTide LL resin (0.2 mmol/g). The amino acid residues (5 equivalents of Fmoc-protected amino acids and 2 equivalents of Alloc-protected amino acids) were activated with 5 equivalents of Oxyma (Ethyl cyanohydroxyiminoacetate) and 10 equivalents of DIC (N,N'-Diisopropylcarbodiimide) were used for each coupling step. One coupling cycle of 4 minutes was performed at 90 °C in DMF (dimethylformamide) for each residue. Deprotection of Fmoc was carried out in 20% piperidine in DMF, twice for 1 minute each. Deprotection of Alloc was carried out in a peptide synthesis flask with 0.3 equivalents of tetrakis(triphenylphosphine)palladium(0) and 6 equivalents of diphenylsilane in DCM (10 mL), three for 15 minutes each. The resin was washed with DMF before every Fmoc deprotection and coupling cycle. Peptides were cleaved from the resin with 95:2.5:2.5 trifluoroacetic acid (TFA):water:triisopropylsilane for 3 hours. Crude peptide materials were purified by reverse phase HPLC using C18 XBridge 5 µm column (Waters) with solvent A as 95:5 water:acetonitrile, 0.1% TFA and solvent B as 95:5 acetonitrile:water, 0.1% TFA. The purified peptides were lyophilized, and identity was confirmed by ESI-LCMS.

Experimental Procedures

Dialkoxynaphthalene (DAN)

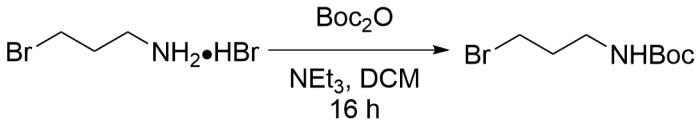

***tert*-Butyl (3-bromopropyl)carbamate:** This compound was synthesized by following a literature procedure.[8] A round bottom flask was charged with 3-bromopropan-1-amine hydrobromide (20.00 g, 91.36 mmol, 1 equiv), Boc_2O (19.94 g, 91.36 mmol, 1 equiv), and DCM (250 mL). The reaction mixture was cooled to 0 °C in an ice water bath. NEt_3 (12.7 mL, 91.36 mmol, 1 equiv) was slowly added via syringe. The reaction mixture was stirred at rt for 16 h. The organic phase was washed with 5 % aq. sodium bicarbonate (3 × 100 mL) and brine (3 × 100 mL), dried over sodium sulfate, filtered, and concentrated *in vacuo* to provide the product as a yellow oil which was used in the next step without further purification (21 g, 91 mmol, quant.), and the acquired ^{1}H NMR spectrum is consistent with the literature spectrum.

Analytical data: **^{1}H NMR** (400 MHz, $CDCl_3$) δ 4.95 (t, *J* = 6.2 Hz, 1H), 3.35 (t, *J* = 6.5 Hz, 2H), 3.17 (q, *J* = 6.4 Hz, 2H), 1.96 (p, *J* = 6.5 Hz, 2H), 1.35 (s, 9H).

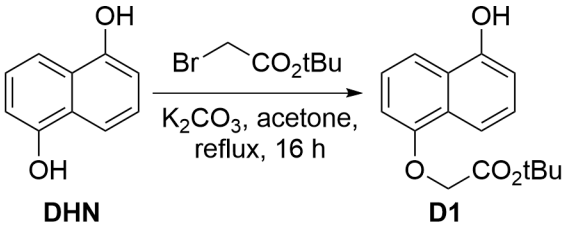

***tert*-Butyl 2-((5-hydroxynaphthalen-1-yl)oxy)acetate (D1):** This compound was synthesized using a modified literature procedure for a similar compound.[8] A round bottom flask equipped with a reflux condenser was charged with **DHN** (4.93 g, 30.8

mmol, 2 equiv), K_2CO_3 (5.31 g, 38.4 mmol, 2.5 equiv), and acetone (150 mL). The reaction mixture was purged with N_2 for 30 min. *tert*-butyl bromoacetate (2.27 mL, 15.4 mmol, 1 equiv) was added, and the reaction mixture was refluxed for 16 h. The reaction was cooled to rt, and the solvent was removed *in vacuo*. The crude residue was suspended in DCM (200 mL, filtered over Celite, and rinsed with DCM (100 mL). The solvent was removed *in vacuo*, and the crude residue (TLC of the mixture of **DHN** (R_f = 0.2), **D1** (R_f = 0.2), and bis-alkylated product (R_f = 0.8) in 20 % EtOAc/hexane) was purified on silica by flash column chromatography (0-5 % methanol/DCM) to provide **D1** as a yellow solid (1.77 g, 6.45 mmol, 42 %).

Analytical data: **^{1}H NMR** (400 MHz, $CDCl_3$) δ 7.96 – 7.88 (m, 1H), 7.77 (dd, *J* = 8.6, 1.0 Hz, 1H), 7.32 (dd, *J* = 8.5, 7.7 Hz, 1H), 7.24 (dd, *J* = 8.5, 7.5 Hz, 1H), 6.79 (dd, *J* = 7.5, 1.0 Hz, 1H), 6.73 – 6.67 (m, 1H), 4.70 (s, 2H), 1.51 (s, 9H); **^{13}C NMR** (101 MHz, $CDCl_3$) δ 168.30, 153.53, 151.20, 126.84, 125.45, 125.43, 124.66, 114.88, 114.66, 109.48, 105.38, 82.62, 77.34, 77.02, 76.71, 65.98, 28.06; **HRMS (ESI$^-$)** Calcd. for [$C_{16}H_{17}O_4^-$] ([M-H]): 273.11, Found: 273.1134; **TLC** (EtOAc/Hex = 20/80): R_f = 0.2.

^{1}H NMR Spectrum of D1

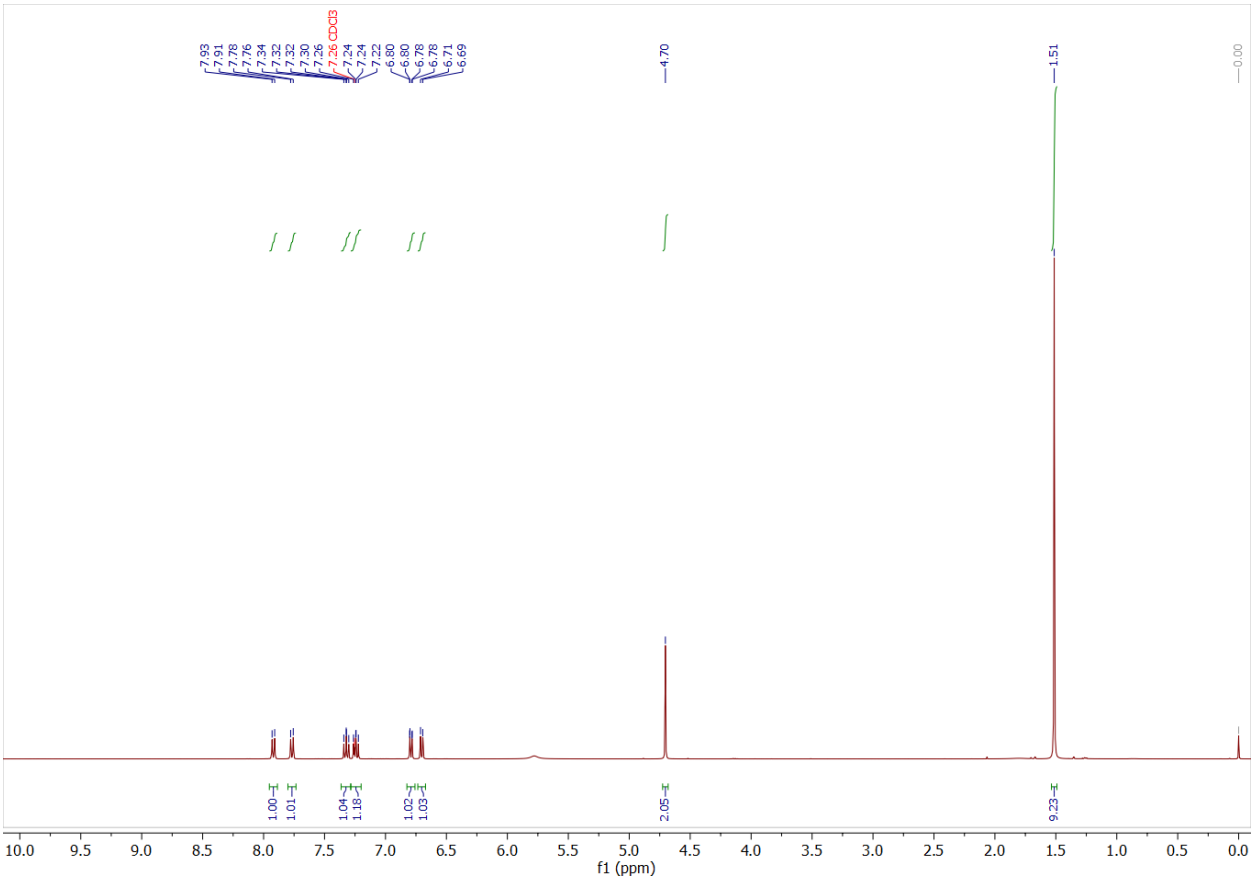

^{13}C NMR Spectrum of D1

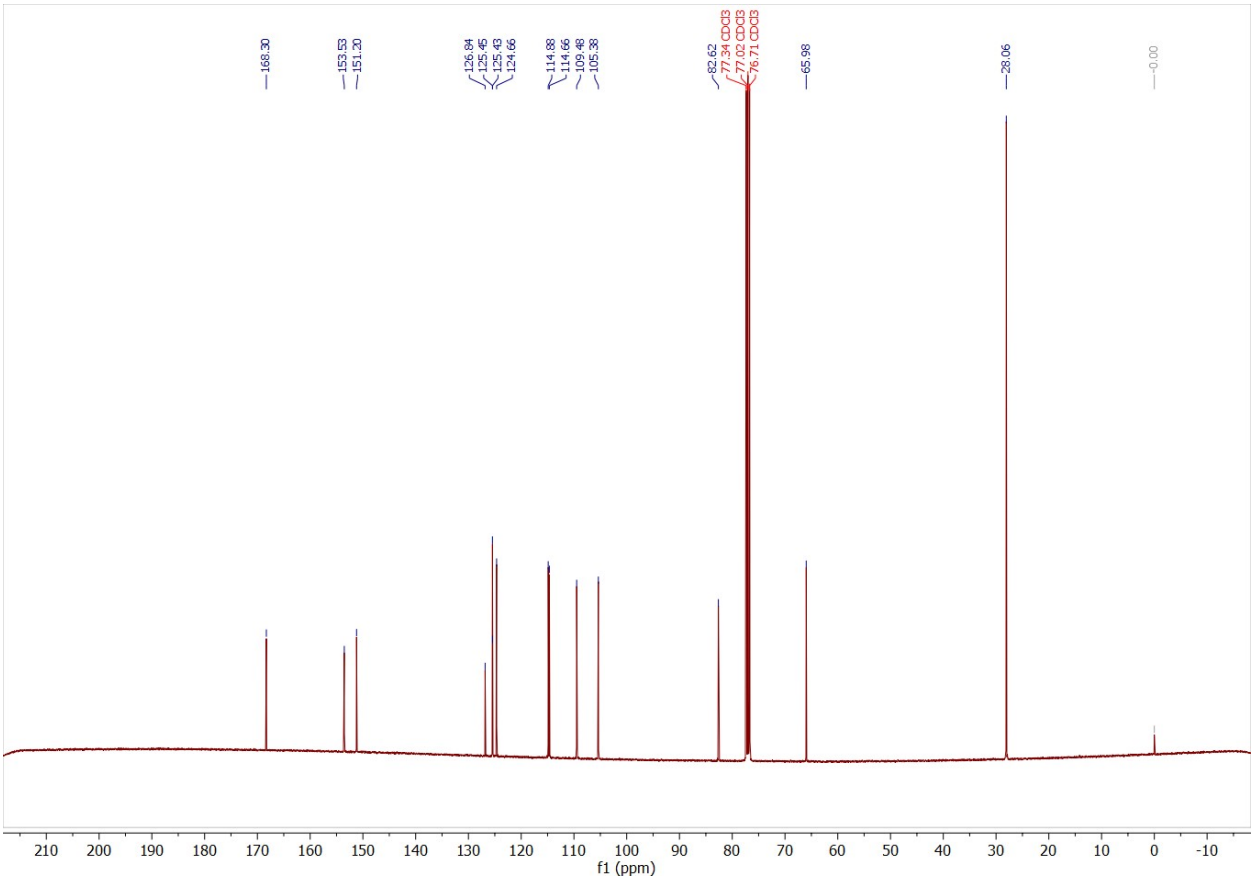

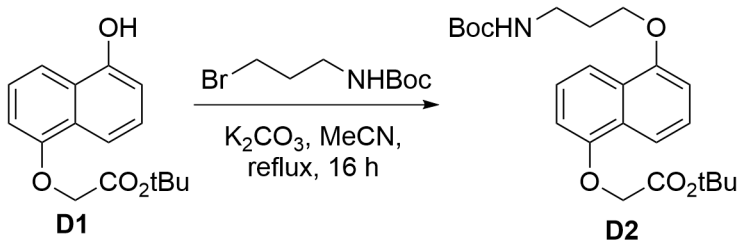

***tert*-Butyl 2-((5-(3-((*tert*-butoxycarbonyl)amino)propoxy)naphthalen-1-yl)oxy)acetate (D2):** This compound was synthesized using a modified literature procedure for a similar compound.[8] A round bottom flask equipped with a reflux condenser was charged with **D1** (1.77 g, 6.45 mmol, 1 equiv), *tert*-butyl (3-bromopropyl)carbamate (2.30 g, 9.68 mmol, 1.5 equiv), K_2CO_3 (2.23 g, 16.1 mmol, 2.5

equiv), and MeCN (30 mL). The reaction mixture was purged with N_2 for 30 min. The reaction mixture was refluxed for 16 h. The reaction was cooled to rt, and the solvent was removed *in vacuo*. The crude residue was suspended in DCM (100 mL), filtered over Celite, and rinsed with DCM (20 mL). The solvent was removed *in vacuo*, and the crude residue was purified on silica by flash column chromatography (40-100 % DCM/hexane, then 0-10 % methanol/DCM) to provide **D2** as a tan solid (1.64 g, 3.80 mmol, 58 %).

Analytical data: **^{1}H NMR** (400 MHz, $CDCl_3$) δ 7.95 (dt, *J* = 8.5, 0.9 Hz, 1H), 7.86 (dt, *J* = 8.6, 0.9 Hz, 1H), 7.36 (ddd, *J* = 18.1, 8.5, 7.6 Hz, 2H), 6.85 (dd, *J* = 7.7, 0.9 Hz, 1H), 6.73 (dd, *J* = 7.8, 0.9 Hz, 1H), 4.90 (s, 1H), 4.69 (s, 2H), 4.19 (t, *J* = 5.8 Hz, 2H), 3.43 (q, *J* = 6.3 Hz, 2H), 2.12 (p, *J* = 6.2 Hz, 2H), 1.50 (s, 9H), 1.44 (s, 9H); **^{13}C NMR** (101 MHz, $CDCl_3$) δ 167.94, 156.00, 154.13, 153.55, 126.63, 126.61, 125.40, 124.85, 115.07, 114.58, 105.68, 105.42, 82.34, 79.18, 77.34, 77.02, 76.70, 66.14, 66.09, 38.34, 29.49, 28.40, 28.05; **HRMS (ESI$^-$)** Calcd. for [$C_{24}H_{32}NO_6^-$] ([M-H]): 430.22, Found: 430.2237; **TLC** (MeOH/DCM) = 5/95): R_f = 0.2.

^{1}H NMR Spectrum of D2

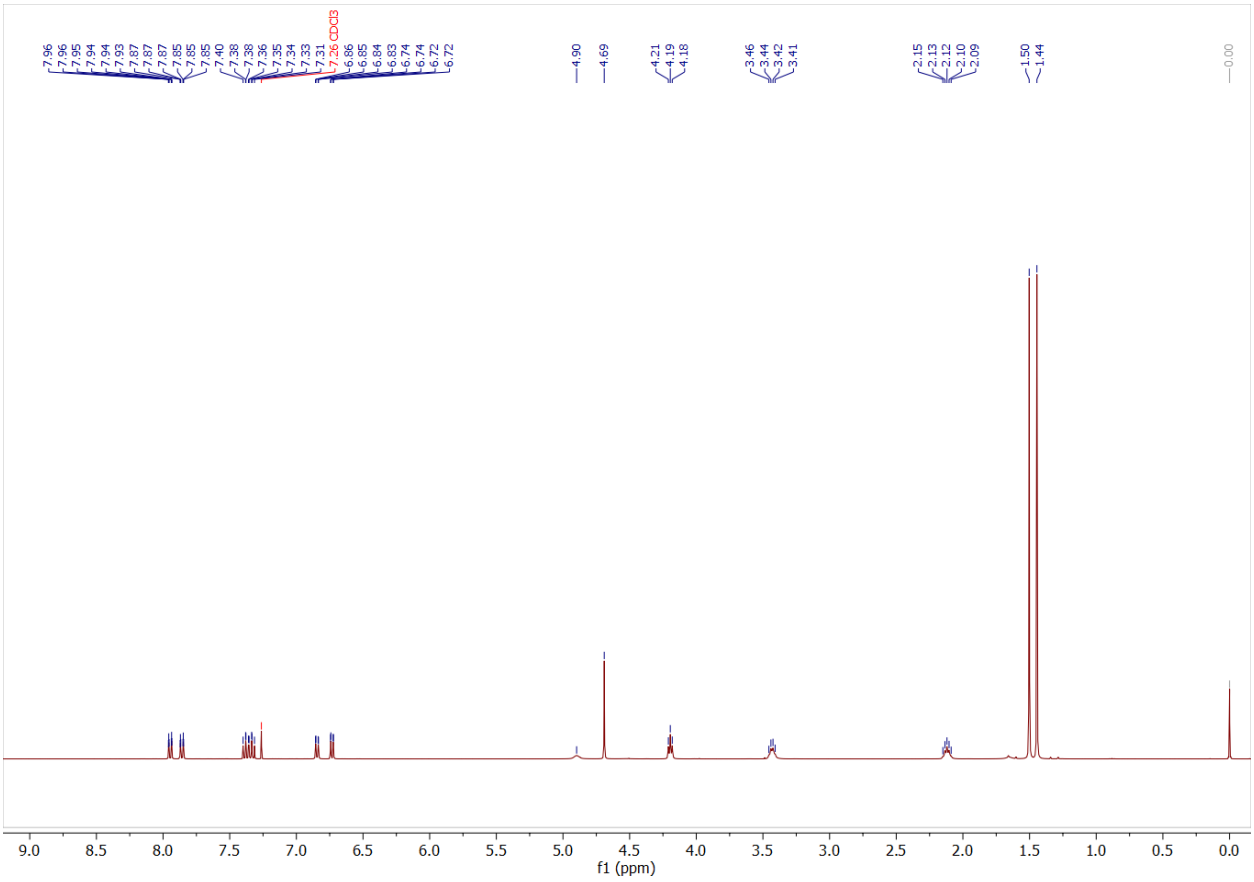

^{13}C NMR Spectrum of D2

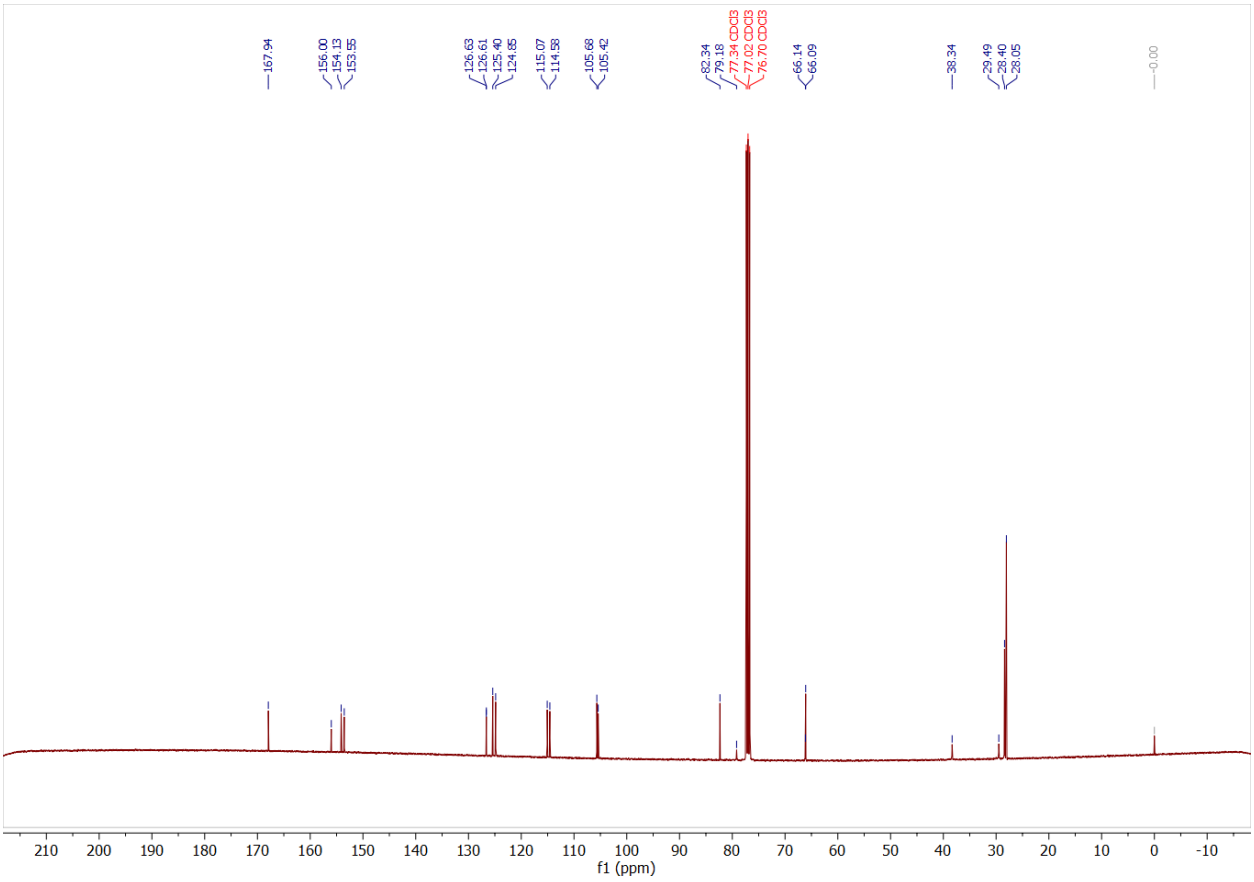

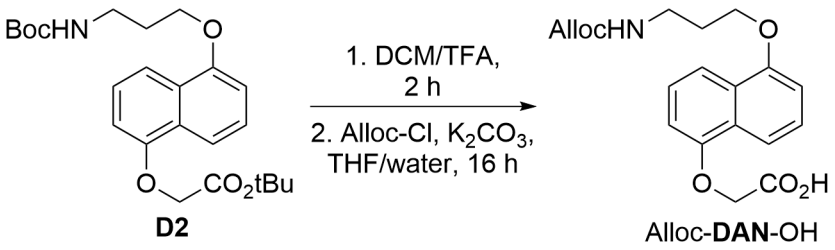

2-((5-(3-(((allyloxy)carbonyl)amino)propoxy)naphthalen-1-yl)oxy)acetic acid (Alloc-**DAN**-OH**):** A round bottom flask was charged with **D2** (1.64 g, 3.80 mmol, 1 equiv), DCM (10 mL), and TFA (10 mL). The reaction solution was stirred at rt for 2 h. The solvent was removed *in vacuo* and azeotroped with toluene (2 × 50 mL) and heptane. The residue and K_2CO_3 (2.63 g, 19.0 mmol, 5 equiv) were dissolved in water (20 mL),

and THF (10 mL) was added. A solution of Alloc-Cl (444 µL, 4.18 mmol, 1.1 equiv) in THF (10 mL) was added in one portion. The reaction mixture was stirred at rt for 16 h. The reaction was quenched with 1 M HCl (50 mL). The aqueous phase was extracted with DCM (3 × 50 mL). The organic layers were combined and washed with 1 M HCl (50 mL) and brine (50 mL), dried over sodium sulfate, filtered, and concentrated *in vacuo* to provide Alloc-**DAN**-OH as a tan solid (1.19 g, 3.31 mmol, 87 %).

Analytical data: **^{1}H NMR** (600 MHz, DMSO-*d*6) δ 7.76 (dd, *J* = 11.4, 8.5 Hz, 2H), 7.39 (dt, *J* = 21.2, 8.1 Hz, 2H), 7.00 – 6.96 (m, 1H), 6.90 (d, *J* = 7.7 Hz, 1H), 5.90 (ddt, *J* = 17.3, 10.6, 5.3 Hz, 1H), 5.27 (dt, *J* = 17.3, 1.8 Hz, 1H), 5.16 (dq, *J* = 10.5, 1.6 Hz, 1H), 4.87 (s, 2H), 4.46 (dd, *J* = 5.4, 1.6 Hz, 2H), 4.16 (t, *J* = 6.0 Hz, 2H), 3.26 (q, *J* = 6.5 Hz, 2H), 1.99 (p, *J* = 6.5 Hz, 2H); **^{13}C NMR** (151 MHz, DMSO) δ 170.56, 156.47, 154.36, 153.54, 134.31, 126.49, 126.29, 126.07, 125.68, 117.37, 115.21, 114.64, 114.13, 106.37, 106.24, 65.85, 65.64, 65.41, 65.30, 64.77, 64.66, 40.49, 40.37, 40.23, 40.09, 39.95, 39.81, 39.67, 39.53, 37.94, 29.65, 15.65; **HRMS (ESI^{+})** Calcd. for $[C_{19}H_{21}NO_6Na]^{+}$ ([M+Na]): 382.13, Found: 382.1266.

^{1}H NMR Spectrum of Alloc-**DAN**-OH

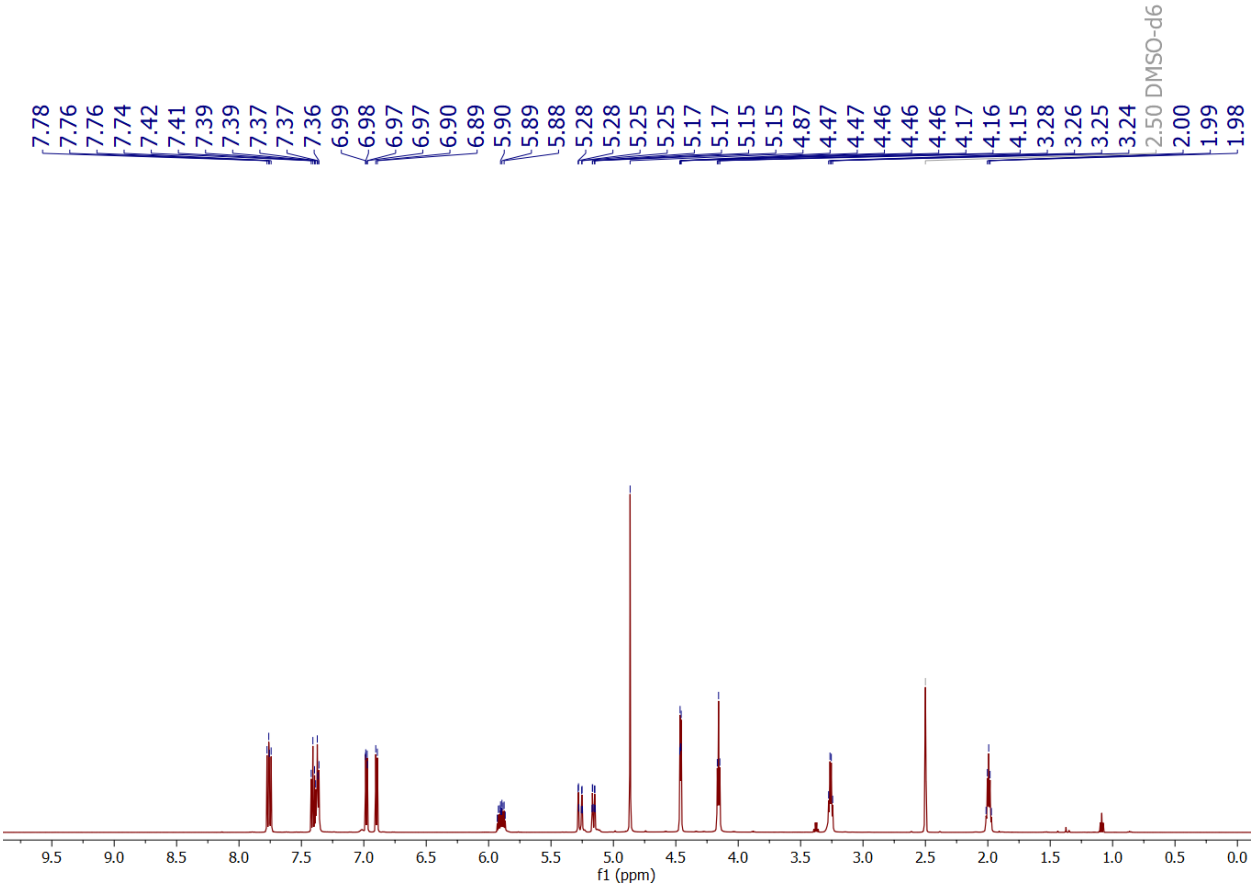

^{13}C NMR Spectrum of Alloc-**DAN**-OH

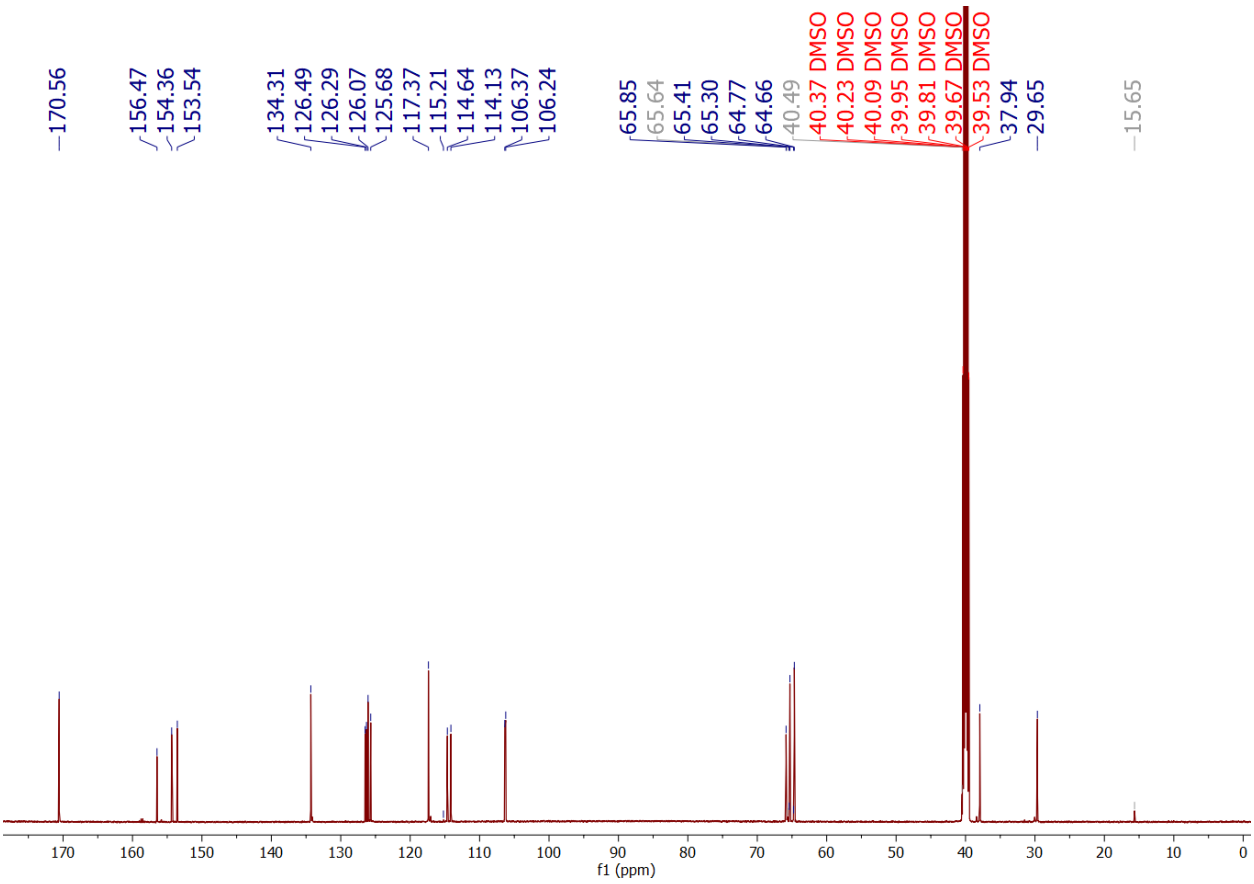

Naphthalenediimide (NDI)

Allyl *tert*-butyl butane-1,4-diyldicarbamate: A round bottom flask was charged with *tert*-butyl (4-aminobutyl)carbamate (4.8 mL, 25 mmol, 1.1 equiv), NEt_3 (3.5 mL, 25 mmol, 1.1 equiv), and DCM (50 mL). The reaction solution was cooled using an ice water bath. While stirring in an ice water bath, allyl chloroformate (2.5 mL, 23 mmol, 1 equiv) was slowly added via syringe. Upon complete addition, the reaction flask was removed from the ice water bath and stirred for 2 h. The reaction solution was diluted

with additional DCM (100 mL), washed with 5 % aq. acetic acid (50 mL), water (50 mL), and brine (50 mL), dried over sodium sulfate, filtered, and concentrated *in vacuo* to provide the product as a white solid which was use used in the next step without further purification (6.3 g, 23 mmol, quant.).

Analytical data: **^{1}H NMR** (600 MHz, $CDCl_3$) δ 5.90 (ddt, *J* = 16.4, 10.8, 5.6 Hz, 1H), 5.24 (dd, *J* = 55.0, 13.8 Hz, 2H), 4.85 (s, 1H), 4.59 (s, 1H), 4.54 (d, *J* = 5.6 Hz, 2H), 3.19 (q, *J* = 6.3 Hz, 2H), 3.11 (t, *J* = 6.2 Hz, 2H), 1.51 (dt, *J* = 8.2, 4.2 Hz, 4H), 1.42 (s, 9H); **^{13}C NMR** (151 MHz, $CDCl_3$) δ 156.42, 156.13, 133.05, 117.74, 79.30, 65.86, 65.57, 41.43, 40.76, 40.25, 28.52, 27.48, 27.38; **HRMS (ESI^{+})** Calcd for $[C_{13}H_{24}N_2O_4Na]^{+}$ ([M+Na]): 295.16, Found: 295.1637.

^{1}H NMR Spectrum of Allyl *tert*-butyl butane-1,4-diyldicarbamate

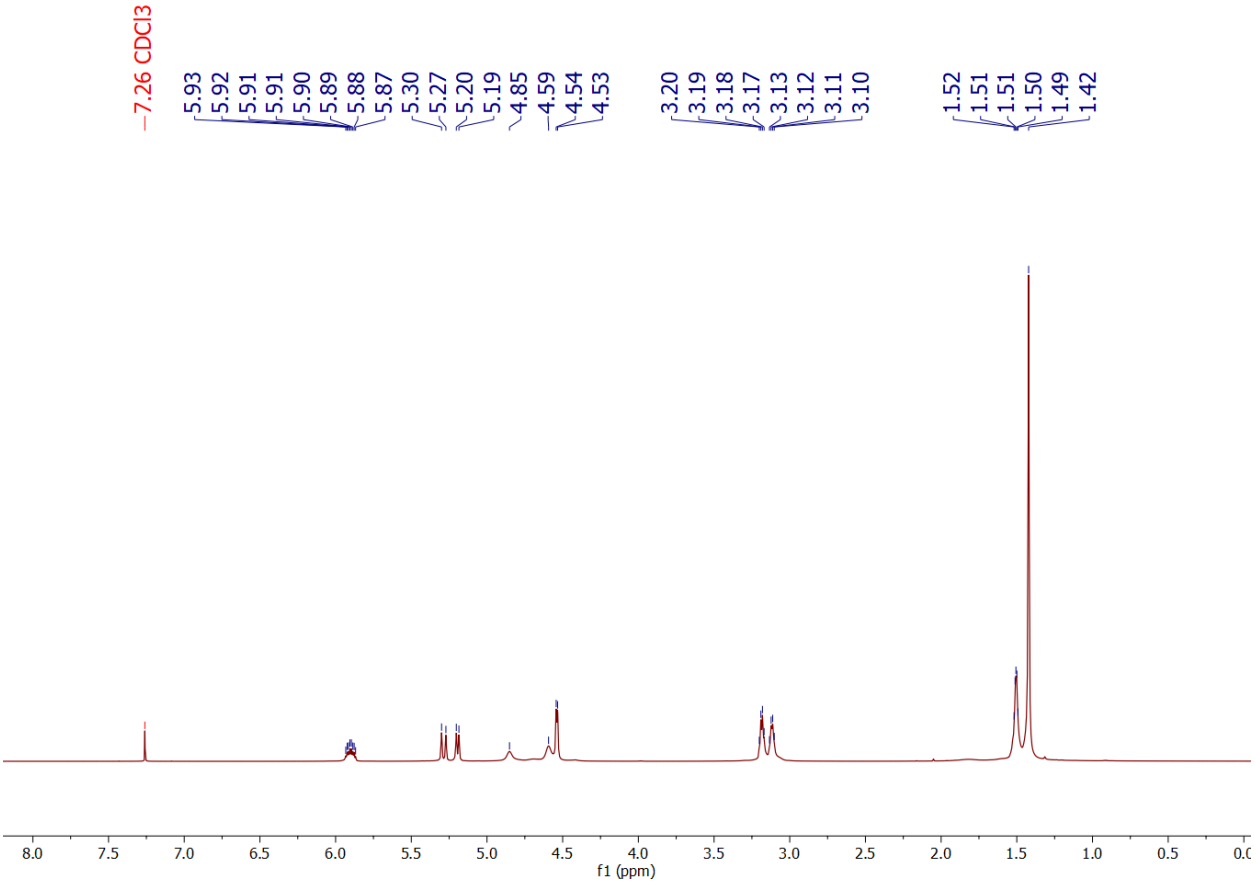

^{13}C NMR Spectrum of Allyl *tert*-butyl butane-1,4-diyldicarbamate

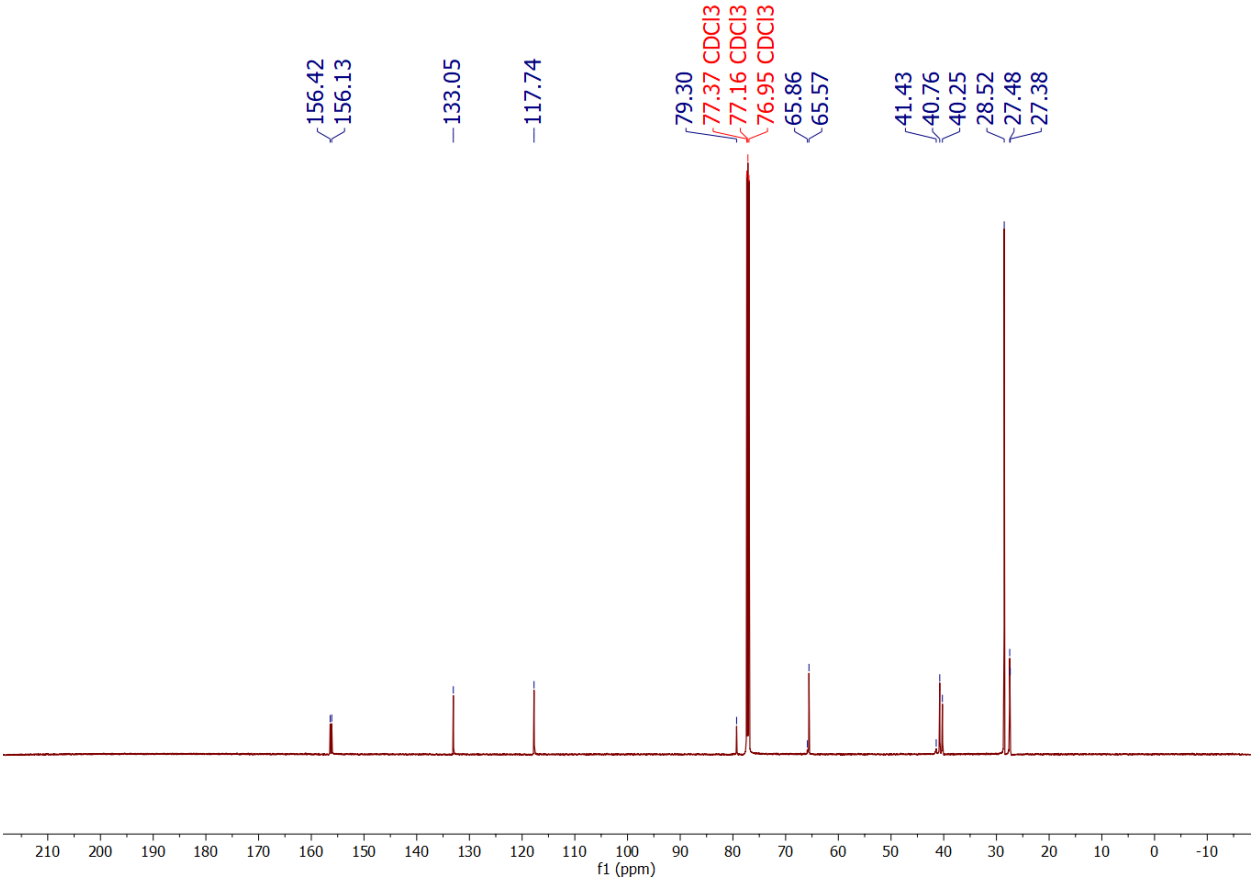

Allyl (4-aminobutyl)carbamate trifluoroacetate: A round bottom flask was charged with allyl *tert*-butyl butane-1,4-diyldicarbamate (1.12 g, 4.10 mmol, 1 equiv) and DCM (10 mL). To this solution, TFA (10 mL) was added, and the reaction was stirred at rt for 2 h. The solvent was removed *in vacuo* and azeotroped with toluene and heptane to provide the product as a clear oil. The compound was used without characterization or purification in the second step of the synthesis for Alloc-**NDI**-OH.

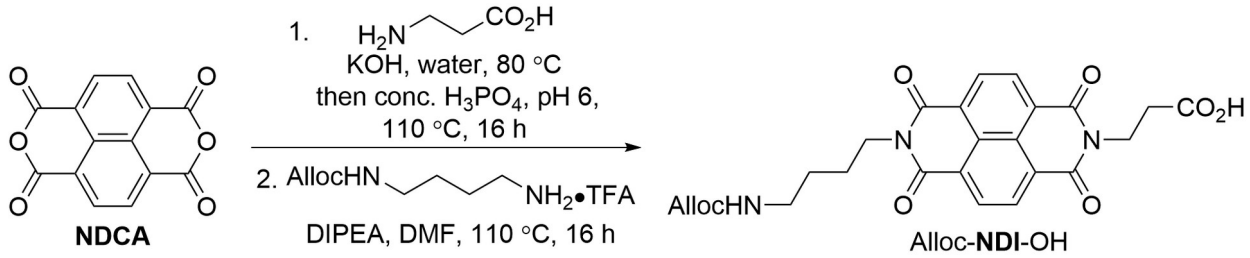

3-(7-(4-(((allyloxy)carbonyl)amino)butyl)-1,3,6,8-tetraoxo-3,6,7,8-tetrahydrobenzo[*lmn*][3,8]phenanthrolin-2(1*H*)-yl)propanoic acid (Alloc-**NDI**-OH**):** This compound was synthesized using the literature procedure for a similar compound.[16] A round bottom flask equipped with a reflux condenser was charged with **NDCA** (1.00 g, 3.73 mmol, 1 equiv) and water (7 mL). The suspension was heated to 80 °C and aq. KOH (1.26 g, 22.4 mmol, 6 equiv in 5 mL water) was added. The suspension was stirred until it completely dissolved to a yellow solution. The pH was adjusted to pH 6 using conc. phosphoric acid. To this aq. solution, β-alanine (365 mg, 4.10 mmol, 1.1 equiv) was added, and the pH was adjusted back to 6. The reaction mixture was refluxed at 110 °C for 16 h. The reaction was cooled to rt and acidified to pH 2 with 1 M HCl. The suspension was stirred while heating to 80 °C for 30 min. The yellow precipitate was filtered on a glass-fritted funnel by vacuum filtration and allowed to completely dry.

The round bottom flask with allyl (4-aminobutyl)carbamate trifluoroacetate was charged with the yellow precipitate and DMF (15 mL). DIPEA (714 µL, 4.10 mmol, 1.1 equiv) was added, and the reaction mixture was heated to 110 °C for 16 h. The reaction was cooled to rt and diluted with chloroform (200 mL). The organic phase was washed with 10 % aq. acetic acid (3 × 100 mL). Each aqueous later was extracted with chloroform (50 mL). The organic layers were combined, washed with 1 M aq. potassium

bisulfate (100 mL) and brine (2 × 50 mL), dried over sodium sulfate, filtered, and concentrated *in vacuo*. The crude residue was dissolved in chloroform and purified by flash column chromatography (0-10 % methanol:chloroform) to provide Alloc-**NDI**-OH as a yellow solid (895 mg, 1.81 mmol, 48 %).

Analytical data: **^{1}H NMR** (600 MHz, DMSO-*d*6) δ 8.61 (s, 4H), 7.22 (t, *J* = 5.7 Hz, 1H), 5.88 (ddt, *J* = 17.2, 10.5, 5.3 Hz, 1H), 5.24 (dq, *J* = 17.2, 1.8 Hz, 1H), 5.14 (dq, *J* = 10.4, 1.6 Hz, 1H), 4.43 (dt, *J* = 5.4, 1.6 Hz, 2H), 4.29 – 4.23 (m, 2H), 4.04 (t, *J* = 7.3 Hz, 2H), 3.35 (s, 2H), 3.02 (q, *J* = 6.6 Hz, 2H), 2.65 – 2.61 (m, 2H), 1.65 (p, *J* = 7.6 Hz, 2H), 1.48 (p, *J* = 7.1 Hz, 2H), 1.38 (p, *J* = 3.3 Hz, 1H), 1.17 (s, 2H); **^{13}C NMR** (151 MHz, DMSO-*d*6) δ 172.47, 162.60, 162.49, 160.94, 155.95, 133.92, 133.89, 130.43, 126.31, 126.20, 126.07, 126.05, 116.88, 64.15, 40.05, 36.82, 36.10, 35.83, 31.99, 30.80, 27.07, 26.91, 26.40, 24.95; **HRMS (ESI^{+})** Calcd for $[C_{25}H_{23}N_3O_8]^+$ ([M+H]): 494.15, Found: 494.1575.

^{1}H NMR Spectrum of Alloc-**NDI**-OH

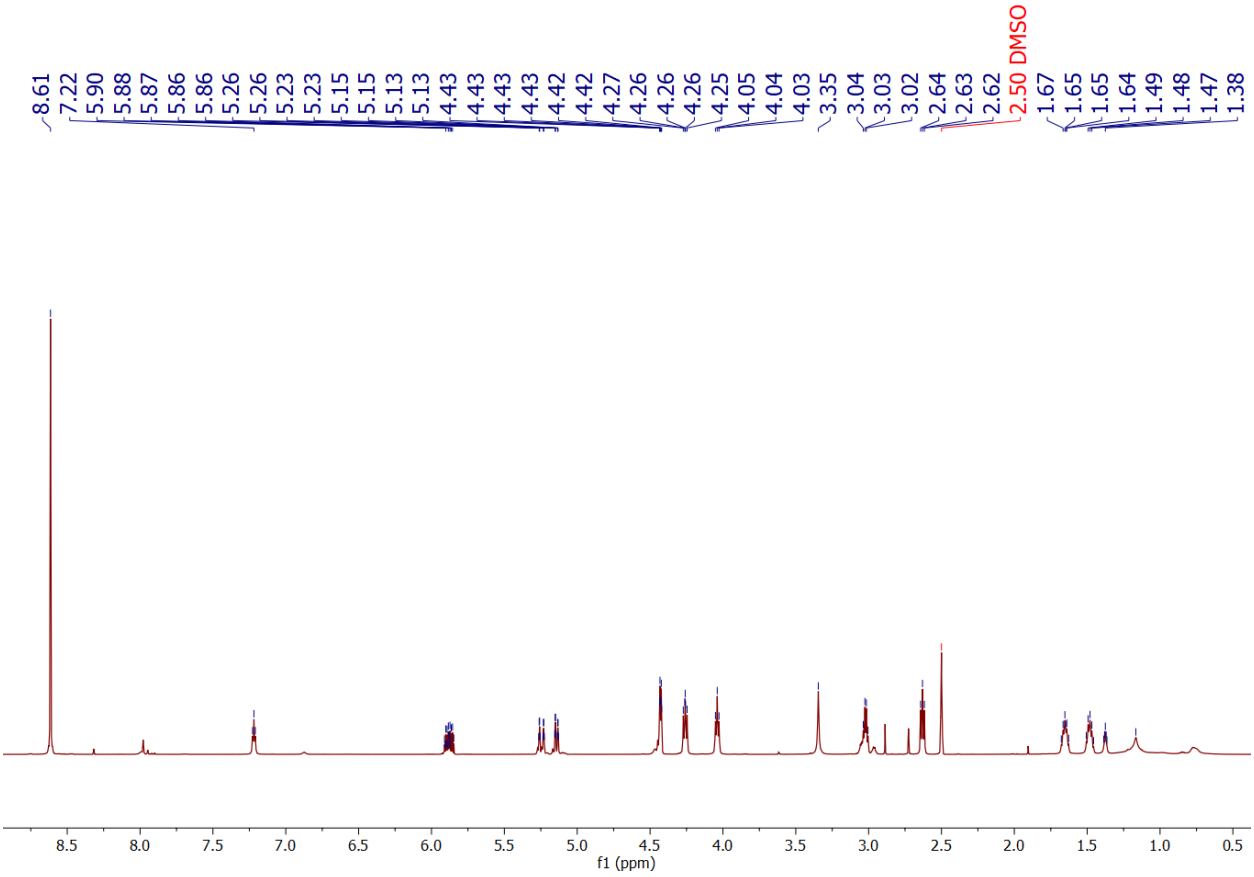

^{13}C NMR Spectrum of Alloc-**NDI**-OH

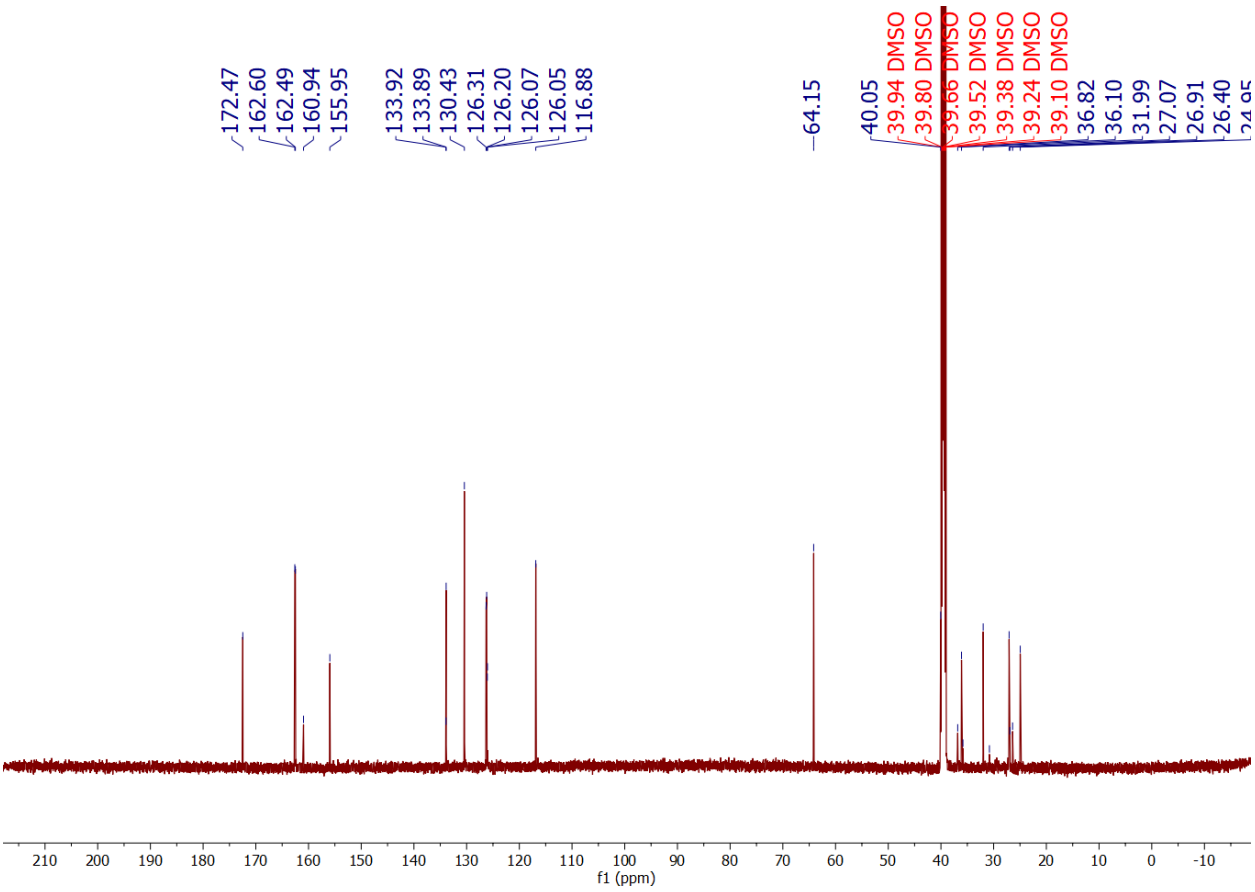

Aminoalkoxynaphthalene (AAN)

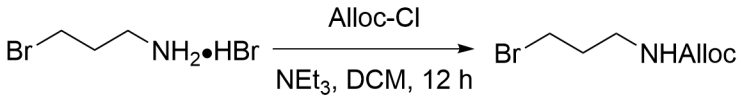

Allyl (3-bromopropyl)carbamate: This compound was synthesized by following a literature procedure.[17] A round bottom flask was charged with 3 bromopropan-1-amino hydrobromide (3.00 g, 13.7 mmol, 1 equiv), NEt_3 (6.69 mL, 47.9 mmol, 3.5 equiv), and DCM (85 mL). The reaction mixture was cooled to 0 °C in an ice water bath. A solution of Alloc-Cl (1.46 mL, 13.7 mmol, 1 equiv) in DCM (10 mL) was slowly added, and the reaction mixture was stirred at 0 °C for 1.5 h. The reaction was warmed to rt and stirred

for an additional 12 h. The reaction mixture was washed with 1 M HCl (20 mL), water (20 mL), and brine (20 mL), dried over sodium sulfate, filtered, and concentrated *in vacuo* to provide the product as a peach-colored oil which was used in the next step without further purification (2.5 g, 11.2 mmol, 82 %), and the acquired ^{1}H NMR spectrum is consistent with the literature spectrum.

Analytical data: **^{1}H NMR** (400 MHz, Chloroform-*d*) δ 5.91 (ddt, *J* = 16.4, 10.9, 5.7 Hz, 1H), 5.34 – 5.17 (m, 2H), 4.89 (s, 1H), 4.56 (dt, *J* = 5.7, 1.5 Hz, 2H), 3.45 (t, *J* = 6.4 Hz, 2H), 3.35 (q, *J* = 6.4 Hz, 2H), 2.07 (p, *J* = 6.5 Hz, 2H).

^{1}H NMR Spectrum for Allyl (3-bromopropyl)carbamate

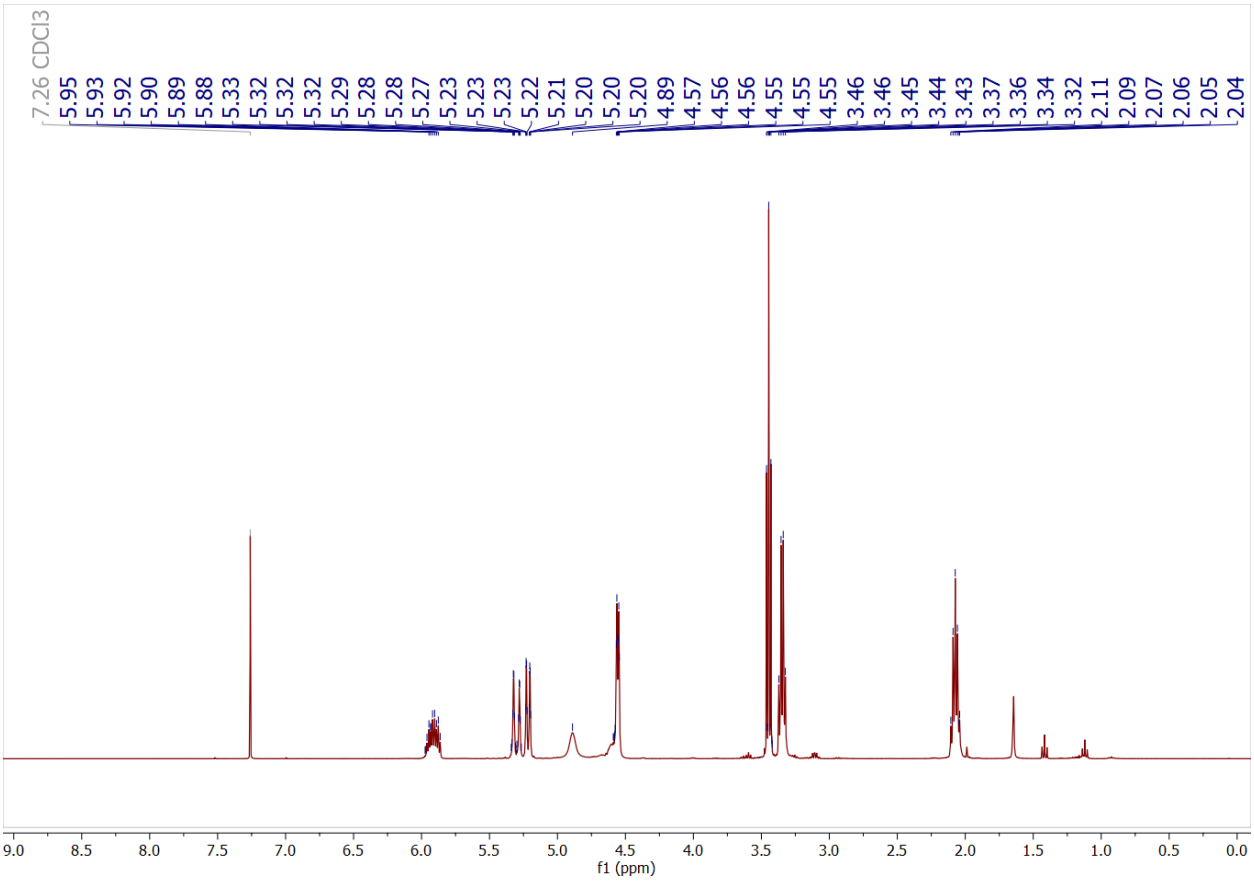

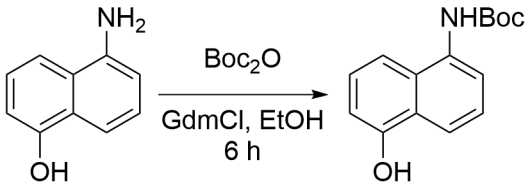

AHN **A1**

***tert*-Butyl (5-hydroxynaphthalen-1-yl)carbamate (A1):** This compound was synthesized by following a literature procedure.[18] A round bottom flask was charged with **AHN** (3.0 g, 18 mmol, 1 equiv), Boc_2O (4.1 g, 18 mmol, 1 equiv), guanidine hydrochloride (GdmCl, 360 mg, 3.8 mmol, 0.2 equiv), and degassed EtOH (50 mL). The reaction solution was stirred under an N_2 atm for 6 h. The reaction solvent was removed *in vacuo*, and the crude residue was dissolved in diethyl ether (100 mL). The organic phase was wash with water (50 mL), filtered, washed with brine (50 mL), and filtered again. After drying over sodium sulfate, the organic phase was concentrated *in vacuo* to provide **A1** as a dark purple solid (4.2 g, 16 mmol, 86 %), and the acquired ^{1}H NMR spectrum is consistent with the literature spectrum.

Analytical data: **^{1}H NMR** (400 MHz, DMSO-*d*6) δ 10.17 (s, 1H), 9.12 (s, 1H), 7.96 (d, *J* = 8.4 Hz, 1H), 7.53 (d, *J* = 6.4 Hz, 1H), 7.47 (d, *J* = 8.4 Hz, 1H), 7.42 – 7.34 (m, 1H), 7.34 – 7.25 (m, 1H), 6.88 (d, *J* = 6.6 Hz, 1H), 1.49 (s, 9H).

^{1}H NMR Spectrum of A1

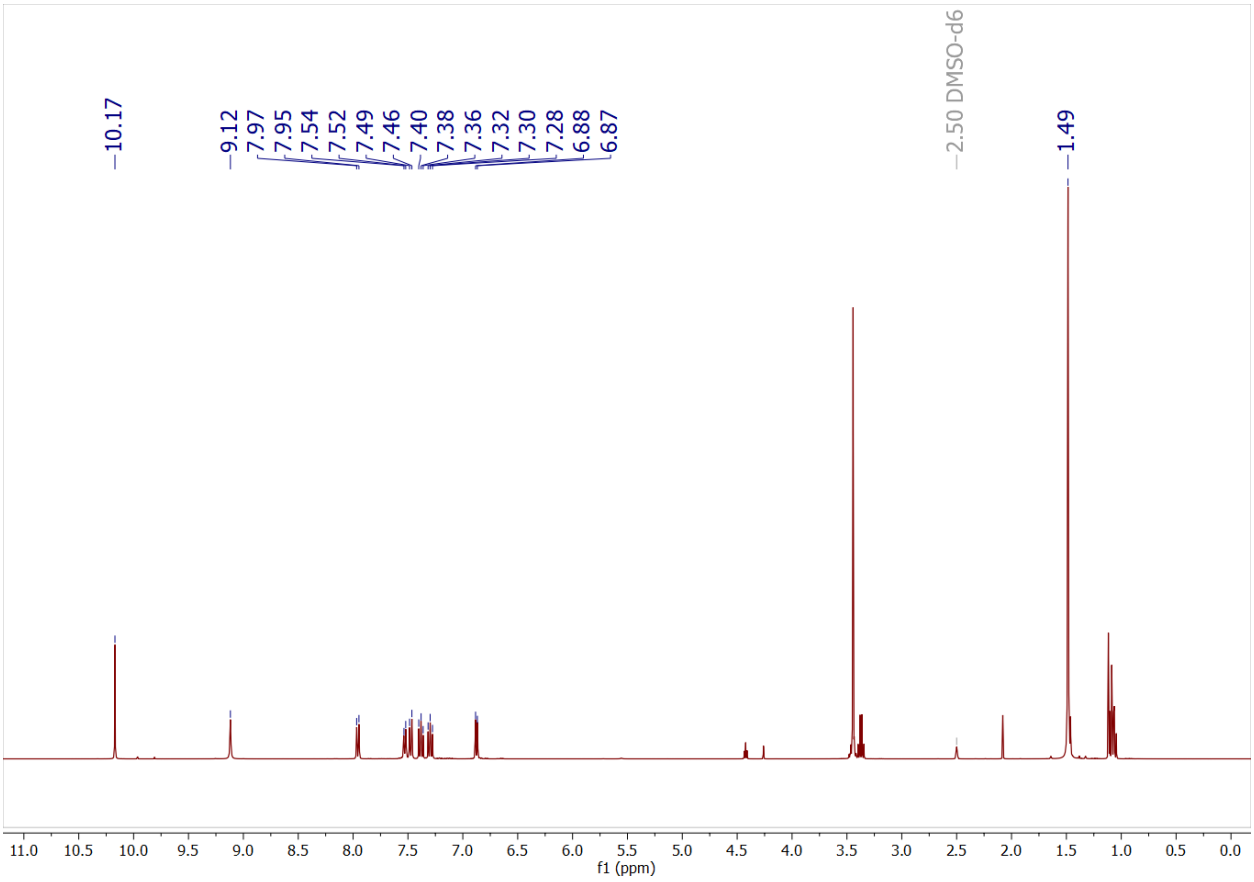

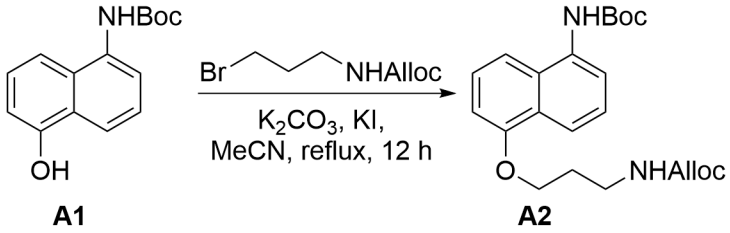

A1 **A2**

***tert*-Butyl (5-(3-(((allyloxy)carbonyl)amino)propoxy)naphthalen-1-yl)carbamate (A2):** A round bottom flask was charged with **A1** (1.7 g, 6.5 mmol, 0.9 equiv), allyl (3-bromopropyl)carbamate (1.6 g, 7.2 mmol, 1 equiv), K_2CO_3 (4.0 g, 29 mmol, 4 equiv), KI (0.24 g, 1.4 mmol, 0.2 equiv), and MeCN (55 mL). The reaction flask was evacuated and purged with N_2 (3x). The reaction mixture was refluxed for 12 h, then cooled to rt. The reaction solvent was removed *in vacuo*, and the residue was dissolved in EtOAc

(100 mL). The organic phase was washed with aq. sodium bicarbonate (50 mL) and brine (50 mL), dried over sodium sulfate, filtered, and concentrated *in vacuo*. The crude residue was purified on silica by flash column chromatography (0-100 % EtOAc/hexane) to provide **A2** as a dark purple solid (2.11 g, 5.27 mmol, 73 %).

Analytical data: **^{1}H NMR** (400 MHz, DMSO-*d*6) δ 9.18 (s, 1H), 7.98 (dt, *J* = 8.4, 1.0 Hz, 1H), 7.58 (t, *J* = 8.2 Hz, 2H), 7.47 – 7.36 (m, 3H), 6.95 (d, *J* = 7.6 Hz, 1H), 5.90 (ddt, *J* = 17.3, 10.6, 5.4 Hz, 1H), 5.30 – 5.14 (m, 2H), 4.46 (dt, *J* = 5.4, 1.5 Hz, 2H), 4.16 (t, *J* = 6.1 Hz, 2H), 3.26 (q, *J* = 6.5 Hz, 2H), 2.04 – 1.96 (m, 2H), 1.48 (s, 9H). **^{13}C NMR** (101 MHz, DMSO) δ 156.06, 154.14, 154.09, 133.90, 129.12, 125.89, 125.72, 124.80, 121.86, 118.29, 116.97, 114.98, 105.12, 78.92, 65.48, 64.25, 37.52, 29.22, 28.22; **HRMS (ESI^{+})** Calcd for $[C_{22}H_{28}N_2O_5Na]^+$ ([M+Na]): 423.19, Found: 423.1890.

^{1}H NMR Spectrum of A2

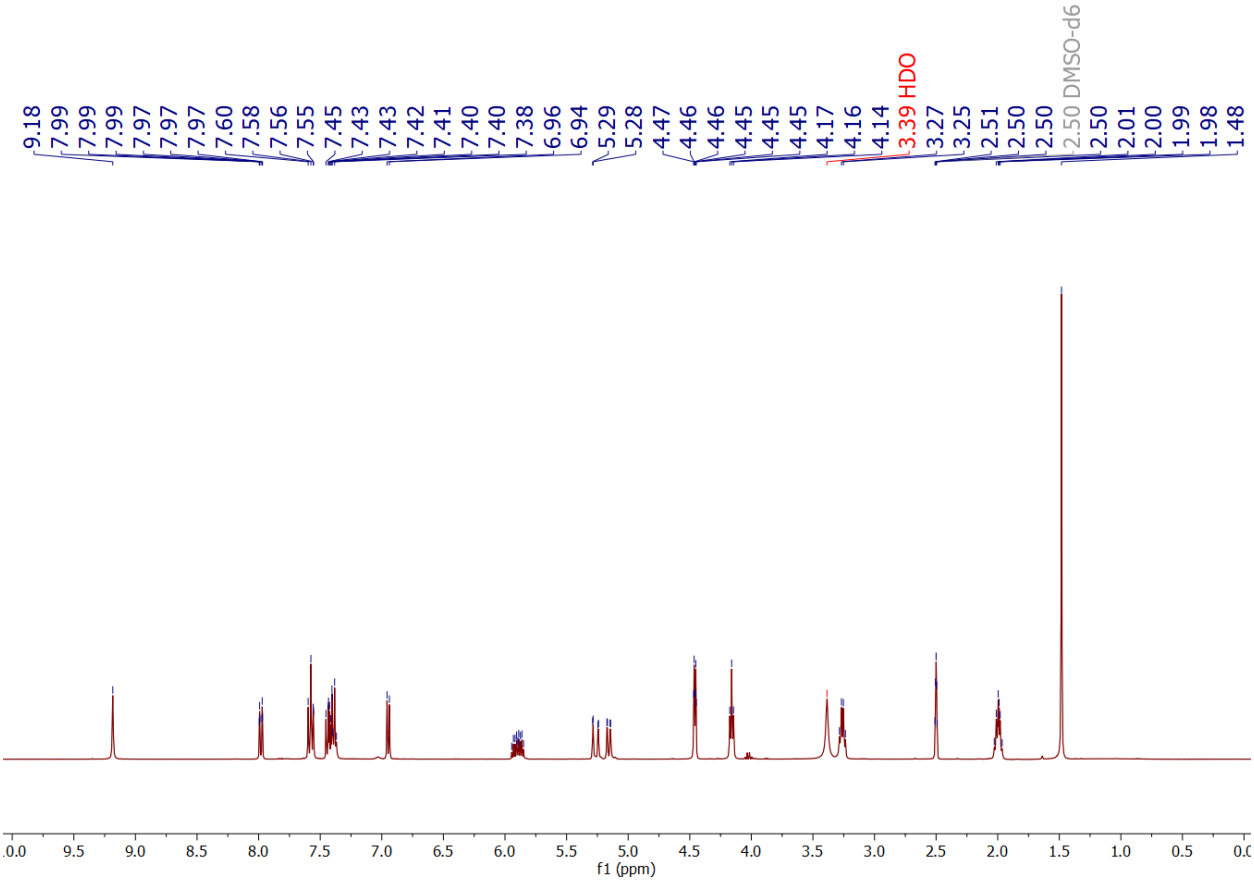

^{13}C NMR Spectrum of A2

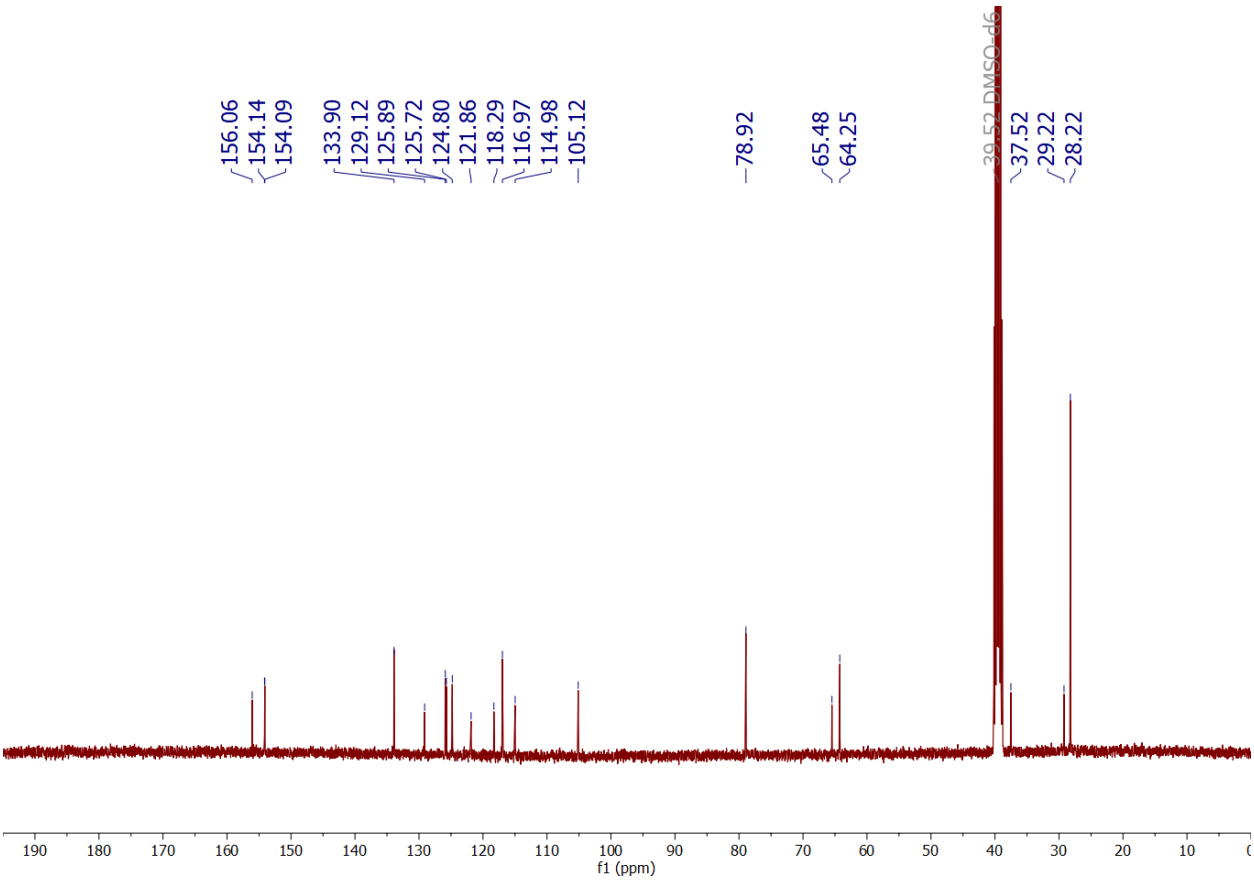

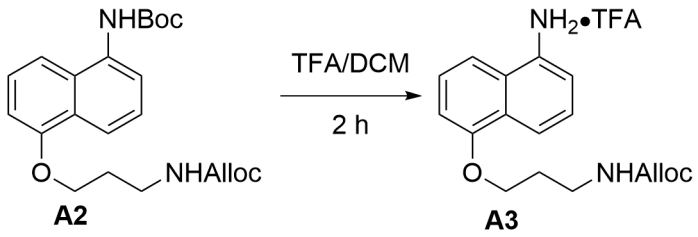

Allyl (3-((5-aminonaphthalen-1-yl)oxy)propyl)carbamate trifluoroacetate (A3): A round bottom flask was charged with **A2** (2.11 g, 5.27 mmol, 1 equiv), DCM (40 mL), and TFA (40 mL). The reaction mixture was stirred at rt for 2 h. The reaction solvent was removed *in vacuo* and azeotroped with toluene and heptane to provide **A3** as a dark purple solid which was used in the next step without further purification or characterization.

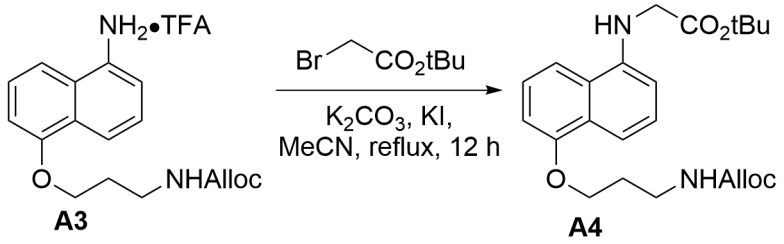

***tert*-Butyl (5-(3-(((allyloxy)carbonyl)amino)propoxy)naphthalen-1-yl)glycinate (A4):**

A round bottom flask equipped with a reflux condenser was charged with **A3** (1.70 g, 4.10 mmol, 1 equiv), *tert*-butyl bromoacetate (1.82 mL, 12.3 mmol, 3 equiv), $KHCO_3$ (1.64 g, 16.4 mmol, 4 equiv), KI (136 mg, 0.82 mmol, 0.2 equiv), and MeCN (25 mL). The reaction flask was evacuated and purged with N_2 (3x), and the reaction mixture was refluxed for 12 h. The reaction mixture was cooled to rt, and the solvent was removed *in vacuo*. The residue was dissolved in EtOAc (100 mL), and the organic phase was washed with aq. sodium bicarbonate (50 mL) and brine (50 mL), dried over sodium sulfate, filtered, and concentrated *in vacuo*. The crude residue was purified on silica by flash column chromatography (0-100 % EtOAc/hexane) to provide **A4** as a light pink solid (1.12 g, 2.70 mmol, 65 %).

Analytical data: **^{1}H NMR** (400 MHz, DMSO-*d*6) δ 7.67 (d, *J* = 8.6 Hz, 1H), 7.47 (d, *J* = 8.4 Hz, 1H), 7.35 – 7.30 (m, 1H), 7.24 (t, *J* = 8.0 Hz, 1H), 6.90 (d, *J* = 7.7 Hz, 1H), 6.38 – 6.30 (m, 1H), 5.91 (ddt, *J* = 17.3, 10.6, 5.4 Hz, 1H), 5.28 (dt, *J* = 17.2, 1.8 Hz, 1H), 5.16 (dt, *J* = 10.5, 1.6 Hz, 1H), 4.48 (d, *J* = 5.4 Hz, 1H), 4.13 (t, *J* = 6.1 Hz, 2H), 3.94 (s, 2H), 3.27 (q, *J* = 6.5 Hz, 2H), 2.00 (p, *J* = 6.5 Hz, 2H), 1.42 (s, 9H). **^{13}C NMR** (101 MHz, DMSO) δ 170.43, 156.02, 154.25, 143.41, 133.85, 125.91, 125.79, 124.28, 123.89, 116.88, 113.56, 109.66, 105.11, 103.74, 80.59, 80.51, 65.31, 64.21, 45.74, 37.57, 29.27,

27.75, 27.66; **HRMS (ESI$^+$)** Calcd for $[C_{23}H_{30}N_2O_5Na]^+$ ([M+Na]): 437.21, Found: 437.2047.

^{1}H NMR Spectrum of A4

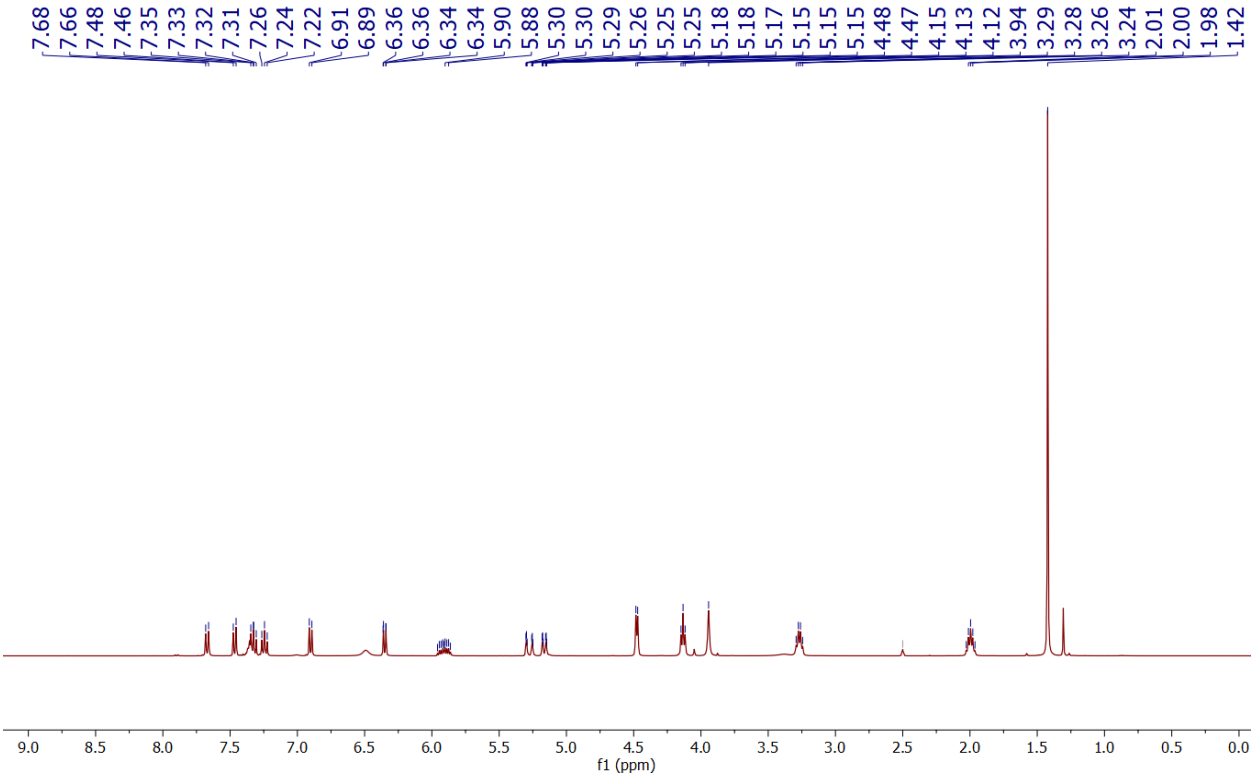

^{13}C NMR Spectrum of A4

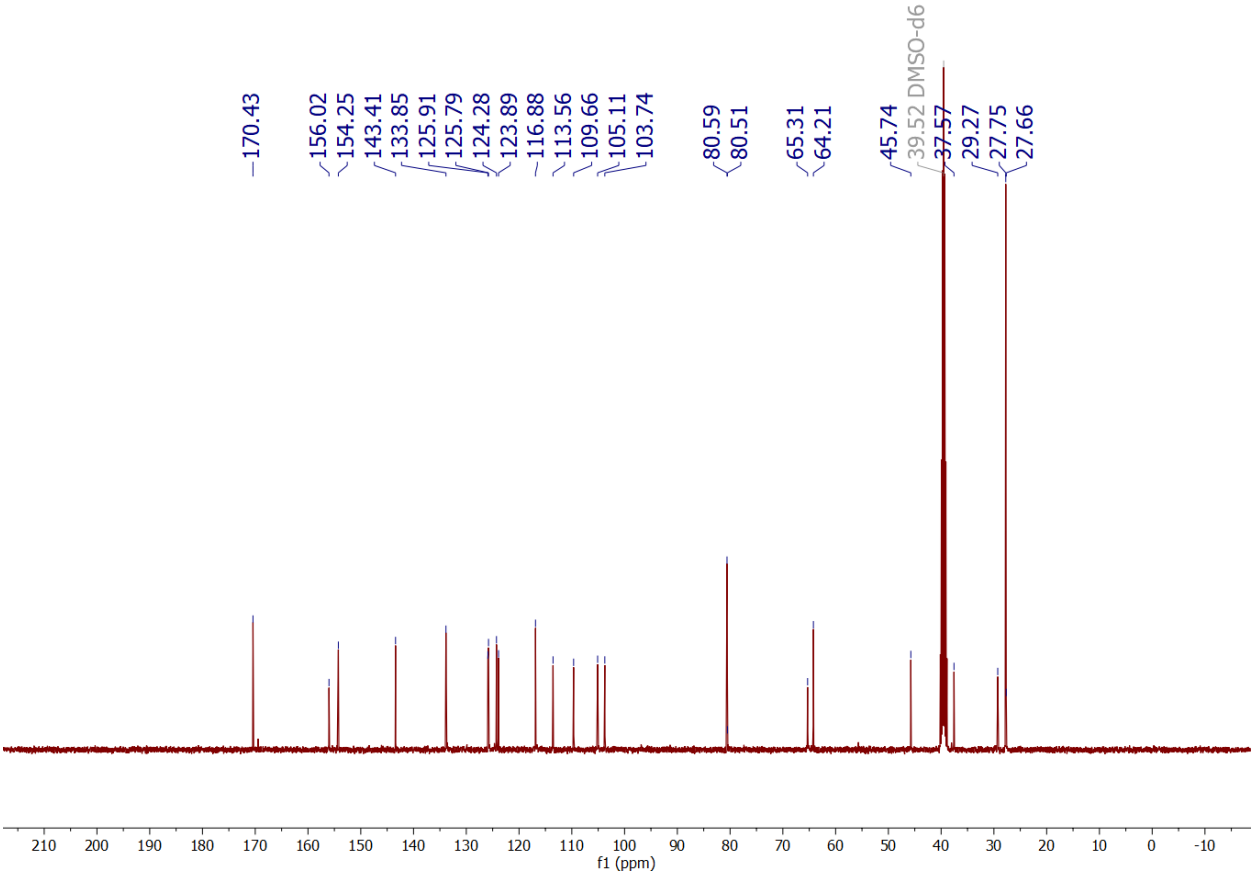

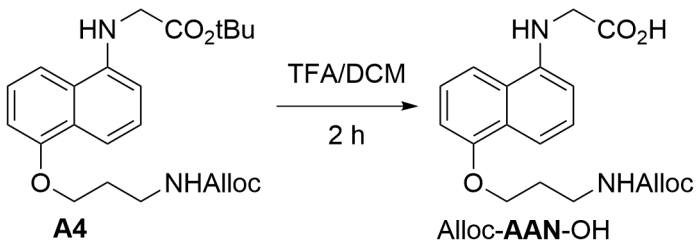

(5-(3-(((allyloxy)carbonyl)amino)propoxy)naphthalen-1-yl)glycine (Alloc-**AAN**-OH**):**

A round bottom flask was charged with **A4** (1.12 g, 2.70 mmol, 1 equiv), DCM (20 mL), and TFA (20 mL). The reaction mixture was stirred at rt for 2 h. The reaction solvent was removed *in vacuo* and azeotroped with toluene and heptane. The oily residue was

suspended in diethyl ether, sonicated and collected by filtration to provide Alloc-**AAN**-OH as a gray solid (1.23 g, 2.61 mmol, 96 %).

Analytical data: **^{1}H NMR** (400 MHz, DMSO-*d*6) δ 7.65 (d, *J* = 8.5 Hz, 1H), 7.45 (d, *J* = 8.3 Hz, 1H), 7.35 – 7.29 (m, 2H), 7.24 (t, *J* = 8.0 Hz, 1H), 6.90 (d, *J* = 7.7 Hz, 1H), 6.37 (d, *J* = 7.6 Hz, 1H), 5.90 (ddt, *J* = 17.3, 10.6, 5.3 Hz, 1H), 5.32 – 5.23 (m, 1H), 5.16 (dd, *J* = 10.4, 1.7 Hz, 1H), 4.47 (dt, *J* = 5.4, 1.6 Hz, 2H), 4.13 (t, *J* = 6.1 Hz, 2H), 3.96 (s, 2H), 3.25 (q, *J* = 6.5 Hz, 2H), 1.98 (p, *J* = 6.5 Hz, 2H); **^{13}C NMR** (101 MHz, DMSO) δ 172.66, 156.02, 154.25, 143.42, 133.86, 125.90, 125.85, 124.28, 123.83, 116.90, 113.52, 109.55, 105.14, 103.72, 65.32, 64.21, 44.95, 37.55, 29.26; **HRMS (ESI^{+})** Calcd for $[C_{19}H_{22}N_2O_5]^+$ ([M+H]): 358.15, Found: 358.1603.

^{1}H NMR Spectrum of Alloc-**AAN**-OH

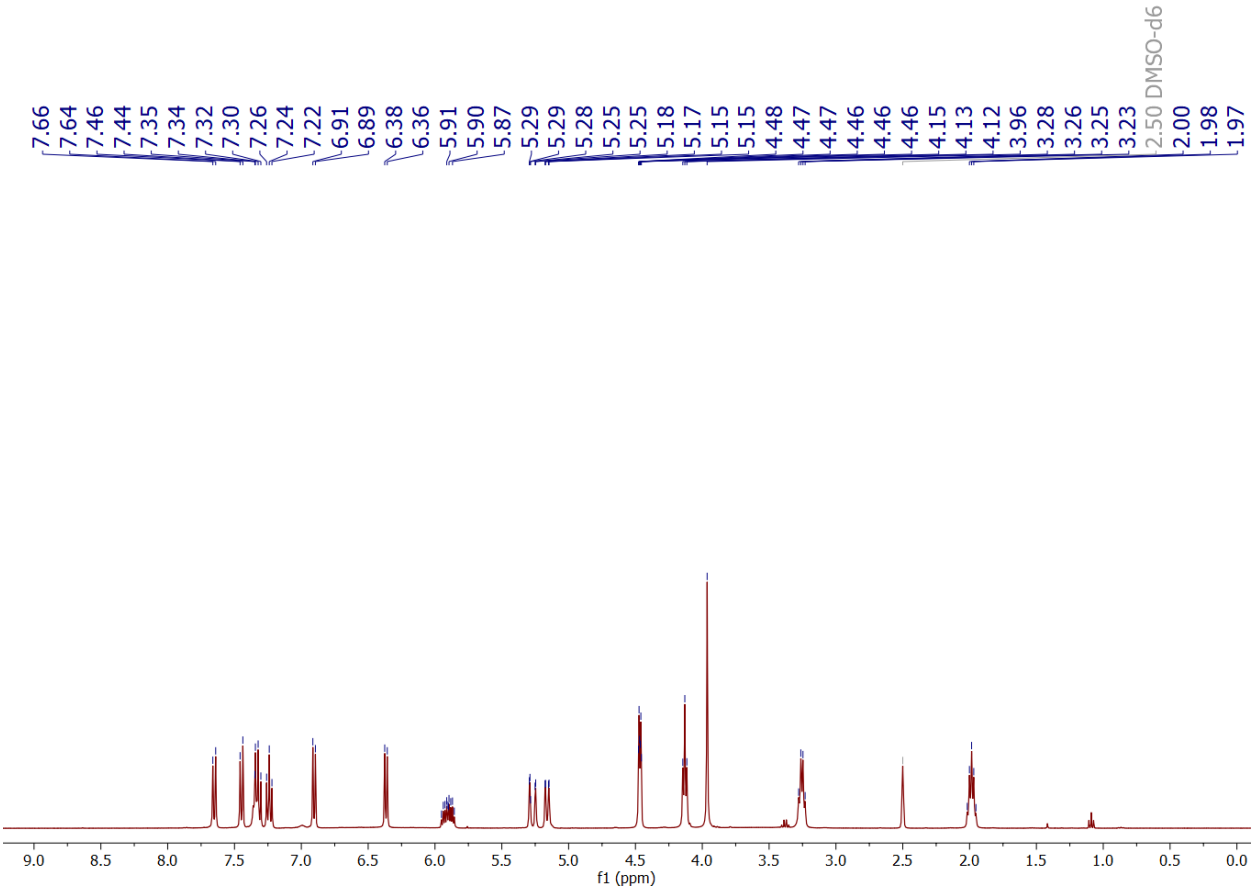

^{13}C NMR Spectrum of Alloc-**AAN**-OH

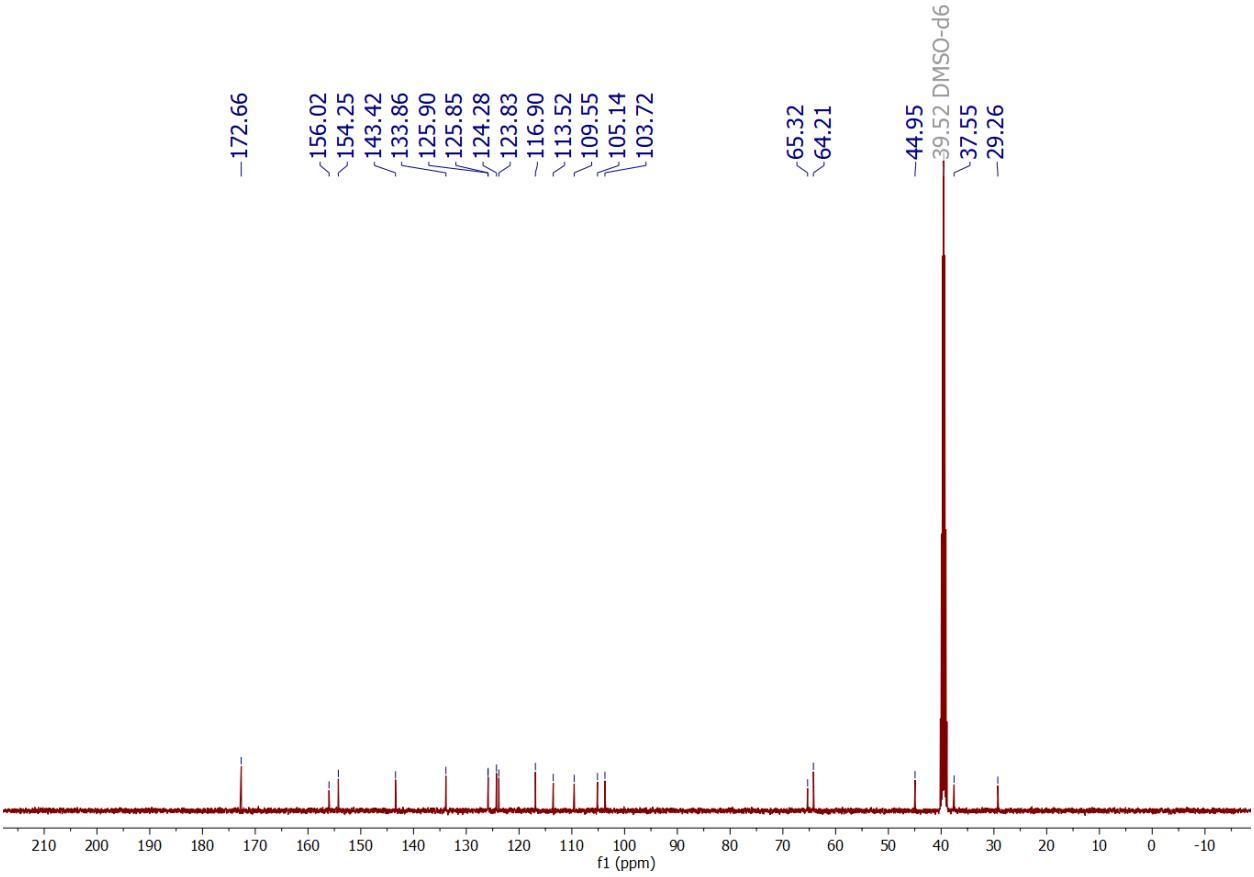

Peptide Sequences

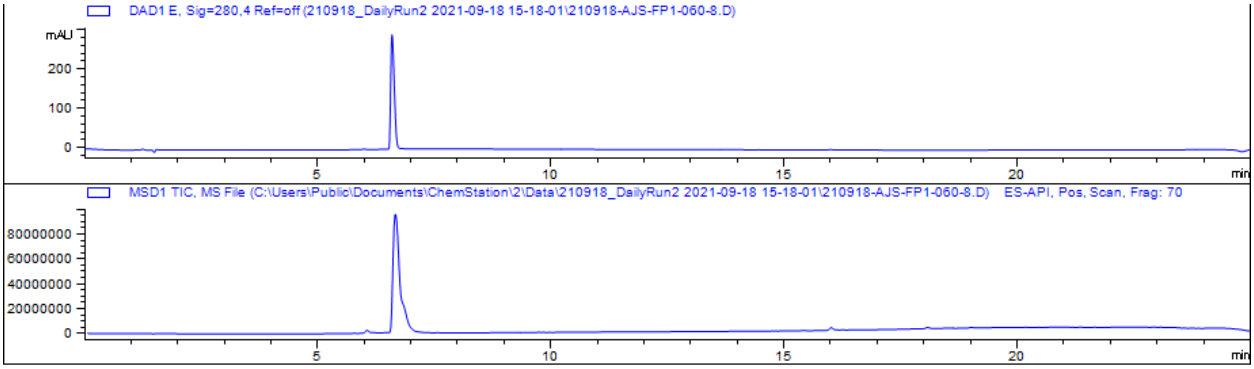

Figure 2-22. Ac-Lys-**DAN**-Lys-NH_2: LCMS UV absorbance trace (280 nm) (top) and TIC (bottom).

DAN monomer peptide was purified with a gradient of 0-100% solvent B in 60 min.

Expected mass: [M+H] 574, [M+2H] 287; Observed mass: [M+H] 574, [M+2H] 287.

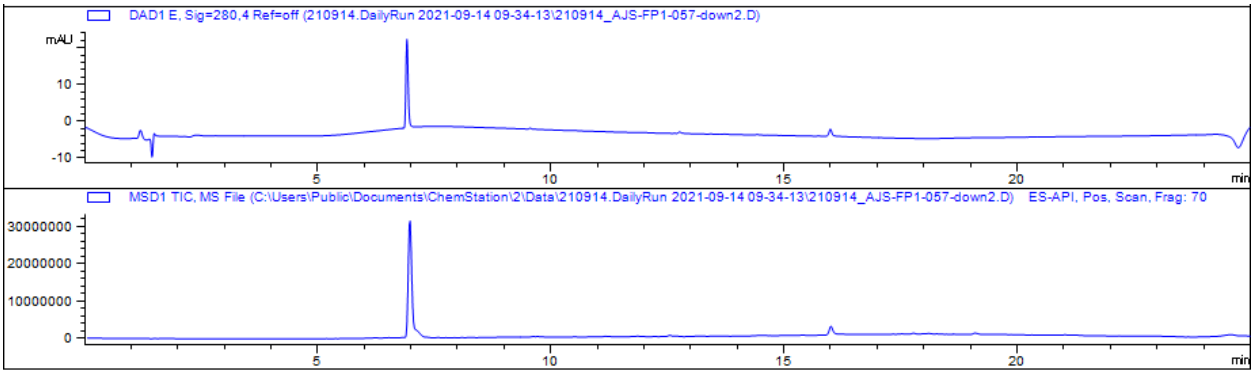

Figure 2-23. Ac-Lys-**NDI**-Lys-NH_2: LCMS UV absorbance trace (280 nm) (top) and TIC (bottom).

NDI monomer peptide was purified with a gradient of 0-100% solvent B in 60 min.

Expected mass: [M+H] 708, [M+2H] 354; Observed mass: [M+H] 708, [M+2H] 354.

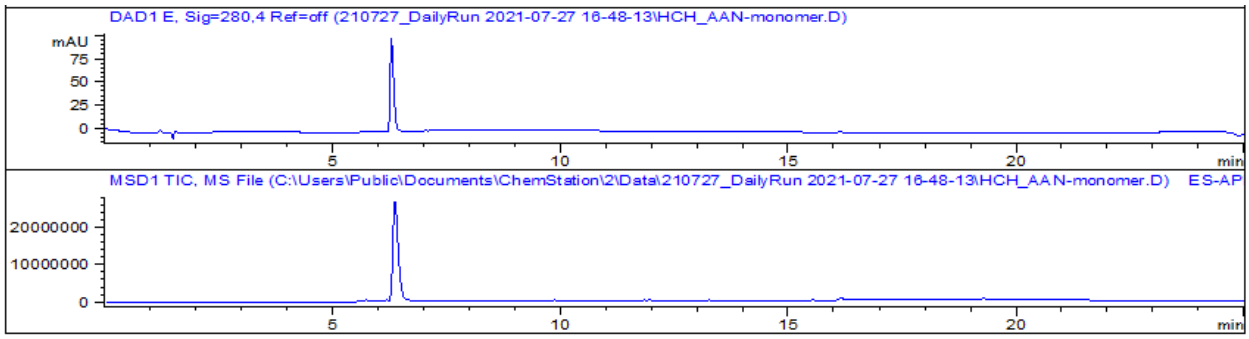

Figure 2-24. Ac-Lys-**AAN**-Lys-NH_2: LCMS UV absorbance trace (280 nm) (top) and TIC (bottom).

AAN monomer peptide was purified with a gradient of 0-100% solvent B in 60 min.

Expected mass: [M+H] 572, [M+2H] 286, [M+3H] 191; Observed mass: [M+H] 572,

[M+2H] 286.

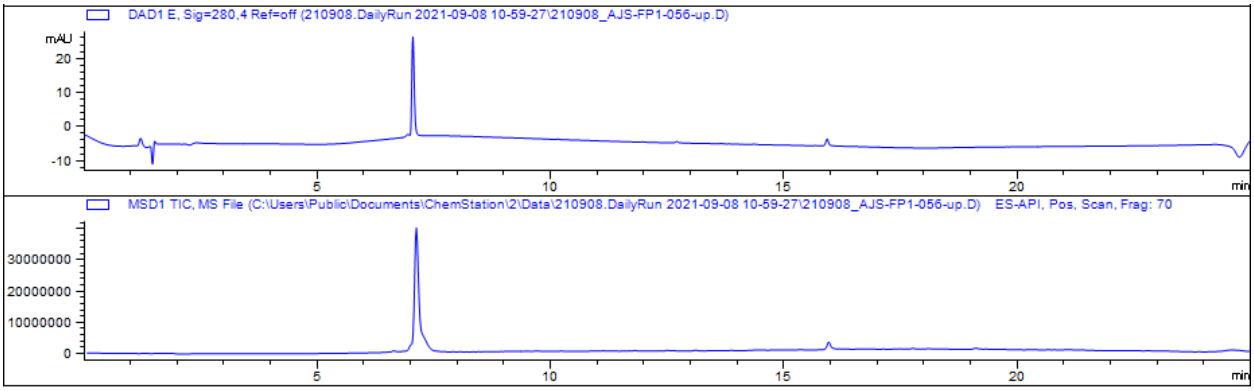

Figure 2-25. Ac-Lys-**NDI**-Lys-**AAN**-Lys-NH_2: LCMS UV absorbance trace (280 nm) (top) and TIC (bottom).

NDI-**AAN** dimer peptide was purified with a gradient of 10-60% solvent B in 60 min.

Expected mass: [M+H] 1092, M+2H] 546, [M+3H] 364, [M+4H] 273; Observed mass

[M+2H] 546, [M+3H] 364, [M+4H] 273.

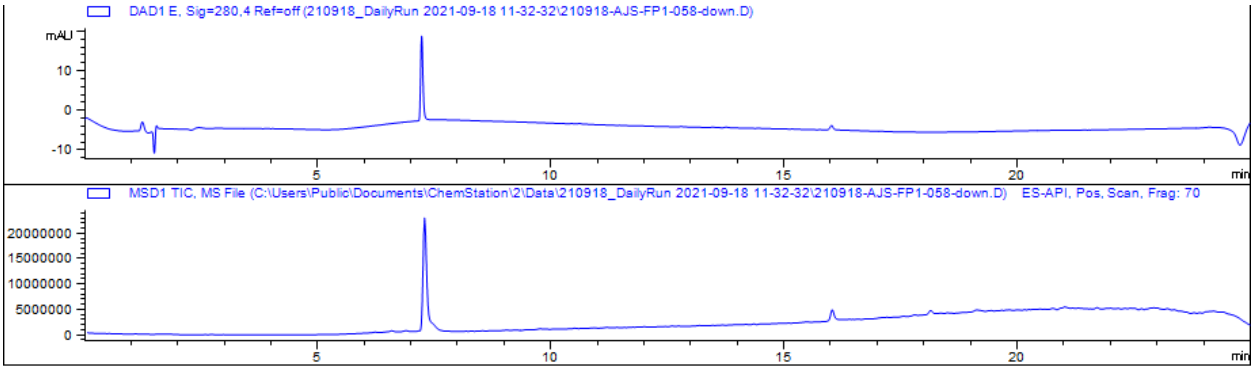

Figure 2-26. Ac-Lys-**NDI**-Lys-**DAN**-Lys-NH_2: LCMS UV absorbance trace (280 nm) (top) and TIC (bottom).

NDI-**DAN** dimer peptide was purified with a gradient of 10-60% solvent B in 60 min.

Expected mass: [M+H] 1093, [M+2H] 546, [M+3H] 365; Observed mass: [M+2H] 546, [M+3H] 365.

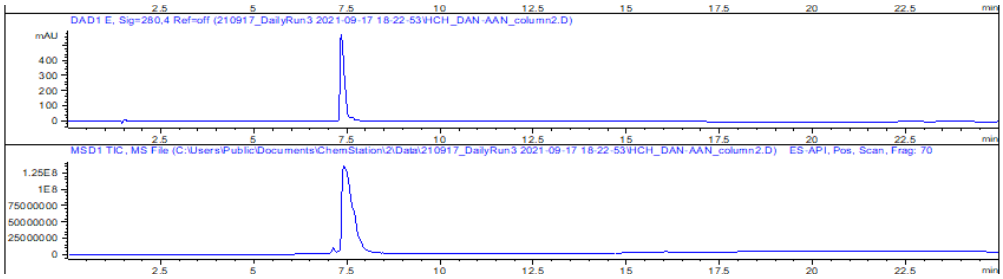

Figure 2-27. Ac-Lys-**DAN**-Lys-**AAN**-Lys-NH_2: LCMS UV absorbance trace (280 nm) (top) and TIC (bottom).

DAN-**AAN** dimer peptide was purified with a gradient of 10-60% solvent B in 60 min.

Expected mass: [M+H] 957, [M+2H] 479, [M+3H] 319, [M+4H] 250; Observed mass: [M+2H] 479, [M+3H] 319, [M+4H] 250.

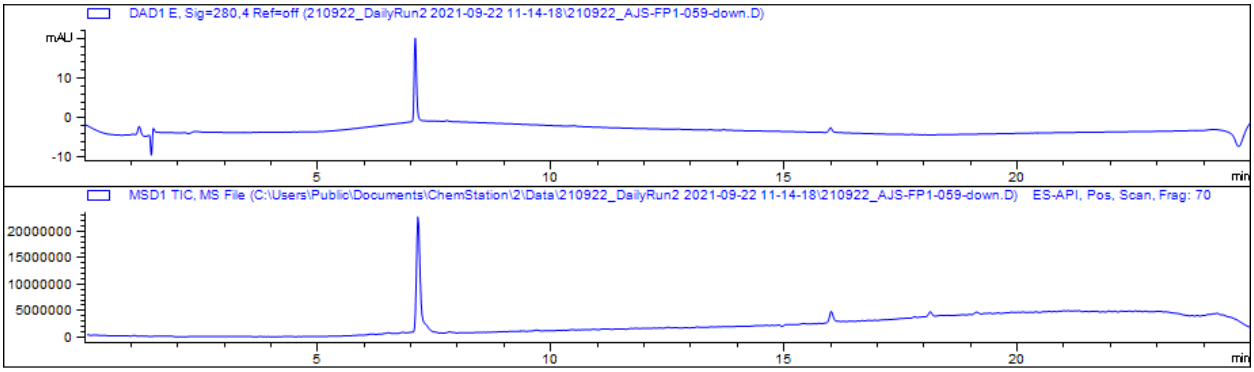

Figure 2-28. Ac-Lys-**NDI**-Lys-**NDI**-Lys-NH_2: LCMS UV absorbance trace (280 nm) (top) and TIC (bottom).

NDI-**NDI** dimer peptide was purified with a gradient of 10-60% solvent B in 60 min.

Expected mass: [M+H] 1227, [M+2H] 613, [M+3H] 409; Observed mass: [M+2H] 613, [M+3H] 409.

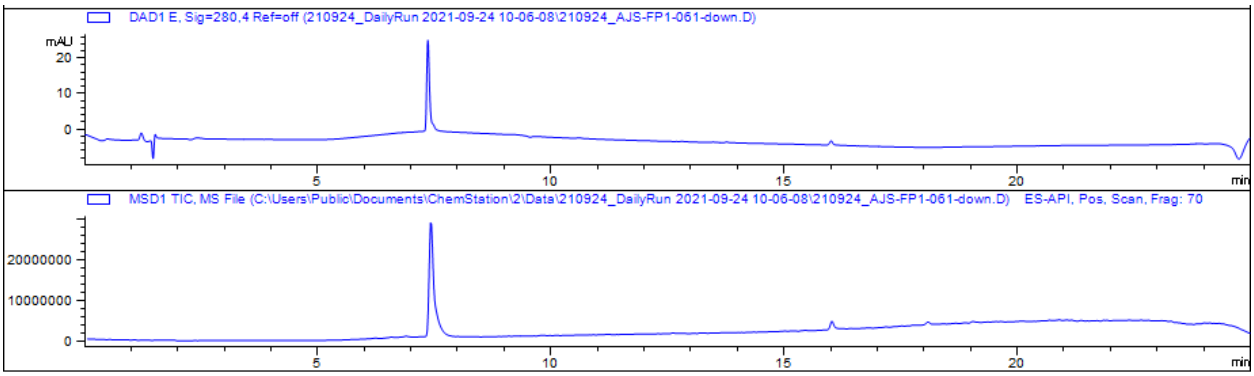

Figure 2-29. Ac-Lys-Lys-**NDI**-Lys-**NDI**-Lys-**DAN**-Lys-**AAN**-Lys-Lys-NH_2: LCMS UV absorbance trace (280 nm) (top) and TIC (bottom).

Gen 1 foldamer peptide was purified with a gradient of 10-50% solvent B in 60 min.

Expected mass: [M+H] 2252, [M+2H] 1126, [M+3H] 751, [M+4H] 536, [M+5H] 451, [M+6H] 376, [M+7H] 322, [M+8H] 282; Observed mass: [M+2H] 1126, [M+3H] 751, [M+4H] 536, [M+5H] 451, [M+6H] 376, [M+7H] 322.

REFERENCES

(1) Ferreiro, D. U.; Komives, E. A.; Wolynes, P. G. Frustration, Function and Folding. *Curr. Opin. Struct. Bio.* **2018**, *48*, 68–73. https://doi.org/10.1016/j.sbi.2017.09.006.

(2) Chung, M.-K.; White, P. S.; Lee, S. J.; Gagné, M. R.; Waters, M. L. Investigation of a Catenane with a Responsive Noncovalent Network: Mimicking Long-Range Responses in Proteins. *J. Am. Chem. Soc.* **2016**, *138* (40), 13344–13352. https://doi.org/10.1021/jacs.6b07833.

(3) Kobilka, B. K. G Protein Coupled Receptor Structure and Activation. *Biochim. Biophys. Acta. Biomembr.* **2007**, *1768* (4), 794–807. https://doi.org/10.1016/j.bbamem.2006.10.021.

(4) Scott Lokey, R.; Iverson, B. L. Synthetic Molecules That Fold into a Pleated Secondary Structure in Solution. *Nature* **1995**, *375* (6529), 303–305. https://doi.org/10.1038/375303a0.

(5) Bryson, A. The Effects of Substituents on the PK_a Values and N-H Stretching Frequencies of 1- and 2-Naphthylamines. *J. Am. Chem. Soc.* **1960**, *82* (18), 4862–4871. https://doi.org/10.1021/ja01503a029.

(6) Cubberley, M. S.; Iverson, B. L. ^{1}H NMR Investigation of Solvent Effects in Aromatic Stacking Interactions. *J. Am. Chem. Soc.* **2001**, *123* (31), 7560–7563. https://doi.org/10.1021/ja015817m.

(7) Ikkanda, B. A.; Iverson, B. L. Exploiting the Interactions of Aromatic Units for Folding and Assembly in Aqueous Environments. *Chem. Commun.* **2016**, *52* (50), 7752–7759. https://doi.org/10.1039/C6CC01861K.

(8) Zych, A. J.; Iverson, B. L. Synthesis and Conformational Characterization of Tethered, Self-Complexing 1,5-Dialkoxynaphthalene/1,4,5,8-Naphthalenetetracarboxylic Diimide Systems. *J. Am. Chem. Soc.* **2000**, *122* (37), 8898–8909. https://doi.org/10.1021/ja0019225.

(9) Gabriel, G. J.; Sorey, S.; Iverson, B. L. Altering the Folding Patterns of Naphthyl Trimers. *J. Am. Chem. Soc.* **2005**, *127* (8), 2637–2640. https://doi.org/10.1021/ja046722y.

(10) Au-Yeung, H. Y.; Cougnon, F. B. L.; Otto, S.; Pantoş, G. D.; Sanders, J. K. M. Exploiting Donor–Acceptor Interactions in Aqueous Dynamic Combinatorial Libraries: Exploratory Studies of Simple Systems. *Chem. Sci.* **2010**, *1* (5), 567. https://doi.org/10.1039/c0sc00307g.

(11) Nguyen, J. Q.; Iverson, B. L. An Amphiphilic Folding Molecule That Undergoes an Irreversible Conformational Change. *J. Am. Chem. Soc.* **1999**, *121* (11), 2639–2640. https://doi.org/10.1021/ja9838920.

(12) Ikkanda, B. A.; Samuel, S. A.; Iverson, B. L. NDI and DAN DNA: Nucleic Acid-Directed Assembly of NDI and DAN. *J. Org. Chem.* **2014**, *79* (5), 2029–2037. https://doi.org/10.1021/jo402704z.

(13) Gabriel, G. J.; Iverson, B. L. Aromatic Oligomers That Form Hetero Duplexes in Aqueous Solution. *J. Am. Chem. Soc.* **2002**, *124* (51), 15174–15175. https://doi.org/10.1021/ja0275358.

(14) Serjeant, E. Zwitterion Ratios of Aminobenzoic Acids. *Aust. J. Chem.* **1969**, *22* (6), 1189. https://doi.org/10.1071/CH9691189.

(15) Pescitelli, G.; Di Bari, L.; Berova, N. Conformational Aspects in the Studies of Organic Compounds by Electronic Circular Dichroism. *Chem. Soc. Rev.* **2011**, *40* (9), 4603. https://doi.org/10.1039/c1cs15036g.

(16) Tanaka, H.; Litvinchuk, S.; Tran, D.-H.; Bollot, G.; Mareda, J.; Sakai, N.; Matile, S. Adhesive π-Clamping within Synthetic Multifunctional Pores. *J. Am. Chem. Soc.* **2006**, *128* (50), 16000–16001. https://doi.org/10.1021/ja066886+.

(17) Méret, M.; Bienz, S. Efficient and Flexible Solid-Phase Synthesis of N-Hydroxypolyamine Derivatives. *European Journal of Organic Chemistry* **2008**, *2008* (33), 5518–5525. https://doi.org/10.1002/ejoc.200800677.

(18) Oh, S.-J.; Hwang, S. J.; Jung, J.; Yu, K.; Kim, J.; Choi, J. Y.; Hartzell, H. C.; Roh, E. J.; Lee, C. J. MONNA, a Potent and Selective Blocker for Transmembrane Protein with Unknown Function 16/Anoctamin-1. *Mol. Pharmacol.* **2013**, *84* (5), 726–735. https://doi.org/10.1124/mol.113.087502.